



UNIVERSIDAD NACIONAL DE COLOMBIA

Study of the interface - interphase of a Mg-CNT composite made by an alternative sandwich technique

**“Estudio de la intercara – interfase de un compuesto Mg-NTC
fabricado por la técnica alternativa tipo sándwich”**

Cesar Augusto Isaza Merino

Universidad Nacional de Colombia
Mines Faculty, Materials and Minerals School
Medellín, Colombia

2017

Study of the interface – interphase of a Mg-CNT composite made by an alternative sandwich technique

**“Estudio de la intercara – interfase de un compuesto Mg-NTC fabricado por
la técnica alternativa tipo sándwich”**

Cesar Augusto Isaza Merino

Thesis or research paper presented as partial requirement to obtain the title of:

Doctor in Engineering – Materials Science

“Doctor en Ingeniería – Ciencia de los Materiales”

Advisor:

PhD Juan Manuel Meza Meza

Associate Professor-Universidad Nacional de Colombia

Co-advisor:

PhD José Martín Herrera Ramírez

Researcher at Centro de Investigación en Materiales Avanzados (CIMAV, México)

Research field:

Metal Matrix Composites

Research group:

Tribology and Surface G

Universidad Nacional de Colombia

Mines Faculty, Materials and Minerals School

Medellín, Colombia

2017

DEDICATION

“This dissertation is dedicated to my wife who has helped me through this process. Her constant encouragement has provided me the strength to complete this dissertation”

ACKNOWLEDGMENTS

I would like to extend my sincere gratitude to Dr. Juan Manuel Meza Meza and Dr. José Martín Herrera Ramirez, my advisors. This dissertation would not have been possible without their efficient planning, management and supervision. I am thankful for the effort and time they have dedicated towards the completion of this thesis, as well as the development of my career. In addition, I would like to extend my gratitude to laboratorio de caracterización de Materiales, Centro de Investigación en Materiales Avanzados (CIMAV) and group of tribology and surfaces for all the help and permission to use their facilities.

I am thankful to Dr. Juan Felipe Santa Marin for allows me to use the facilities of the laboratorio de polimeros from ITM (instituto técnico metropolitano). I am grateful to Dr. José Miguel Yacaman from Texas University for allows to use the facilities from the Kleberg microscopy laboratory center, as well as all researchers from the Department of Physics and Astronomy for help me during my stay in Texas University at San Antonio.

Finally, I would like to extend my gratitude to MSc José Ernesto Ledezma from CIMAV for his dedication and collaboration during this research and Dr. Hugo Armando Estupiñan for allows me to use the laboratory of corrosion and his facilities such as Raman and AFM microscopies, and finally the scanning electron microscopy. I am thankful with Colciencias for the financial support by the national program for doctorates and the internal projects at the Universidad Nacional de Colombia (Cod. 29072, 29072 and 35845).

There are many who I may have left out in the acknowledgment, but whose co-operation during this research was very important.

Abstract

Carbon nanotubes (CNTs) have been studied as potential reinforcement for Metal Matrix Composites (MMC) for improving the mechanical properties. However, dispersion and alignment of CNTs in the matrix has been very difficult due to their tendency to form clusters. In the present investigation, the synthesis of AZ31B magnesium alloy reinforced with multi-walled carbon nanotubes (MWCNTs) have been developed via the “sandwich” technique. This technique produces a material comprised of a metallic matrix and banded structures-layers of MWCNTs, where a polymeric solution is used to disperse and align the MWCNTs. As a result, a better dispersion and alignment of the CNTs in metal matrix composites was obtained.

The results obtained showed a good interface between the metal matrix and the MWCNTs, allowing a very good interfacial bonding; thus, the mechanical properties, both at the nano level and in bulk, always showed a good behavior. For this characterization, several microscopy techniques including TEM in situ testing, nanomechanical tests and bulk mechanical tests were used. In the studied zones, interphases between the metal matrix and MWCNTs were not found, phases which could hamper the proper load transference between the matrix and reinforcement.

HRTEM analysis allowed to identify the interactions between the metal matrix composites and MWCNTs. In the HRTEM images a semi-coherent and coherent interface between the metal matrix and MWCNTs was found. Additionally, two type of dislocations at the interface were identified: stacked and some dislocations formed to accommodate the Mg crystalline cell in order to produce a semi-coherent surface. No intermediate interphases were found in the studied zones.

Notched micro-cantilever in situ TEM tests showed the dependency of the fracture toughness with the MWCNTs added in the magnesium matrix. Suggesting that the fracture toughness of the reinforced zone increases with the MWCNTs percentage added. This

changes in the fracture toughness is due to the different strengthening mechanisms such as grain size, dislocation activity and finally to the reinforcements action. On the other hand, microtraction test of the composite clearly shown an increasing in the ultimate strength, stiffness and fracture toughness while the main final failure mechanism of the composite was delamination.

Finally, PEO (plasma electrolytic oxidation) coatings were applied on the composite surfaces in order to protect them against corrosion. The results showed a good mechanical and electrochemical behavior of the coating. These results allow thinking in using this kind of composites in medical applications.

Key Words: Metal Matrix Composites, Carbon Nanotubes, Mechanical Properties, Dispersion and Alignment, Interface and Interphases.

Resumen

Los nanotubos de carbono (CNTs, por sus siglas en inglés) han sido usados como un refuerzo ideal para mejorar las propiedades mecánicas de los materiales compuestos de matriz metálica. Sin embargo, su dispersión y alineación dentro de la matriz es difícil debido a su tendencia a aglomerarse. En la presente investigación, se sintetizó magnesio reforzado con nanotubos de carbono de pared múltiple (MWCNTs, por sus siglas en inglés) por medio de una nueva técnica denominada tipo sándwich, la cual permite una mejor dispersión y alineación de los nanotubos de carbono en la matriz metálica. Esta técnica produce un material compuesto de matriz metálica por medio de un apilamiento de láminas metálicas y láminas de polímero reforzado con MWCNTs, donde el material polimérico es usado para dispersar y alinear los MWCNTs.

Los resultados obtenidos mostraron un muy buen comportamiento de la intercara entre la matriz metálica y los MWCNTs, permitiendo una muy buena unión interfacial; por lo tanto, las propiedades mecánicas, a nivel nano y en volumen, mostraron siempre un buen comportamiento. Para la caracterización se utilizaron varias técnicas de microscopía, pruebas in situ, pruebas nanomecánicas y pruebas mecánicas en volumen. En las zonas de estudio no se hallaron interfases entre la matriz metálica y los MWCNTs, que pudieran dificultar la adecuada transferencia de esfuerzos entre la matriz y los MWCNTs.

El análisis HRTEM permitió identificar las interacciones entre los compuestos de matriz metálica y los MWCNT. En las imágenes HRTEM se encontró una interfaz semi-coherente y coherente entre la matriz metálica y los MWCNT. Además, se identificaron dos tipos de dislocaciones en la interfaz: apilamiento y formación de dislocaciones, esta última con el fin producir una superficie semi-coherente. Finalmente, no se encontraron interfases intermedias en las zonas estudiadas.

Las pruebas de TEM in situ mostraron la dependencia de la tenacidad a la fractura con los MWCNT añadidos en la matriz de magnesio. Los resultados sugieren que la resistencia a la fractura de la zona reforzada aumenta con el porcentaje de MWCNT añadido. Estos cambios en la resistencia a la fractura se deben a los diferentes mecanismos involucrados, como el tamaño del grano, la actividad de dislocación y finalmente a la acción de los

refuerzos. Por otro lado, la prueba de micro-tracción del material compuesto mostró claramente un aumento en la resistencia final, la rigidez y la tenacidad a la fractura, mientras que el mecanismo de falla final principal del compuesto fue la de-laminación.

Por último y como trabajo adicional, en las superficies de los materiales compuestos se aplicaron recubrimientos de PEO (oxidación electrolítica por plasma) para protegerlos contra la corrosión. Los resultados mostraron un buen comportamiento mecánico y electroquímico. Estos resultados permiten pensar en el uso de este tipo de compuestos para aplicaciones médicas.

Palabras clave: Materiales compuestos de matriz metálica, Nanotubos de carbono, Propiedades mecánicas, Dispersión y Alineación, Intercara e Interfaces.

Contents

	Pág.
Abstract	XI
Figures captions	XVII
Table captions	XXI
Introduction	1
1. Literature review	5
1.1 Carbon nanotubes (CNTs).....	5
1.1.1 Carbon nanotubes synthesis.....	6
1.1.2 Carbon nanotubes properties.....	7
1.2 Metal matrix composites processing	8
1.2.1 Powder metallurgical processing.....	9
1.2.2 Melting and solidification process.....	13
1.2.3 Electrochemical routes.....	15
1.2.4 Other Novel Techniques.....	16
1.3 Mechanical properties of metal matrix composites reinforced with CNTs	17
1.3.1 Prediction models for mechanical properties	17
1.3.2 Mechanical properties of aluminum and magnesium composites	19
1.4 Interfacial behavior between metal matrix (Aluminum and Magnesium) composites and CNTs.....	23
1.4.1 Other interactions between CNTs and metal matrix	24
1.5 Protective coatings for metal matrix composites (additional work)	24
2. Experimental procedure	27
2.1 Materials used in this study.....	27
2.1.1 Metal matrix	27
2.1.2 Carbon nanotubes.....	28
2.1.3 Polyvinyl Alcohol	28
2.2 Experimental procedure.....	29
2.3 Metal matrix composites synthesis.....	31
2.3.1 Polymer matrix composites synthesis.....	31
2.3.2 Metal matrix composites synthesis.....	32
2.4 Dispersion and alignment quantification for both, polymer and metal matrix composites.....	34
2.5 Micro-structural characterization	36
2.6 Mechanical properties characterization.....	38
2.6.1 Ex situ mechanical characterization	38

2.6.2	In situ testing characterization: Fracture toughness	39
2.6.3	Corrosion characterization (additional work)	42
2.7	Experimental analysis.....	43
3.	Results and discussions	45
3.1	Multi-walled carbon nanotubes characterization	45
3.2	Dispersion and alignment quantification in polymer matrix composites.....	47
3.2.1	Mechanical properties for dispersion and alignment verification.....	52
3.3	Bulk microstructural bulk characterization in metal matrix composites.....	55
3.3.1	Dispersion and alignment quantification of MWCNTs in a metal matrix	58
3.4	Interface characterization between magnesium matrix and MWCNTs	60
3.4.1	Interface characterization between magnesium sheets: layer of Mg reinforced with CNTs and diffusion zone	60
3.4.1	Interface characterization between MWCNTs and metallic matrix.....	68
3.5	Mechanical properties characterization in the metal matrix composites	77
3.5.1	Nano mechanical testing characterization	77
3.5.2	Nano-scratch testing characterization	79
3.5.3	In situ TEM testing characterization and crack growth	81
3.5.4	Fracture toughness analysis	87
3.5.5	Bulk mechanical testing in the composites.....	89
3.5.6	Cracking characterization after tensile testing	91
3.5.7	Theoretical models for metal matrix composites	95
3.6	PEO coating characterization in metal matrix composites (additional work). 102	
3.6.1	Micros-structural and morphological PEO coating characterization... 102	
3.6.2	Mechanical testing in the composites coating	104
3.6.3	Corrosion testing in the composites coating.....	107
4.	Conclusions and future work.....	115
4.1	Conclusions.....	115
4.2	Future works	118
A.	Annex: Publications in this dissertation	120
References	128

Figures captions

	Pág.
Figure 1-1. a) Single-walled carbon nanotubes and b) multi-walled carbon nanotubes.....	6
Figure 1-2. Number of publications in composites reinforced with carbon nanotubes	8
Figure 1-3: Representation of the disintegrated melt deposition process [69].	15
Figure 1-4: Distribution of tensile and shear stresses into a short fiber embedded into a matrix.	17
Figure 2-1: Micro-structural changes after recrystallization and deformation process. a) raw material, b) annealed material and c) hot rolled material.....	28
Figure 2-2: TEM image of the MWCNTs used in this study.....	28
Figure 2-3: Methodology used in this research	30
Figure 2-4: Synthesis of polymer matrix composites reinforced with MWCNTs.....	31
Figure 2-5: Synthesis route diagram of the Mg-PVA/MWCNTs composites.....	33
Figure 2-6: a) Outlines the composite sections studied and b) transversal study zone close to the interface (SEM-SE image).....	33
Figure 2-7: Representatives images divided into 10x10 grid lines for quantification.....	36
Figure 2-8: a) Sample extraction in the reinforced zone, b) cantilever bend geometry for the in situ test and c) images before in the situ test.	40
Figure 2-9: (a) Schematic AFM sensor and (b) SEM image of the sensor tip.....	41
Figure 2-10: Box plot and whiskers representation.	43
Figure 3-1: (a) FESEM images of MWCNTs and (b) outer diameter distribution.	46
Figure 3-2: (a to c) HRTEM images of MWCNTs and (d) inner diameter distribution.	46
Figure 3-3. TEM images of the polymer matrix reinforced with 0.25 wt.% of MWCNTs. a) Not aligned – as-synthesized and b) aligned.	48
Figure 3-4: TEM images of the polymer matrix reinforced with 0.5 wt.% of MWCNTs. a) Not aligned – as-synthesized and b) aligned.	49
Figure 3-5. TEM images of the polymer matrix reinforced with 1.0 wt.% of MWCNTs. a) Not aligned – as-synthesized and b) aligned.	50
Figure 3-6. Angle frequency distribution of the alignment quantification. PVA reinforced with a) 0.25, b) 0.5 and c) 1.0 wt.% of MWCNTs.	51
Figure 3-7. Load versus indenter displacement curves for the nanoindentation tests performed on: a) not aligned – as-synthesized and b) aligned samples.....	52
Figure 3-8. a) Elastic modulus and b) hardness measure by nanoindentation test.	53
Figure 3-9. Stress versus strain curves obtained by DMA for the composites tested in two directions (longitudinal and transverse to the stretching direction).....	55
Figure 3-10: Optical microscopy images of the microstructures of magnesium reinforced with MWCNTs: a) 0.25, b) 0.5 and c) 1 wt.%.	56

Figure 3-11: FESEM images of magnesium reinforced with MWCNTs: a) 0.25, b) 0.5 and c) 1 wt.%.....	57
Figure 3-12: FESEM-EDS mapping analysis of the interface zone.....	57
Figure 3-13: XRD patterns of magnesium reinforced with 0.25, 0.5 and 1 wt.% of MWCNTs.....	58
Figure 3-14: FE-SEM images of the metal matrix reinforced with MWCNTs. a) 0.25 wt.% and b) 0.5 wt.%.....	59
Figure 3-15: STEM EDS mapping in the study zone. 1. Lamella extracted close to the study zone (Diffusion zone). 2. Detail from diffusion zone. (see also Fig. 3-16).....	61
Figure 3-16: EDS analysis at the interface between magnesium sheets: Diffusion zone comprised of transition and High content CNTs zones.....	62
Figure 3-17: a) HRTEM image and b) diffraction pattern of the composite in zone 1 (Spectrum 1).	62
Figure 3-18: a) TEM image and b) diffraction pattern in zone 2 (spectrum 2).	63
Figure 3-19: a) HRTEM image and b) diffraction pattern in Zone 3 (Spectrum 3).	64
Figure 3-20: Bright field images for magnesium reinforced with 0.25 wt.% of MWCNTs. a) transition zone, b) detail of MWCNTs and c) detail of recrystallized zone.....	65
Figure 3-21: Bright field images for magnesium reinforced with 0.5 wt.% of MWCNTs. a) transition zone, b) detail of MWCNTs and c) detail of recrystallized zone.....	65
Figure 3-22: Bright field images for magnesium reinforced with 1.0 wt.% of MWCNTs. a) transition zone and b) detail of MWCNTs.	66
Figure 3-23: Dark field images for magnesium reinforced with 0.25 wt.% of MWCNTs. ..	66
Figure 3-24: Dark field images for magnesium reinforced with 0.5 wt.% of MWCNTs.	67
Figure 3-25: Dark field images for magnesium reinforced with 1.0 wt.% of MWCNTs.	67
Figure 3-26: HRTEM images for the composites reinforced with 0.25 wt.% of MWCNTs. The dislocation stacking can be seen (HRTEM filter).	69
Figure 3-27: HRTEM images for the composites reinforced with 0.25 wt.% of MWCNTs. The dislocation formation can be seen (HRTEM filter).	69
Figure 3-28: HRTEM images for the composites reinforced with 0.5 wt.% of MWCNTs. MWCNTs in grains borders can be seen (HRTEM filter).	70
Figure 3-29: HRTEM images for the composites reinforced with 0.5 wt.% of MWCNTs. grains directions can be seen (HRTEM filter).	70
Figure 3-30: HRTEM images taken at the interface zone for the composites reinforced with 0.5 wt.% of MWCNTs (HRTEM filter).	71
Figure 3-31: HRTEM images for the composites reinforced with 1.0 wt.% of MWCNTs, (HRTEM filter).....	72
Figure 3-32: HRTEM images for the composites reinforced with 1.0 wt.% of MWCNTs, coherence of the interface between MWCNTs and metal matrix is shown (HRTEM filter).	72
Figure 3-33: Orientation analysis at the interface between magnesium matrix and MWCNTs for images HRTEM (analysis by VESTA software).....	73
Figure 3-34: EDS mapping performed in the Mg/0.5 wt.% MWCNTs composite.	76
Figure 3-35: Elemental spectrogram from the study zone from the Figure 3-34.	76

Figure 3-36: EELS analysis between MWCNTs and the metal matrix in the interface of the 0.5 wt.% of MWCNTs sample).....	77
Figure 3-37: Elastic modulus, b) hardness c) load vs displacement and d) the indentations done close to the interface between Mg sheets.	79
Figure 3-38: Variation of the friction coefficient as a function of scratch length for all composites studied.....	80
Figure 3-39: Nano-scratch tests in the study zones for all Mg composites containing a) 0.0, b) 0.25, c) 0.5 and d) 1.0 wt.% of MWCNTs.....	81
Figure 3-40: Frames images of the in situ test for the composite reinforced with 0.25 wt.% of MWCNTs.....	82
Figure 3-41: Ex situ fracture analysis for the composite reinforced with 0.25 wt.% of MWCNTs.....	83
Figure 3-42: Frames images for the in situ testing for the composite reinforced with 0.5 wt.% of MWCNTs.	84
Figure 3-43: Ex situ fracture analysis for the composite reinforced with 0.5 wt.% of MWCNTs.....	85
Figure 3-44: Frames images of the in situ testing for the composite reinforced with 1.0 wt.% of MWCNTs.....	85
Figure 3-45: Ex situ fracture analysis for the composite reinforced with 1.0 wt.% of MWCNTs. BF: Bright field, DF: Dark field and DP: Diffraction pattern.	86
Figure 3-46: Nano-cantilever beam for the K_{1c} in situ test.....	87
Figure 3-47: a) Schematic illustration showing how strength and fracture behavior can be considered in terms of intrinsic (plasticity) versus extrinsic (shielding) toughening mechanisms associated with crack extension and b) schematic illustration for dislocation pile up at the neutral axis.....	89
Figure 3-48: Mechanical properties by tensile test for the composites: a) stress-strain curves and b) ultimate and yield strengths.....	90
Figure 3-49: Interlaminar fracture in the composites studied.....	91
Figure 3-50: Fracture mechanism for magnesium sheets in the composites studied.	91
Figure 3-51: Tensile Fracture for the composite reinforced with 0.25 wt.% of MWCNTs.	92
Figure 3-52: Tensile Fracture for the composite reinforced with 0.5 wt.% of MWCNTs... ..	93
Figure 3-53: Tensile Fracture for the composite reinforced with 1.0 wt.% of MWCNTs... ..	94
Figure 3-54: Raman spectra for PVA, MWCNTs and PVA/MWCNTs.	96
Figure 3-55: Effects of embedment and cooling on the frequency shift of the D*-band	96
Figure 3-56: Experimental and theoretical values for the elastic modulus and b) stress for all composites studied.	99
Figure 3-57: Experimental and theoretical values for ultimate stress for all composites studied in the basal crystal orientation.....	100
Figure 3-58: Cross-section micrographs of the PEO-film in the a) AZ31B alloy, b), c) and d) the composites reinforced with 0.25, 0.5 and 1.0 wt.% of MWCNTs, respectively.	104
Figure 3-59: SEM-EDS mapping analysis of the interface and coating zone for the composite reinforced with 1.0 wt.% of MWCNTs.	104
Figure 3-60: Nanoindentation results for the coating in all composites: a) load-displacement curve, b) elastic modulus and c) hardness.....	105

Figure 3-61: Scratch test results using a normal load from 0.5 to 100 mN. Lateral force and penetration depth as a function of the scratch distance for: a) AZ31B and b) 0.25 wt. %.....	107
Figure 3-62: EIS (Nyquist) plots of the AZ31B alloy reinforced with MWCNTs and coated by PEO.	108
Figure 3-63: EIS (Bode) plots of the AZ31B alloy reinforced with MWCNTs and coated by PEO.	108
Figure 3-64: Equivalent circuit used for impedance data fitting of AZ31B magnesium alloy reinforced with MWCNTs and coated by PEO.....	111
Figure 3-65: Surface morphology of the AZ31 alloy reinforced with MWCNTs and coated by PEO technique: a) 0.25, b) 0.5 and c) 1.0 wt. % of MWCNTs.....	112

Table captions

	Pág.
Table 1-1: Mechanical properties of CNTs.....	8
Table 1-2: Mechanical properties in metal matrix composites reinforced with CNTs.....	21
Table 2-1: Nominal chemical composition (wt.%) of the AZ31B magnesium alloy.	27
Table 2-2: Sigma Aldrich material specifications (http://www.sigmaaldrich.com).	29
Table 3-1. Measured and calculated parameters for the PVA-MWCNTs composites.....	52
Table 3-2: Measured and calculated parameters for the Mg-MWCNTs composites.....	60
Table 3-3: Parameters and fracture toughness after in situ testing.	88
Table 3-4: Parameters and elastic modulus for MWCNTs used in this research.....	97
Table 3-5: Results for Ultimate strength by Tabor's equation. The ultimate strength for Mg matrix is 307 MPa.....	98
Table 3-6: Parameters for in situ testing and calculated mechanical properties.....	101
Table 3-7. EIS fitting results for the AZ31B alloy with different content of MWCNTs and coated by PEO (T stands for charge transfer and P for phase).....	111

Introduction

Since their discovery by Iijima [1] in the 1990s, the carbon nanotubes (CNTs) began to be the cornerstone in several scientific branches, from Physics to Chemistry, going through Medicine and Biology. In materials science, technology and applied engineering, a large number of studies has been conducted on carbon nanotubes, due to their extraordinary mechanical, thermal and physical properties. During three decades, several research centers and universities groups had tried understanding the carbonaceous behavior in carbon nanotubes, and an outstanding potential of this kind of materials for structural applications as a reinforcement in composites materials with polymeric, ceramic and metallic matrices.

Dispersion within a matrix is maybe the most important and difficult challenge in the fabrication of composites reinforced with CNTs. CNTs consist of graphene layers arranged concentrically in a tube form, with dimensions of some nanometers and large specific surface area up to $200 \text{ m}^2\text{g}^{-1}$. Therefore, they tend to agglomerate and form clusters owing to van der Waals forces. Good dispersion of the reinforcement is needed for efficient use of the properties, because CNTs clusters have lower strength, higher porosity and serve as discontinuities, which decrease the mechanical, electrical or thermal properties of the composite. Recent developments on this field seek for processes that promote a good dispersion of CNTs in the matrix without causing them damage, bringing about at the same time, high CNTs density and effective load transfer between reinforcement and metal matrix [2]. The mechanical properties of the composite depends on the chemistry, atomic structure and the bonding at the interface, because this is the region where the mechanical load is transferred from the matrix to the reinforcement [3, 4].

Since 1990s, automotive and aeronautic engineers have increasingly focused on magnesium and aluminum alloys and their composites due to their low density and high specific strengths. In the last century, magnesium alloys suffered from low corrosion resistance, usually due to iron, copper and nickel impurities, but nowadays magnesium

alloys with good corrosion behavior are available. In a few words, researchers are currently studying the magnesium reinforced with different kind of reinforcement like SiC [5, 6], Al₂O₃ [7], SiO₂ [8], Y₂O₃ [9], CNTs [10-12] and graphene nanoplates [13, 14]. On the other hand, several metal matrix composites manufacturing techniques involve high temperature, which can produce some damages to the CNTs and compromise their stability during the fabrication of the composite.

Among the main routes for processing metal matrix composites (MMCs) reinforced with carbon nanotubes are:

Liquid metallurgy processing: MMCs are simple to manufacture in large quantities by a conventional casting equipment. However, there are difficulties for achieving homogeneous dispersion of CNTs, poor wetting and preferential formation of harmful interfacial products. Melt processing techniques can be classified into melt stirring, melt infiltration and laser deposition [14]. Gupta et al. [15] developed a disintegrated melt deposition processing for producing MMCs reinforced with CNTs, with very good mechanical properties.

Spray forming: thermal spray for producing MMCs have many applications in automotive engines, aerospace turbine blades, orthopedic prostheses and electronic devices by forming coatings on their surfaces. The coating can be particles, fibers or CNTs, as it has been demonstrated by Bakshi et al. [16].

Powder metallurgy processing, it is the most economical and easy technique for manufacturing MMCs due to its simplicity and flexibility. The process involves mechanical blending of CNTs with metal powders in a mill, followed by other processes like compaction and sintering, cold isostatic pressing, hot pressing/hot isostatic pressing, or spark plasma sintering. These processes are followed by secondary mechanical deformation treatments such as hot extrusion, hot forging, or hot rolling to consolidate the compacts into full-dense products. However, in some cases these processing techniques do not lead to a major increase of the mechanical properties due to the agglomeration of CNTs into the metal matrix. It should be noted that in magnesium composites the reactivity decrease with the reinforcement, which is less than other metals like aluminum [17, 18]. All these techniques will be discussed in more detail in the literature review section.

In this research, a new process that allows obtaining well dispersed and aligned MWCNTs in the magnesium metal matrix composite was implemented. It is worth saying that the

process could be implemented to produce several types of composites with any type of metallic matrices. This technique takes advantage of the easy incorporation and dispersion of the carbon nanotubes in polymer matrices, mainly because the rheology of the mixture is adequate and low processing temperatures are required (below 200°C). In fact, there are some polymers like polyvinyl alcohol (PVA) which can be dissolved by hot water, producing a low viscosity solution, which allows an easy dispersion of some nanostructures like CNTs. In addition, by stretching processing of the PVA, the mechanical alignment of CNTs can be reached [19]. In this work, a new method to produce MMCs was developed, which promises to overcome some problems of dispersion and alignment of the CNTs that are typical of thermo-mechanical manufacturing techniques.

Focus of the Present Research Work

The overall aim of the present research is to study the interface and interphases of metal matrix composites reinforced with MWCNTs by the alternative technique called sandwich. The specific objectives of this work are as follows.

- Establish an appropriate methodology for manufacturing polyvinyl alcohol reinforced with MWCNTs.
- Quantify the dispersion and alignment of MWCNTs in the polymer matrix.
- Establish an adequate methodology for manufacturing magnesium reinforced with carbon nanotubes by an alternative technique.
- Quantify the dispersion and alignment of MWCNTs in the metal matrix composite.
- Study the physical, chemical and mechanical behavior at the interface between MWCNTs and metal matrix in the composites.
- Study the mechanical behavior of the composite material (magnesium reinforced with MWCNTs).
- Identify the mechanisms of crack growth of the composites submitted to static loads.

The research work carried out in this study will be documented in this dissertation in various sections: introduction, literature review, experimental procedure, results and discussion, conclusion and recommendations for future work. The appendix includes the first page of the publications in international journals arising out of this research work.

1. Literature review

In this literature review the recent progress of metal matrix composites based on light metallic materials is shown; particular emphasis is made for both magnesium and aluminum alloys with applications in the aerospace and automotive structural industry. Some techniques for producing carbon nanotubes and their mechanical properties, which are of great interest to improve the properties of the composite, are described in this review. The process of metal matrix composites comprises several manufacturing techniques that are described from the viewpoint of the process. Finally, the properties and relevant theoretical models for metal matrix composites, mechanical properties and physical properties such as: theoretical prediction, interfacial phenomenon and fracture toughness will be described.

1.1 Carbon nanotubes (CNTs)

Reported by Iijima in 1991 [1] CNTs consist of concentric graphene cylinders produced in a low current furnace. However, since 1970 Endo and collaborators had already obtained carbon nanotubes [20], through a controlled process of benzene and ferrocene pyrolysis at 1000°C, but they could not prove it. The CNTs are characterized by having distances between layers of about 3.4 Å, and are slightly larger than the distance between graphite layers (3.35 Å). Iijima attributes these morphological characteristics to the curvature of the tube and the van der Waals interactions between successive cylinders. The CNTs are obtained in inert atmosphere and optimum conditions of current and pressure. In the 1990s, multiple layer nanotubes (MWCNT) and single layer nanotubes (SWCNT) were introduced in the scientific community (Figure 1-1). Since then, the development of these new materials has been increased, finding different and new applications because of their exceptional physical, mechanical and chemical properties.

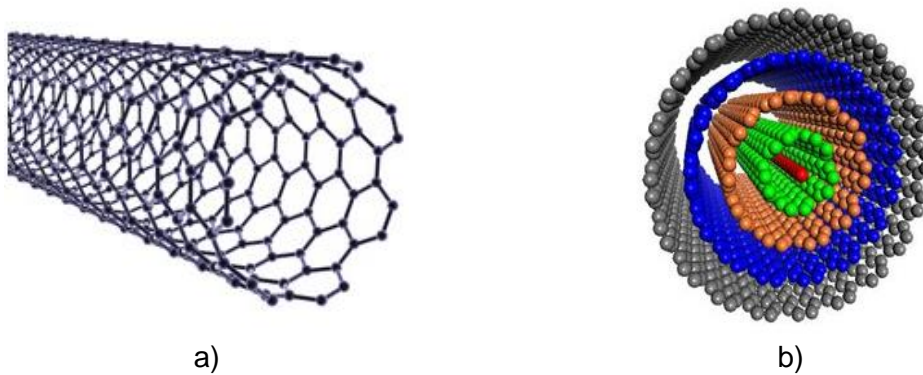


Figure 1-1. a) Single-walled carbon nanotubes and b) multi-walled carbon nanotubes

The CNTs have three different structures, which define their most important characteristics such as electrical and thermal conductivity, and mechanical properties. Each of these structures has a different geometry and depends on the carbon chains location respect to the nanotube axis.

1.1.1 Carbon nanotubes synthesis

CNTs have three different manufacturing processes; each technique has its advantages and disadvantages, and depend on the costs and CNTs quality. In this section, the CNTs manufacturing methods will be mentioned, without going into details.

- **Arc discharge**

The arc discharge method consists on producing an electric discharge between two electrodes of graphite. This method evaporate electrodes in approximately 60% nanoparticles and 40% CNTs, and the temperature reached at the moment of graphite evaporation is between 3000 and 4000 °C. This technique is appropriated for producing single or multi-walled CNTs with excellent quality [21]. Currently the technique has had several improvements that is reflected in the CNTs quality and manufacture control, such as the purification influence, magnetic field for controlled growth, alignment and dispersion in in situ manufacturing [22-24].

- **Laser ablation**

The laser ablation method uses a pulsating laser light to evaporate the graphite, which is mixed with a small part of cobalt and / or nickel, in order to obtain single-walled carbon

nanotubes [25]. In this technique, the material is preheated at approximately 1200°C, after that, both the laser pulses and gas start working at the same time, being the gas, which collects the CNTs, produced to deposit them in a cold room. The technique allows that the conditions of synthesis are controlled and maintained over a long period, producing a more uniform vaporization of the CNTs and better quality. Similarly, the authors have tried implementing other raw materials and variations in the manufacturing processes, which have allowed improve the quality and properties of CNTs [26-28].

- *Chemical vapor deposition (CVD)*

Chemical vapor deposition technique is based on the hydrocarbons decomposition at high temperatures. In this process, a catalyst is heated in a furnace, then the raw material (hydrocarbon in the gaseous state) flows through the furnace, after that, the CNTs are cooled to room temperature. This method allows the control of CNTs diameters [29] and the number of CNTs concentric tubes during the manufacture process [30, 31]. This method is the most used because allows the manufacture of large quantities of CNTs with few defects and at a relatively low cost.

1.1.2 Carbon nanotubes properties

The CNTs have exceptional mechanical properties, Table 1-1 summarizes some values measured by several researchers. The values measured for the Young modulus are higher in comparison to the traditional materials used in engineering. This fact has motivated researchers to try to develop composite materials reinforced with CNTs. Since the 1990s, this kind of research has had a great impact; however, after 2000s, the most relevant research results related to structural applications started to appear using CNTs as reinforcement material in polymeric, ceramic and metallic matrices, being polymeric matrix reinforced with CNTs the most studied, as shown in the graph of Figure 1-2.

On the other hand, the United States is the main producer of CNTs with approximately 13 industries followed by Japan and China. Consequently, these are the countries that have more academic production in CNTs for different applications, both structural and functional applications.

Table 1-1: Mechanical properties of CNTs

TECHNIQUE	MODULUS	REFERENCES
Thermal vibrations amplitude of the MWCNTs at different temperatures	$E = 0.4-4.15$ TPa	[32]
Fixed displacement-force curve by AFM	$E = 1.28 - 0.59$ TPa	[33]
Electromagnetic resonance frequency	$E = 1-0.1$ TPa For MWCNTs	[34]
Tension test by SEM	$E = 270-950$ GPa Strength = 11-63 GPa	[35]
Single bending tests	$E = 870$ GPa for MWCNTs by arc discharge and 27GPa for MWCNTs by CVD	[36]
Finite element simulation	$E = 1 - 1.06$ TPa	[37]

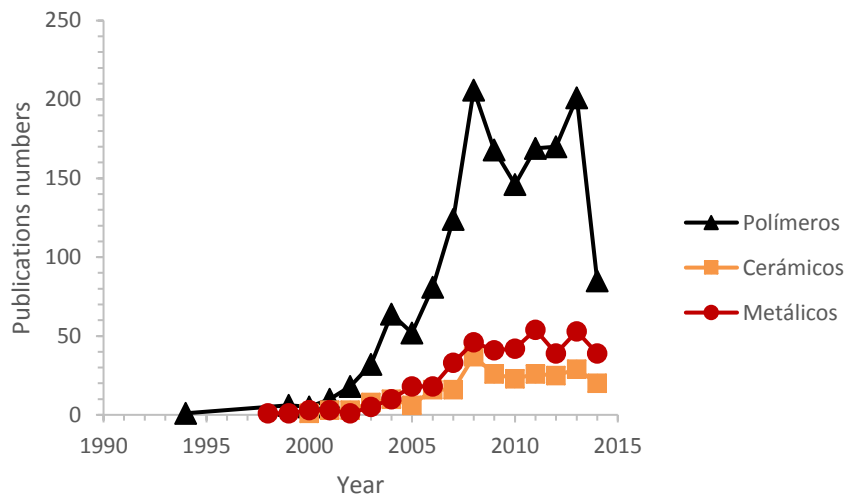


Figure 1-2. Number of publications in composites reinforced with carbon nanotubes

1.2 Metal matrix composites processing

Due to their properties showed in Table 1-1, the CNTs have been used as a reinforcement in materials to contribute their properties to the base material (polymer, ceramic or metals).

Metallic and ceramic matrices have some disadvantages compared with polymeric ones such as low dispersion, low alignment and a bad interfacial bounding. However, composites processing techniques have been forth optimized, and every year the mechanical properties of the metal matrix composites are better. Such techniques are presented below:

1.2.1 Powder metallurgical processing

Powder metallurgy processes for manufacturing metal matrix composites are widely used, but they have some disadvantages, such as low dispersion, low alignment and in some cases CNTs damage due to processing. However, this process is the most inexpensive and good mechanical properties in the composites can be obtained. However, in some cases, interfacial problems are generated due to the formation of harmful phases for the composite. In magnesium, this process is not the most used owing to the low magnesium plastic deformation and because it does not allow a good dispersion of the CNTs.

Several processes for the metal matrix composite manufacturing reinforced with CNTs based on powder metallurgy such as sintering, hot pressing, plasma deformation and sintering processes will be described in this section.

- Sintering process

Sintering is the most conventional process used in the metal matrix composites fabrication. CNTs are mixed and incorporated within the matrix (metal powders) by mechanical stirring and finally compacted and sintered. In order to obtain a composite with good mechanical properties, a very good CNTs dispersion must be made before compacting and sintering, otherwise, these agglomerations will be presented as pores avoiding a good performance of the material. This is, the CNTs agglomerations have a direct influence in the mechanical properties of the composites.

Stein et al. [38], studied AA5083 aluminum powders mixed with MWCNTs; the dispersion process was done mechanically and the composites were sintered and extruded. The authors found non-significant increases of elasticity modulus, although both the maximum stress and yield strength considerably increased using high dispersion energy by ball milling with 1.5 wt.% of CNTs. Li et al. [39] made grow CNTs in aluminum powders and the composite was sintered at 550°C. They achieved, with 0.8 wt.% of CNTs, a maximum

improvement of some mechanical properties like hardness and strength. An increment in the CNTs content resulted in a mechanical properties decreasing. Other studies [40] evaluated the temperature sintering effect of Al6061 aluminum powders reinforced with CNTs made by mechanical stirring. In this process, the authors used mechanical stirring during 30 h (CNTs were added in the last 2 h) and then the composites were compacted and sintered at three different temperatures. The authors obtained good dispersion, although several CNTs damages were evidenced. Others studies were carried out on electrical and tribological properties for aluminum reinforced with CNTs [41].

For manufacturing magnesium reinforced with CNTs, several authors have tried to integrate different techniques to increase the mechanical properties. A novel approach to prepare Mg matrix composite reinforced with CNTs- Al_2O_3 was proposed by Li et al. [42], where the CNTs were synthesized and dispersed using alumina as a vehicle to promote the dispersion of CNTs in the Mg matrix; the mechanical properties of the composite were improved.

Sun et al. [43] used the in situ synthesis: CNTs were synthesized on the Mg powder by acetylene decomposition at 480°C . After that, mechanical mixing for greater dispersion and homogenization of the reinforcement was done, and finally, the powders were cold compacted and sintered at 580°C , followed by a process of Extrusion to enhance their properties. The hardness of the Mg/CNTs composites was improved by 25%, and the tensile strength reached about 285 MPa, which is a 45% increase over commercial pure Mg. However, bigger amounts of CNTs produced a decreasing of mechanical properties, which was possibly due to CNTs dispersion problems and possible surfaces reactivity between CNTs and magnesium matrix.

Habibi et al. [44, 45] combined different materials for making hybrids. In this study, the manufacturing process was done in two steps using a conventional solid-state powder metallurgy technique. First, the aluminum powder was mixed with CNTs and finally this composite was mixed with magnesium powders. In the manufacturing process, a rapid microwave sintering and hot extrusion were used to synthesize near-dense Mg nano-composites containing a mixture of nanopowdered Al and CNTs. Properties such as elastic modulus, yield and ultimate strength were increased as the amount of aluminum in the hybrid composite was increased. The authors explained that the strength enhancement can

be attributed to: reduction in average matrix grain size, crystallographic texture changes, dislocation generation due to elastic modulus mismatch and coefficient of thermal expansion mismatch between the matrix and ball milled Al–CNT nanoparticles, as well as the Orowan strengthening mechanism.

- ***Hot compaction process***

Hot pressing and hot forming process are techniques, generally used before sintering process. However, some authors have found these techniques unfavorable for the CNTs dispersion in the aluminum matrix [46]; in addition, the thermal process and possible clusters of CNTs allow easy phase formation such as: AlC and Al₄C₃, which, evidence the reactivity between CNTs and aluminum. Kwon et al. [47, 48], used this technique for manufacturing aluminum reinforced with CNTs; in order to obtain a good bonding between matrix and reinforcement, silicon carbide was added; however, although in low percentages, Al₄C₃ phase was formed. Shin et al. [49] used a technique which includes sintering and hot-pressing steps, they were able to process aluminum reinforced with CNTs and showed that the post-processing step improved the mechanical properties in the composites studied.

Magnesium reinforced with carbon nanotubes by hot compaction process has been well explored by Gupta et al. [50]. They used this technique as an additional process before making the sintering process. For the composites synthesis, mechanical mixing of the magnesium powders was done, followed by a hot pressing; finally, they made a pressureless sintering process. The results of the mechanical behavior characterization revealed that an increasing volume fraction of CNTs in the magnesium matrix lead to an improvement of 0.2% in the yield strength, ductility and fracture toughness. An increase in the ductility was observed up to 0.18 wt % of CNTs in Mg. Shimizu et al. [51], used a mechanical mixture of CNTs and magnesium powders in argon atmosphere; they did not found CNTs clusters evidence in the magnesium matrix after hot pressing and extrusion process.

- ***Deformation processing***

Deformation process is used as a post-processing step in different manufacturing techniques, generally used after sintering or hot compaction processing for manufacturing metal matrix composites. Deformation process includes techniques such as hot and cold

rolling and extrusion, whose aim is to eliminate pores, refine the grain and in some cases help to orient the reinforcement; however, for CNTs the reorientation is more difficult due to their size. Liu et al. [52], } used a combination of spark plasma sintering and hot extrusion, founding that during the process there was a new phase formation between aluminum and CNTs; however the mechanical properties of the composite increased with the CNTs amount. In addition, after the extrusion process they found areas with CNTs aligned in the extrusion direction, which increased the mechanical properties of the composites. In the same way, Jiang et al. [53] carried out the powder metallurgy process for manufacturing aluminum reinforced with CNTs, using extrusion as a post-process, which enhanced the mechanical properties of the composite. In this process, the authors did not found evidence of the harmful phases precipitation.

The post- processing allows CNTs to explore their longitudinal properties. This fact improves the dislocation storage capability, which guarantees both enhanced strength and ductility over the nanocomposites composed of the same constituents but with randomly distributed CNTs. However, Kwon, et al. [54] found some damages on the CNTs after the extrusion process, making it difficult to take full advantage of the reinforcing characteristics, as well as undesired phases in the interfaces between nanotubes and aluminum matrix.

In the manufacturing of magnesium reinforced with CNTs, the deformation processes are used as a post-process for enhancing the mechanical properties. As did Paramsothy et al. [55], ZK60A magnesium was extruded after being processed by solidification process. The material manufactured showed an increase in its ductility and mechanical strength, but its compressive strength decreased, which was attributed to the little formation of intermetallic phases after the manufacturing process. Other authors [42] extruded a hybrid material: a pre-dispersion of CNTs into alumina particles was subsequently mixed with magnesium powders. The authors found a little improvement in the mechanical strength and elastic modulus. Besides, several authors have improved the mechanical properties of magnesium by extrusion as a post-process [44, 56, 57].

- Plasma sintering process

This technique uses electrical pulses for heating the matrix powders. It has been found an improvement of the fracture toughness and crack propagation behavior in metal matrix

composites such as H. Kwon et al. [58] demonstrated. In their research, they used this technique combined with the extrusion process for manufacturing aluminum reinforced with CNTs. The authors found that the properties of the composite increase with the percentage of CNTs. However, the formation of harmful phase and CNTs clusters were observed. Other authors [17, 59-61], reported that the dispersion of MWCNTs was very difficult to do; despite this, there was a significant increase in the mechanical properties. In magnesium composites the technique is not frequently used due to the CNTs dispersion difficulties into the matrices, in addition to the possible formation of harmful phases during the process. Fukuda et al. [57], used the plasma sintering process followed by an extrusion process for manufacturing AZ 61B magnesium reinforced with CNTs. The authors found that the ductility improved with the percentage of CNTs, although the modulus, creep and mechanical strength were kept unchanged. A recent study [62] of magnesium reinforced with graphene nanoplates manufactured by plasma sintering process showed that the mechanical properties decreased in comparison with pure magnesium, however for the addition of 2 wt.% of nanoplates, the ductility of the material increased.

1.2.2 Melting and solidification process

This technique is the most primitive for manufacturing metal alloys; however, for composites manufacturing it has some limitations, being the main is the need of using low melting point matrix materials. High melting point matrix materials would produce reinforcement damages. Another limitation is that due to the CNTs surface tension, they tend to agglomerate and create clusters, which prevents to obtain good final properties on the composite; in addition, around the clusters the formation of undesired phases is prone to occur.

- *Melting process*

This technique uses the metal in the molten state to disperse the CNTs into the matrix; this procedure has some limitations, such as the difficulty in dispersing the CNTs into the matrix. Notwithstanding, the common drawback of the melting based process, researchers [12] have manufactured aluminum reinforced with CNTs by high-pressure casting technique, founding a decreasing of the yield strength as the CNTs are added, although the maximum strength of the composite was maintained. Other techniques such as semi-solid processes, were explored by Wu et al.[63], who found that the mechanical properties decrease for high

percentage of CNTs (up to 2wt.%); the authors explained this decrement to the phases formation between CNTs and the matrix.

A recent work [64] shows the changes in the magnesium microstructure due to the rate of solidification done by the cast mixing technique. The authors found that low solidification rates lead to the CNTs agglomeration at the grain boundaries and that high solidification rates help to capture the CNTs inside the magnesium grains; in addition, they reported good bonding between the metal matrix and CNTs.

- ***Infiltration processing***

The metal infiltration process consists on preparing a porous preform containing dispersed reinforcements, which is subjected to a molten material and, finally, the molten metal is distributed in the reinforced structure by pressure.

Besides common problems of melting processes, the pressure used in this process could cause CNTs agglomeration. Zhou et al. [65] used powder metallurgy with materials such as aluminum and magnesium with CNTs dispersed in the powders as preforms, which were then pressed. Finally, the compacted material with high percentage of pores is infiltrated using pressure and an aluminum aqueous solution. The authors concluded that as the CNTs are added, the hardness increases and the coefficient of friction decreases, i. e., the wear resistance increases. A very interesting work was reported by Park et al. [66], which use pressure casting for manufacturing magnesium reinforced with CNTs. They put a silicon film onto the CNTs in order to improve the bonding between the matrix and CNTs; since the surface tension of the silicon allows a good interface with CNTs.

- ***Disintegrating melt deposition process (DMD)***

The disintegrating melt process is a relatively new technique for manufacturing metal matrix composites reinforced with CNTs. The technique consists on melting the metal matrix in an oven with controlled atmosphere, then the CNTs are dispersed into the casting by mixing; in the lower part of the crucible, the casting is evacuated by a nozzle, to be finally deposited in an ingot for allowing its solidification, as shown in Figure 1-3. This technique has been used for manufacturing hybrid materials as reported by Paramsothy et al. [56]. They combined both AZ31 and A5083 alloys reinforced with CNTs by DMD technique and finally used the extrusion to enhance the mechanical properties of the composite; however, the

mechanical properties were not changed, except for the ductility that was increased with the CNTs percentage. Other researchers have made similar studies with similar results [55, 67, 68]. Hassan et al. [69], } synthesized a AZ31/1.0CNTs nanocomposite by the DMD technique coupled with hot extrusion process. The nanocomposite had superior strength and ductility. CNTs as a reinforcement allowed to an enhanced softening and increased ductility of the AZ31 alloy within the limit of the high temperature used in the study.

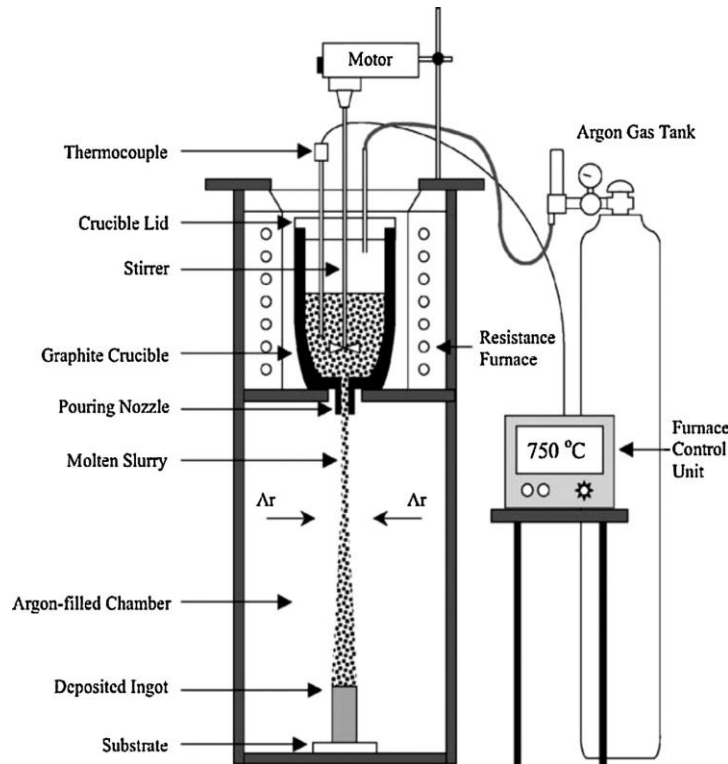


Figure 1-3: Representation of the disintegrated melt deposition process [69].

1.2.3 Electrochemical routes

After powder metallurgy techniques, electrochemical deposition is the second most popular route for manufacturing metal matrix composites. It is primarily used for thin composite coatings. This technique has also been used for coating CNTs with metals for producing different types of nanosensors, electrodes, interconnections and magnetic recorder heads in computer applications. Electrolytic deposition technique uses the catalytic action, which decomposes a material and deposits it on the surface of other material. The deposition mechanisms in electrolytic processes are based on the thermo-chemistry system; in other words, the temperature and pH values play a very important role in the composition and morphology of the manufactured material. The synthesis of composites of aluminum and

magnesium reinforced with CNTs was not found by these techniques, but they are widely used for manufacturing nickel composites. The techniques consist on depositing particles of some material on the CNTs surface by an electric current. The CNTs are deposited between the matrix layer (cathode) and the electrode (anode) and, by galvanic effect, the matrix particles are deposited on the CNTs imperfections. Electrodeposition techniques are widely used for manufacturing composites with nickel and copper matrices to control their electrical and magnetic properties.

1.2.4 Other Novel Techniques

There are other techniques for manufacturing both, aluminum and magnesium matrix composites reinforced with CNTs, which were not mentioned above. These techniques have a high-energy consumption and high costs during their production. Among these techniques are: thermal spraying, which has been well used for coating manufacturing, in which CNTs reinforcement is deposited on the matrix surface [70-72], friction mixing processes which have been widely used for manufacturing aluminum reinforced with CNTs [46, 73, 74]. For magnesium, these techniques have not been reported, probably because the magnesium structure does not allow an easy CNTs incrustation.

Another technique for manufacturing this kind of composites is the sandwich technique, which consists on stacking different layers of materials and finally making compaction and rolling processes. Yu et al. [75] have used this technique for manufacturing aluminum reinforced with CNTs. In their research, they staked aluminum and resin reinforced with CNTs and then all materials were compacted. They found that the fracture toughness improves significantly with the CNTs content. Others works were reported by Isaza Merino et al. [76-78], in which sheets of polyvinyl alcohol reinforced with CNTs (PVA/CNTs) are staked with aluminum or magnesium sheets; finally, they made a hot compaction process. The technique has had very good results in terms of mechanical properties, such as the elastic modulus, yield strength and hardness in areas close to the interface between metals layers, as well as on the hybrid material itself. In the present work, the sandwich technique will be studied in deeper detail.

1.3 Mechanical properties of metal matrix composites reinforced with CNTs

In this section, the models to predict the most relevant mechanical properties will be described, in order to have a theoretical approach of mechanical behavior of metal matrix reinforced with CNTs. In addition, the recent evolution in mechanical properties of aluminum and magnesium reinforced with CNTs will be briefly shown.

1.3.1 Prediction models for mechanical properties

The theoretical prediction of the mechanical properties for composites requires an understanding of the state of stresses and deformations of the materials. The micro-mechanical models predict the composites response from the individual properties of the materials that the composites have. These models evaluate the local stresses state and strains of the phases; which depend on their properties and geometries. Cox et al. [79], proposed the "shear lag" model in which short fibers in a metal matrix are perfectly anchored, i. e., the shear stresses are completely transmitted between reinforcement and matrix, the maximum stress at tension is reached at the fiber longitudinal center, while the shear stress reaches its maximum towards the fiber ends; this occurs because the fibers are aligned in the direction of the applied load as shown schematically in Figure 1-4.

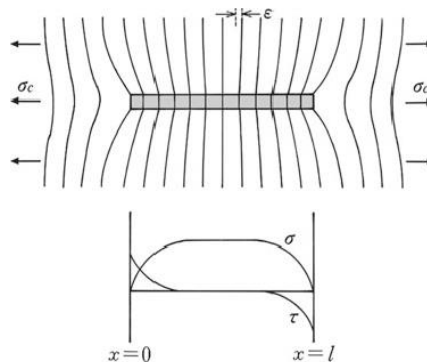


Figure 1-4: Distribution of tensile and shear stresses into a short fiber embedded into a matrix.

Assuming that distribution, composite Young's modulus E_c could be predicted using the law of mixtures (Equation 1-1):

$$E_c = \eta E_f V_f + E_m (1 - V_f) \quad \text{Equation 1-1}$$

where, E_f is the fiber Young's modulus, E_m the matrix Young's modulus, V_f is the fiber volumetric fraction into the composites and η is a load transfer efficiency factor (which is a function of the geometry of the fiber) and is generally 0.20 for nanocomposites, but for composites structures a value of 1 is used, which is defined as the Hooke's law on a fiber cross section. For the composite studied in this research, que factor was calculated using Equation 1-2.

$$\eta = \left[1 - \frac{\tan h(\beta\alpha)}{\beta\alpha} \right] \quad \text{Equation 1-2}$$

where, α is the ratio between the length and diameter (l/d) of the fiber, and β is given by Equation 1-3.

$$\beta = \sqrt{\frac{2E_m}{E_f(1 + V_m)\ln\left(\frac{1}{V_f}\right)}} \quad \text{Equation 1-3}$$

where, V_m is the matrix Poisson relation.

For a good performance of the composite, the matrix must not fail first than the reinforcing material; for this goal be achieved, fiber must have a minimum length. This length was called by Kelly and Macmillan [80] "critical fiber length" and is given by Equation 1-4.

$$\frac{l_c}{d} = \frac{\sigma_{fu}}{2\tau} \quad \text{Equation 1-4}$$

where d is the fiber diameter, τ is the matrix shear yield stress and σ_{fu} is the fiber ultimate stress.

Now the fracture stress of the composites can be redefined from the critical fiber length as shown in the Equation 1-5 and Equation 1-6.

$$\sigma_c = \tau \left(\frac{l}{d} \right) + \sigma_m(1 - V_f) \quad \text{para } l < l_c \quad \text{Equation 1-5}$$

$$\sigma_c = \sigma_{fu}V_f \left(1 - \frac{l_c}{2l} \right) + \sigma_m(1 - V_f) \quad \text{for } l > l_c \quad \text{Equation 1-6}$$

where, σ_m is the matrix stress and l is the fiber length.

Equation 1-6 shows that when the fiber length is infinite, the behavior is similar to a continuous fiber, which is defined by Equation 1-7 (law of mixtures again):

$$\sigma_c = \sigma_{fu} V_f + \sigma_m (1 - V_f) \quad \text{Equation 1-7}$$

Halpin and Tsai [81] developed a semi-empirical model to predict the composite's stiffness with unidirectional fibers; this model also introduces some geometrical aspects of the reinforcement which have important effects on the mechanical properties of the composites. However, these models will not be used in this research due to the orientation degree achieved is not enough for use it, as will be seen later.

Other theoretical models, such as that of Hashin-Shtrikman [82], which is based on the variational principles, provides the upper and lower modulus limit in the composite material.

In manufacturing processes of metal matrix reinforced with CNTs, the phase formation is highly possible due to temperatures involved in the process, , therefore the CNTs can react forming new phases in the interlayers and, in some cases, they can interfere with the stresses transmission between the matrix and CNTs. However, in some cases these phases in the interface help to transmit the stresses between the reinforcement and matrix. Coleman et al.[83], proposed the model of Equation 1-8 to predict the composite strength.

$$\sigma_c = \left(\frac{1+2b}{D} \right) \left[\frac{\sigma_{shear} l}{D} - \left(\frac{1-2b}{D} \right) \sigma_m \right] v_f + \sigma_m \quad \text{Equation 1-8}$$

where σ_{shear} is the shear stress at the interface (which is not easy to measure), σ_m is the maximum stress in the matrix, b is the interface thickness and D is the CNT diameter.

Another model for the strengthening is the resistance increment due to the dislocations in the metallic matrix reinforced with CNTs. As studied by Lahiri et al. [84] the dislocations stacked in close areas between the metallic matrix and CNTs can be modelled using the Taylor relationship [85]. For this model it is necessary to observe and quantify the dislocation density close to the CNTs walls.

1.3.2 Mechanical properties of aluminum and magnesium composites

The main lead force to manufacture these kind of composites is controlling the mechanical properties of the matrix. In order to get good mechanical properties in the composites, an effective stress transference between reinforcement and matrix must be achieved, thus it

is necessary an adequate manufacturing process, good interface between CNTs and matrix; good CNTs dispersion and alignment in the matrix; and the use of the adequate CNTs.

From section 1.2 it can be concluded that with the current manufacture methods the maximum strength and yield strength are increased by the presence of CNTs in the aluminum and magnesium matrices; however, the elastic modulus does not have a notable increase. Nonetheless, after a certain amount of CNTs (close to 2 wt.%), most of the properties starts to decrease. The most relevant mechanical properties reported by recent studies, for both aluminum and magnesium reinforced with CNTs are shown in Table 1-2.

Table 1-2: Mechanical properties in metal matrix composites reinforced with CNTs

Matrix material	CNTs content (wt.%)	Technique	Post-processing	Elastic modulus	Maximum strength	Yield strength	Ductility	Hardness (HV)	Ref.
AA5083 powder	1.5	Mechanical dispersion in powder, Isotactic pressure.	Extrusion	76.0	427	328	4.8	135	[38]
Aluminum powder + Ni particles	0.8	(CNTs in situ growing. Hot compaction and sintering	Cold compaction	--	78	--	--	50	[39]
Al 6061 in powder	2	Mechanical dispersion. Compaction and sintering by different temperatures	--	--	--	--	--	76	[40]
Pure aluminum	2	Mechanical dispersion by 15 h, compaction and sintering	--	--	--	--	--	364	[41]
Al 2009 powder	1	Cold and hot compaction	Friction mixing (4 passes)	--	477	385	8	--	[46]
Pure aluminum powder	1	Powder metallurgy (CNTs embed in PVA)	Extrusion	--	375	300	12	--	[53]
Pure aluminum powder	0.5	Ball milling and spark plasma sintering (CNTs embedded in GBs)	Extrusion	--	206	--	--	58	[52]
Aluminum powder	1	Mechanical mixing, hot extrusion	--	--	298	263	9.1	95	[54]
Aluminum (Al239D, AlSi10Mg)	1	High pressure melt	--	--	250	--	6	--	[12]
Pure aluminum	15	Aluminum infiltrate into CNTs–Mg–Al	--	--	--	--	--	175	[65]
Matrix Material	% of CNTs added	Technique	Pos-processing	Elastic modulus	Maxima strength.	Yield strength	Ductility	Hardness (HV)	Ref.
Pure Mg	4	CNTs in situ grow on Al ₂ O ₃	Extrusion	45	230	181.3	--	65	[42]

Study of the interface - interphase of a Mg-CNT composite made by an alternative sandwich technique

		Compaction and sintering							
Mg AZ31 powder	0.33	Mechanical mixing. Compaction and sintering	--	--	205	140	0.18	--	[86]
Pure Mg	2.4	CNTs in situ grow on Co/Mg compaction and sintering with Mg powder	Extrusion	--	285	130	1.9	--	[43]
Pure Mg (Mg/1.00Al-0.3% CNT)	0.3	Hybrid materials, Al + CNTs and Mg compaction and sintering	Hot extrusion	--	227	160	8.6	60	[44, 45]
Mg AZ91 D	1	Hot compaction	Extrusion	49	388	295	5		[51]
Mg ZK60A in block	1	DMD	Hot extrusion	--	295	180	15	114	[55]
AZ31 and AA 5083	1	DMD	Hot extrusion	--	321	221	12	137	[56]
Mg AZ61 powder	0.74	Spark plasma sintering	Hot extrusion	--	330	230	11	--	[57]
Mg AZ91	1	Melt mixing	--	--	420 (compression)	130 (compression)	24 (compression)	--	[12]
Mg 6% Zn	1	Melt mixing	Solidification control	--	181	100	6.9	--	[64]
AZ91	3	Mg infiltrate in Si-CNTs	--	--	296	253	1.3	160	[66]
Block of AZ31	1	DMD	Hot extrusion	43.5	302	237	16.8	92.8	[67]
Mg AZ81	1.5	DMD	Hot extrusion	--	328	209	13.7	114	[68]
Mg AZ31	1	DMD	Hot extrusion	--	307	190	17.5	--	[87]

1.4 Interfacial behavior between metal matrix (Aluminum and Magnesium) composites and CNTs

The prediction capability of the models presented in section 1.3.1 depends on how the matrix interacts with the reinforcing material. These interactions are influenced among other factors by the wettability of the reinforcement, interface strength and residual stresses. In this section, it will be discussed some concepts such as thermodynamic reactions and anchoring mechanisms at the interfaces between the metal matrix and CNTs.

The stresses transmission in CNTs reinforced composites can occur by these kind of external loads:

If CNTs are in the direction perpendicular to the load, the stress transmission will be through the interface, whereby the mechanical properties will depend on the permissible stresses of the interfacial material (i.e. the shear stress). It is important to mention that, if there is not phase's formation, the anchoring could be through weak attractive forces between CNTs and matrix (this mainly occurs when the matrix metal is reinforced with single-walled CNT).

If CNTs are aligned in the loading direction, the stresses transfer can occur through two mechanisms. The first is at the CNTs ends and the second is in the CNTs surfaces. In these kinds of mechanisms, the composite stresses are transmitted by interface shear stress. The properties prediction by this mechanism was already shown in Equation 1-8, which takes into account the phase formation in the interface between CNTs and metal matrix.

The interactions between CNTs and metal matrix can be given by interactions at the ends (two faces) and superficial longitudinal (one face) zones of the CNTs. At the ends zone, sigma-like links to the matrix by coherent interface formation can be developed. In superficial longitudinal face, the bonds can also be coherent or may be weaker. It is necessary the presence of some defects to promote the interfaces formation, which finally will allow for a good transfer of stresses.

Other important aspect for the stresses transferring between CNTs and matrix is the wettability, which is the interaction of the surface energies; this parameter is represented by the Young's equation (Equation 1-9 and Equation 1-10):

$$\cos \theta = \frac{\gamma_{sv} - \gamma_{ls}}{\gamma_{lv}} \quad \text{Equation 1-9}$$

$$W_A = \gamma_{lv}(1 + \cos\theta) \quad \text{Equation 1-10}$$

where θ is the contact angle, γ_{sv} , γ_{ls} and γ_{lv} are the surface energies of solid - vapor, liquid - solid and liquid - vapor, respectively. Finally, W_A is the adhesion work between the liquid and the substrate. For a good wettability between the liquid matrix and CNTs, a low liquid - vapor angle is required. On the other hand, to achieve a good wettability and anchoring, silicon particles have been deposited [88] onto the CNTs surface.

1.4.1 Other interactions between CNTs and metal matrix

Surface roughness of the reinforcement has a very important role; it can allow the mechanical transfer of the loads through a “hook” effect; moreover, it can modify the wettability of the surface.

Other important aspect to consider is the chemical or physical functionalization, a properly designed allows good CNTs anchoring in the matrix. In that way, a good interface allows an adequate stresses transfer to improve the mechanical properties. The chemical functionalization is based on the covalent bonding between functional carbons in the CNTs surface or CNTs ends. The functionalization is associated with a change in hybridization of the sp^2 orbitals to sp^3 and a simultaneous loss of π -conjugations of the graphene layers [89]. A study conducted in 2012 [90], shows amino-functionalization as a way to generate strong bonds between CNTs and aluminum matrix. Currently it is possible to buy functionalized CNTs in considerable amounts and cheap prices.

1.5 Protective coatings for metal matrix composites (additional work)

The main disadvantages of magnesium (Mg) alloys and their composites are their low wear and corrosion resistances [91, 92], These disadvantages are in part due to the high magnesium electrochemical activity. To overcome these weaknesses, a broad range of coating systems have been developed [93, 94] including ceramic, polymer and composite

protective layers. In an additional work, the conversion coating method was used [95] to transform the composite surface into an oxide layer by means of an electrochemical process. In this process, the oxide layer grows, at the same time, inwards and outwards of the original metal surface, therefore the geometry of the component changes. Conversion coatings arise in a complex interaction of metal dissolution and precipitation, usually during treatments in aqueous solutions. The chemical conversion layers are obtained by immersion of substrates in a bath solution producing, in the case of magnesium alloys and composites, a coating comprised besides magnesium oxide and magnesium hydroxide, of mixtures of other metal oxides and hydroxides, which arise from the dissolved ions in the bath. As conversion coatings are grown in situ, their adhesion to the substrate is generally very good. Plasma electrolytic oxidation (PEO) is a special technique which works with high voltages at the breakdown potential [96]. The first studies for protecting Mg alloys by PEO coatings showed a lower corrosion current density than uncoated samples, additionally, immersion and wear tests have been done for showing the behavior of the PEO-treated sample surfaces, which contain magnesium/aluminum oxide, magnesium silicate and magnesium/aluminum silicates [94, 97, 98]. Some authors have demonstrated the effects of voltage on the morphology of the PEO layer [99]. The increasing in voltage led to an increase in the layer thickness of the PEO coating, but some pores in the morphology were found, which decreased the corrosion resistance and modified the cell growing onto the surface.

2. Experimental procedure

This chapter focuses on the processing details for the synthesis of the magnesium reinforced with MWCNTs by the sandwich technique. Characterization techniques and equipment used for studying the microstructure and mechanical properties of the raw and composite materials are described.

2.1 Materials used in this study

2.1.1 Metal matrix

An annealed and cold rolled AZ31B magnesium alloy was used in this study. The nominal chemical composition is shown in Table 2-1. The aluminum content is an important element due to its affinity with carbon, which promotes the formation of aluminum-carbide phases, as will be discussed later.

Table 2-1: Nominal chemical composition (wt.%) of the AZ31B magnesium alloy.

Mg	Al	Zn	Mn	Si	Cu	Ca	Fe	Ni
Balance	2.9	0.62	>0.2	<0.10	<0.05	<0.04	<0.005	<0.005

The magnesium sheets were annealed at 350°C and then were hot rolled at 250°C until obtaining a thickness about 150 µm was obtained; both processes were performed in environmental atmosphere, which allowed having a more homogeneous composite after the hot compaction. The rolling process changed the microstructural morphology, as shown in Figure 2-1; particularly the grain size is changed during the process. The raw material microstructure evidences different grain size and some twins (Figure 2-1a), after the annealing process, the grain grows and twins disappear (Figure 2-1b). Finally, the grain size decreases after the hot rolling process, while twins formation is not clearly seen (Figure

2-1c). Same experiments were carried out with aluminum as a matrix for synthesizing aluminum reinforced with MWCNTs; these results were reported by Isaza-Merino et al. [78].

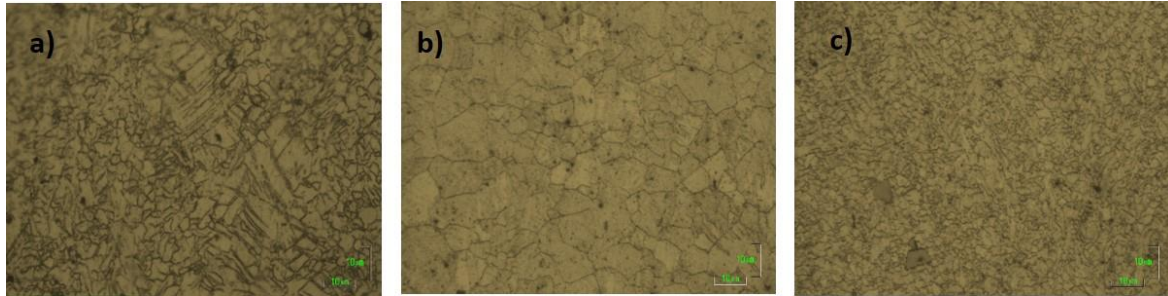


Figure 2-1: Micro-structural changes after recrystallization and deformation process. a) raw material, b) annealed material and c) hot rolled material.

2.1.2 Carbon nanotubes

MWCNTs were supplied by Nanostructured & Amorphous Materials Inc. They have outer diameters of 10-40 nm and inner diameters of 10 - 20 nm as shown in Figure 2-2, with a length of 30-50 μm . Details will be described in the results chapter.

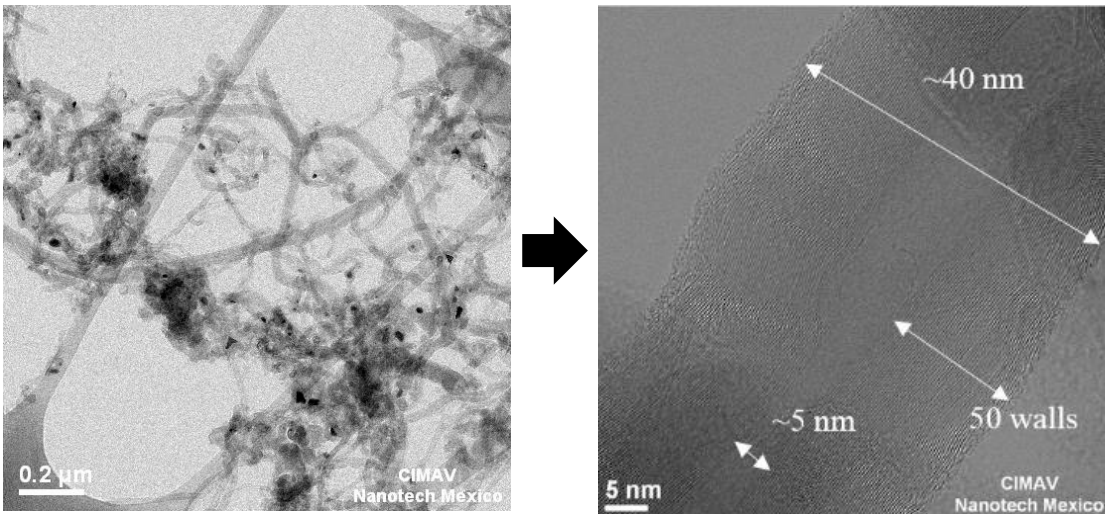


Figure 2-2: TEM image of the MWCNTs used in this study.

2.1.3 Polyvinyl Alcohol

Polyvinyl alcohol (PVA) was supplied by Sigma Aldrich with a molecular weight of 85,000-124,000 and 87-89% hydrolyzed. Table 2-2 shows the polyvinyl alcohol specifications. The PVA reinforced with MWCNTs (PVA/MWCNTs) was successfully characterized by different

techniques and used as a vehicle for dispersing and aligning the MWCNTs onto metal matrix composites as will be described later.

Table 2-2: Sigma Aldrich material specifications (<http://www.sigmaaldrich.com>).

Prod. number	Appearance (Form)	Assay % Hydrolyzed	Loss on Drying	Residue on ignition (Ash)	Viscosity C=4%, H ₂ O	pH C=4%, H ₂ O
363081	Powder	87.0- 89.0 %	≤ 5%	≤ 5%	23.0- 27.0 cps	4.5- 6.5

2.2 Experimental procedure

The project was carried out in the three stages shown in Figure 2-3: The steps I and II focused on the experimentation for the composites manufacturing such as polymer and magnesium matrix composites, while the step III on the characterization and understanding of the mechanical and microstructural behavior in the composites. For this, different characterization techniques were used, as will be described below. The mechanical tests at macro, micro and nano levels were used to show the changes in the mechanical properties of the composites at different scales. In the next sections, detail of this techniques and material synthesis will be described.

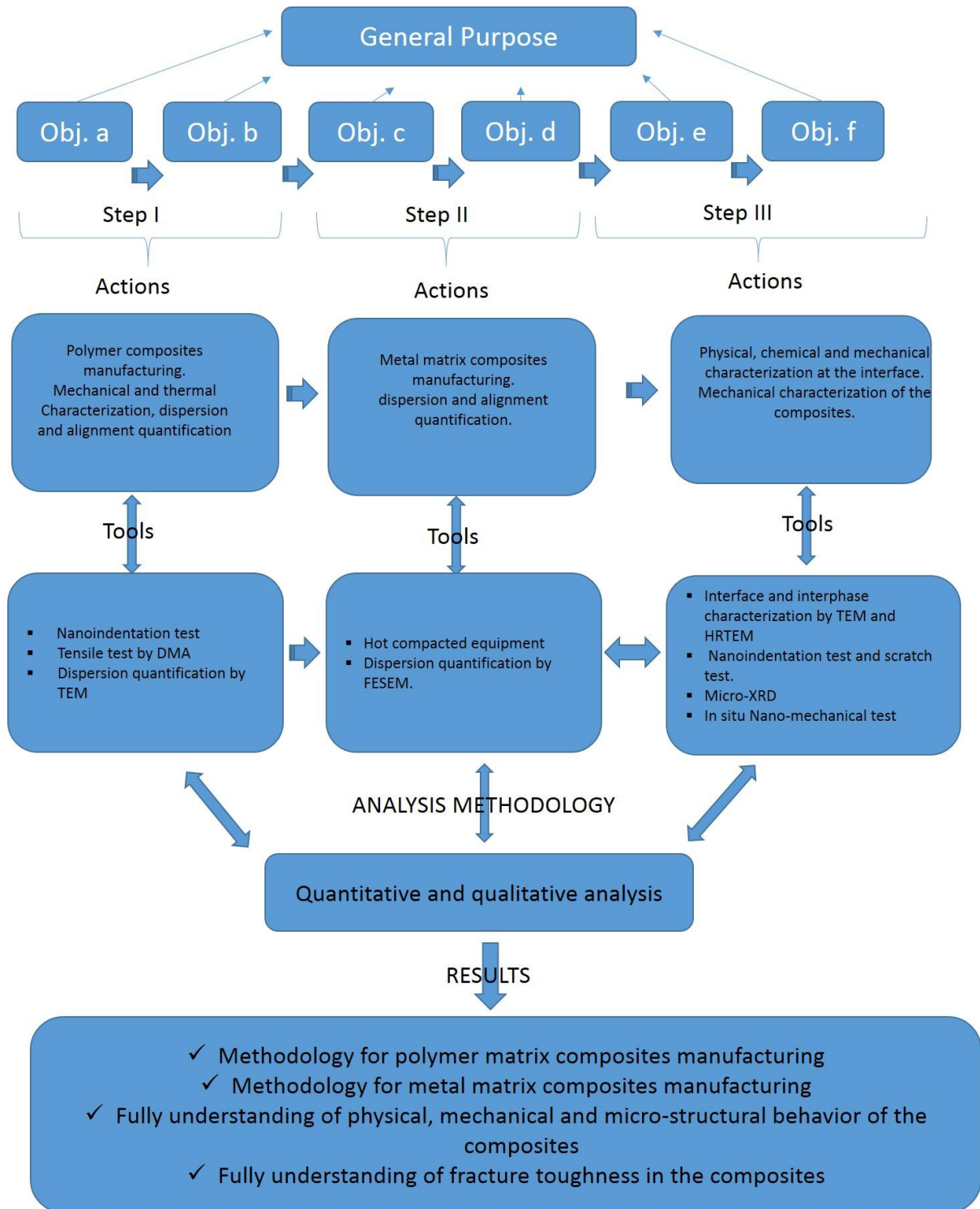


Figure 2-3: Methodology used in this research

2.3 Metal matrix composites synthesis

Metal matrix composite manufacturing was done in two steps; the first step was the MWCNTs pre-dispersion and pre-alignment in the polymeric matrix (PVA). The second step was the manufacture of the metal matrix composites by the sandwich technique.

2.3.1 Polymer matrix composites synthesis

For the synthesis of the polymer matrix composite, pellets of fully hydrolyzed PVA were diluted in hot distilled water to produce a solution of 4 wt.% of PVA. MWCNTs were introduced into the PVA solution in percentages of 0.25, 0.5 and 1.0 wt.%, where they were dispersed by magnetic stirring during 1 h at an average speed of 600 - 900 rpm followed by a sonication in a Vibra Cell series CLC equipment, which was set to a power of 100 W and an amplitude of the probe of 20%; the dispersion maximum energy was 60 - 70 kJ in order to prevent the damage of the CNTs [100, 101]. The polymer solution was poured into Petri acrylic dishes and dried during 24 h at 37°C for allowing the polymer to cure. From this composite, strips of 150 mm x 20 mm with average thickness around 200 μm were stretched using a Monsanto tensile machine at a speed of 1-2 mm/min and at a temperature of 60°C. In this way samples with thicknesses ranging from 100 to 200 μm of polymer reinforced with 0.25, 0.5 and 1.0 wt.% were obtained. The diagram of synthesis of polymer matrix composites reinforced with MWCNTs is shown in Figure 2-4.

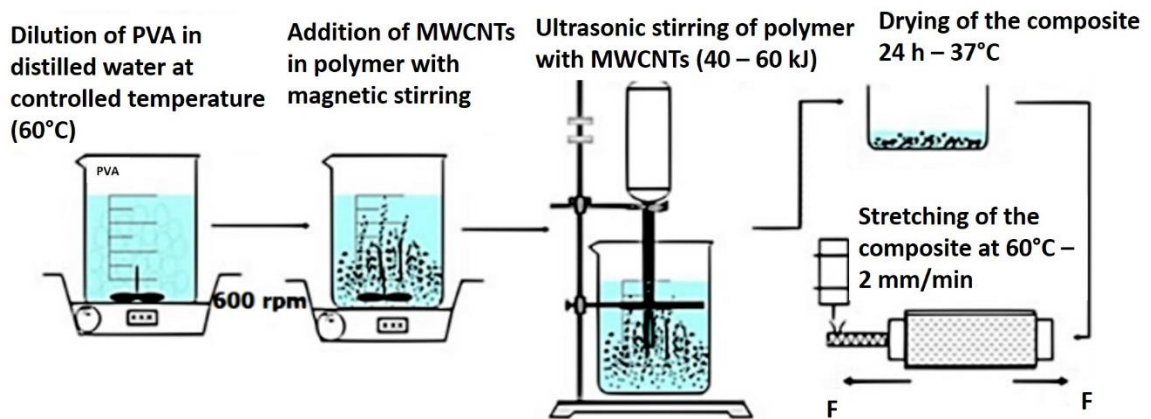


Figure 2-4: Synthesis of polymer matrix composites reinforced with MWCNTs.

2.3.2 Metal matrix composites synthesis

Figure 2-5 shows schematically the synthesis route of Mg-PVA/MWCNTs composites: Two composite sheets of PVA/MWCNTs were alternately stacked with three magnesium sheets. Finally, the stacking was hot compacted in a die using an argon atmosphere to prevent the MWCNTs oxidation during the process. Thermo-gravimetric analysis, performed in a previous work [102], showed that when an argon atmosphere is used the minimum temperature to totally evaporate the PVA and to leave the CNTs is about 500°C. However, both PVA evaporation rate and magnesium diffusion rate depend on time and temperature, which is why in this work the processing temperature was set near the magnesium melting point, in order to increase both rates. Thereby, the temperature was gradually raised during 1.5 h until 580°C were reached; the pressure was also gradually raised up to 40 MPa. This was followed by a holding period of 1.5 h for allowing the PVA to evaporate and the magnesium to diffuse between the sheets, and then the composites were annealed during 30 min and hot rolled at 350°C. The final thickness of the composite was approximately 300-400 µm, the reinforced zones located between the sheets of magnesium named “study zones” in Figure 2-6, were subjected to a close inspection in this research.

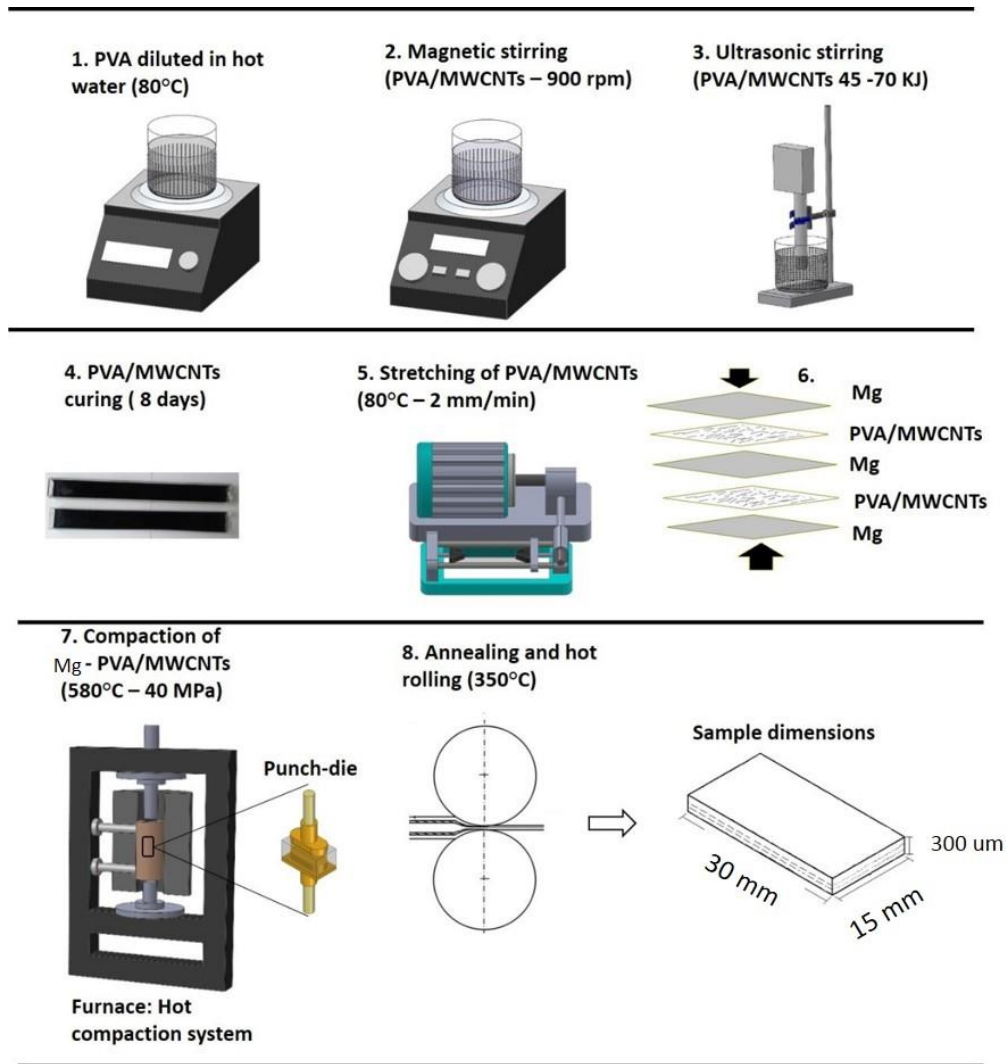


Figure 2-5: Synthesis route diagram of the Mg-PVA/MWCNTs composites.

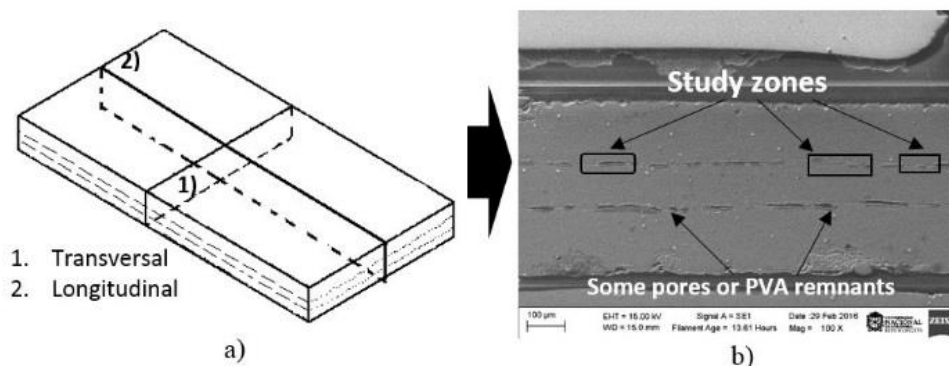


Figure 2-6: a) Outlines the composite sections studied and b) transversal study zone close to the interface (SEM-SE image).

2.3.3 PEO coating synthesis on composites surfaces (additional work)

For the PEO process, samples of 1 cm² were cut from the composites describe above. A surface conditioning was made as follows: surfaces were progressively polished using SiC emery papers up to 1200 grit size, then cleaned in an ultrasonic bath during 3 min using acetone and finally dried in hot air stream. Then, the samples were put in an electrolytic solution of 8.0 g/L of Na₂SiO₃·5H₂O and 1.5 g/L of KOH in distilled water. An electric circuit consisting of sample, electrolyte and a stainless steel foil as counter electrode was powered by a regulated DC power supply PAS 1000 W type; a current density of 100 μA/cm² in the sample was used.

2.4 Dispersion and alignment quantification for both, polymer and metal matrix composites

Both the dispersion and alignment quantification were done using the same methodology. In polymer composites, the samples were sectioned parallel to the stretching direction by a RMC Boeckeler PT-PC Power Tome ultramicrotome using a diamond knife; films of about 200 nm in thickness were obtained. One sample for each reinforcement percentage was used for transmission electron microscopy (TEM) characterization in scanning mode. For metal matrix composites, the samples were cut in cross and longitudinal sections and metallographically polished to be characterized by scanning electron microscopy (SEM); section 2.5 will provide more details of the equipments and techniques used for this characterization. Representative images of 1 by 1 μm were divided into 10x10 grid lines along the horizontal and vertical directions, as shown in Figure 2-7. Then the spacing, both horizontal and vertical, between nearest MWCNTs was measured at each grid intersection using a free software Gwyddion [103]. These images were also used to quantify the alignment degree of the reinforcement and the angle of each CNT with respect to the stretching direction was measured. These data were analyzed using the statistical distribution model [104] showed in Equation 2-1.

$$f(x) = \frac{1}{xn\sqrt{2\pi}} \exp \left[-\frac{1}{2} \left(\frac{\ln x - m}{n} \right)^2 \right], \text{ for } x > 0, \quad \text{Equation 2-1}$$

and

$$f(x) = 0, \text{ for } x \leq 0,$$

where $m = \ln \frac{u^2}{\sqrt{u^2 + \sigma^2}}$ and $n = \sqrt{\ln \frac{u^2 + \sigma^2}{u^2}}$, x is the free-path distance, u is the mean and σ is the standard deviation for the free-path distance measured.

A dispersion parameter, $D_{0.1}$, defined as the probability of the free-path distance distribution, was set in the range of $0.9u - 1.1u$. The distance distribution usually obeys a lognormal distribution model, in which $D_{0.1}$ is formularized as in Equation 2-2.

$$D_{0.1} = 1.1539 * 10^{-2} + 7.5933 * 10^{-2} * \left(\frac{u}{\sigma}\right) + 6.6838 * 10^{-4} * \left(\frac{u}{\sigma}\right)^2 - 1.9169 * 10^{-4} * \left(\frac{u}{\sigma}\right)^3 + 3.9201 * 10^{-6} * \left(\frac{u}{\sigma}\right)^4$$

Equation 2-2

Since in this method $D_{0.1}$ is deduced from the free-path distance distribution, a higher $D_{0.1}$ value indicates more spacing data close to the mean u . A dispersion of 100% means that all of the reinforcements are equally spaced; i.e., different percentages of addition of MWCNTs can have the same values of the $D_{0.1}$ parameter. Moreover, $D_{0.1}$ measures the amount of reinforcements that is at the same distance, regardless of its value. In reality any value of $D_{0.1}$, $D_{0.2}$, $D_{0.3}$, etc. can be chosen, in order to describe the dispersion of the CNTs. The bigger the range the bigger the value of D , i.e there is more probability to find more data in the range, in fact as it was stated before, $D_{1.0} = 100\%$. In consequence, low range values give information about the quantity of CNTs which are equally spaced at a value near to the mean value (well dispersed), high range values give no information about dispersion. This is the reason why we choose 0.1 as the range value. Either way values of 0.2 are also used by other authors [104]. The same analysis was done for the alignment quantification of the MWCNTs into the composites and the statistical distribution model described above was used. In this quantification, the angle between MWCNTs and the stretching direction was measured in three representative TEM images for each composite.

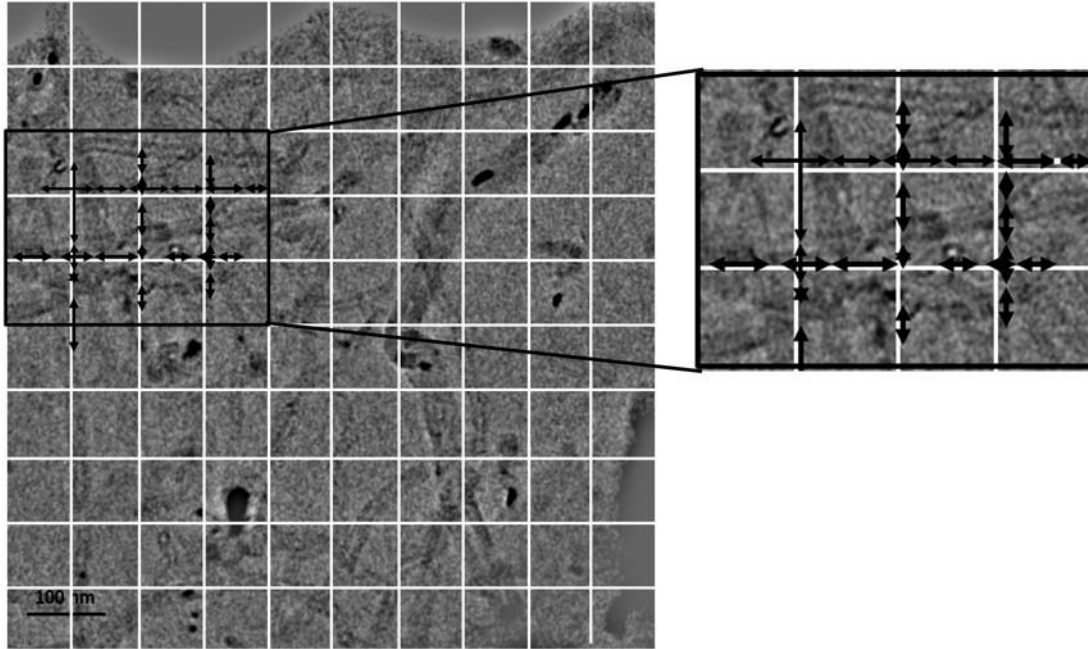


Figure 2-7: Representatives images divided into 10x10 grid lines for quantification.

2.5 Micro-structural characterization

For the microstructural characterization, different techniques were used to study the interaction between the metal matrix and MWCNTs. These interactions and behavior were characterized by different microscopy techniques, such as optical microscopy (MO), scanning electron microscopy (SEM), transmission electron microscopy (TEM), high-resolution transmission electron microscopy (HRTEM) and scanning transmission electron microscopy (STEM). Other techniques such as X-ray diffraction (XRD) and TEM diffraction patterns were used for the phases and interface study between the metal matrix and MWCNTs.

Techniques such as energy dispersion spectroscopy (EDS) and electron energy loss spectroscopy (EELS) were used to identify the chemical elements in the composite, as well as to identify the chemical interaction between the metal matrix and MWCNTs. Atomic force microscopy (AFM) in pin point mode was used to study the morphology and to qualitatively identify the elastic modulus changes along the interfaces in the composite. A brief description of all these techniques is provided below.

Optical Microscopy (OM). Samples of the MMCs were cut perpendicularly and longitudinally to the longitudinal axis and then were progressively polished using SiC emery papers and a finishing cloth loaded with 1 μm diamond paste. Finally, the samples were etched with a mixture of picric acid, acetic acid and water to reveal their microstructure. The microstructure was characterized by an optical microscope Nikon LV100 series coupled to a Nikon digital camera.

Scanning electron microscopy. The same sample preparation used for OM was used for the SEM characterization; a FESEM JEOL JSM-7100F microscope was used for this purpose.

Transmission electron microscopy (TEM and HRTEM). For the polymer characterization by TEM, the samples were sectioned parallel to the stretching direction by a RMC Boeckeler PT-PC Power Tome ultramicrotome using a diamond knife; films of about 200 nm in thickness were obtained. For the metal matrix composites, transversal sections of the composites were prepared by a focused ion beam system (JEOL JEM 9320FIB). High-resolution transmission electron microscope (HRTEM) JEOL JEM2200FS and JEOL 2010 field emission transmission electron microscope were used as tools for image, structural and chemical analysis. The JEOL 2010 TEM has a high-resolution pole piece, with a resolution of 1.9 \AA . The images of the composites and the interface between the metal matrix and MWCNTs were obtained using diffraction contrast (BF and DF) and phase contrast (HRTEM). For the characterization by TEM diffraction, the selected area electron diffraction mode was used.

For atomic resolution images at the interface between the metal matrix and MWCNTs, a JEOL ARM 200 Atomic Resolution Microscope with aberration-corrected probe and a spatial resolution of 0.78 \AA (STEM mode) and 1.2 \AA (TEM mode) was used. Spatially-resolved elemental analysis by X-ray energy dispersive spectrometry and localized electronic structure measurements by EELS were used to identify the chemical elements in the composite and to identify the chemical interaction between the metal matrix and MWCNTs.

X-Ray Diffraction (XRD). A multi-purpose vertical X'Pert Pro MPD diffractometer (θ - θ) with Cu K α radiation and a high-resolution goniometer with a step size 0.0001 $^\circ$ and 2 θ linearity

$\pm 0.01^\circ$ over the whole angular range was used. The diffractometer is equipped with two detectors: a standard proportional detector and a PIXcel3D detector.

2.6 Mechanical properties characterization

Different techniques were used for the mechanical characterization. Tension test under conventional testing and dynamical mechanical analysis (DMA) were used to measure the tensile mechanical properties of MMCs and PMCs (polymeric matrix composites), respectively.

Nanoindentation and nanoscratch techniques were used for identify the mechanical properties such as elastic modulus, hardness, coefficient of friction and adhesion of PEO coatings deposited onto the MMMCs. These tests were carried out in the study zone showed in Figure 2-6. All these test are detailed below:

In-situ nanoflexion tests in a TEM equipped with an AFM probe were made to measure crack propagation along the “study zone” and to measure K1c, details of these test will be provided in section 2.6.2.

2.6.1 Ex situ mechanical characterization

Tensile tests. Tensile tests were carried out in accordance with the ASTM E8M standard, in order to guarantee a plane stress state. Five samples were used for each metal matrix composite studied. Dog-bone type samples were cut along the longitudinal direction (parallel to the CNTs alignment direction) by using a controlled water jet machine; their dimensions were: 23 mm in gage length, 10 mm in width and 300–400 μm in thickness. The tests were carried out using an AG Shimadzu model GX testing machine at a constant crosshead speed of 0.5 mm/min.

Dynamic Mechanical Analysis (DMA). In order to investigate the effect of the reinforcement alignment direction in the PVA/MWCNTs composites, DMA tests were performed. Strips of 4 mm x 3 mm with thicknesses of 200 - 400 μm were cut for both stretching (longitudinal) direction and perpendicular (transverse) direction. A RSA3 TA *instruments* equipment in tensile mode using a clamp speed of 0.005 mm/s was used for these tests which were performed at room temperature.

Nanoindentation tests. The nanoindentation tests were performed in an IBIS Authority Fischer-Cripps nanoindenter with a diamond Berkovich indenter tip. For the metal matrix composites, a peak load of 1 mN was held during 5 s to reduce the creep effects during the final unloading step. The data were acquired in open loop mode in order to produce quick tests and minimize the thermal creep effects. Loading-unloading cycles last 20 s. A matrix of 10×10 indentations was set, being the lines parallel to the interface. The distance between the indentations was 3 μm . The hardness and elastic modulus were calculated by the Oliver and Pharr method; average values were reported.

The elastic modulus and hardness of the PMCs, were also measured using nanoindentations, twenty indentations were made and averaged for each sample. The maximum indentation load was 100 mN with a loading and unloading rate of 1 mN/min.

The scratch test performed on the study zone was made following the next parameters: constant load of 10 mN, displacement speed of 10 $\mu\text{m/s}$, travel distance of 150 μm , spherical diamond tip of 10 μm . Five scratches were performed for each sample. All tests were carried out at 23°C. Tracks observation was performed under an optical microscope Nikon LV 100 series.

2.6.2 In situ testing characterization: Fracture toughness

For in situ testing characterization, a focused ion beam (FIB Carl Zeiss, Germany) was used to obtain micro-cantilever beams of all composites studied. The cantilever beams with a nominal beam length of 3.2 μm , a width of 900 nm and a thickness of 200 nm were milled with a high current Ga⁺-ion beam (30 keV, 7 nA, 700 and 300 pA), followed by fine milling at low currents (30 keV, 50 pA), the cantilevers were notched using the same FIB conditions (30 keV, 50 pA), at a distance of 800 nm away from the cantilever beam support. The samples were extracted from the study zone in the cross section showed in Figure 2-6. The cantilever was extracted from the homogenous zones in the interface between magnesium layers. The homogenous zone is an isotropic material, as was corroborated by EDS analysis presented in the results section.

Figure 2-8 shows a zone where a samples for is situ testing were extracted and shows the geometry of the cantilever used for this type of test. For in situ testing, a Nanofactory Instruments nano-force AFM sensors intended for in situ TEM measurement was used.

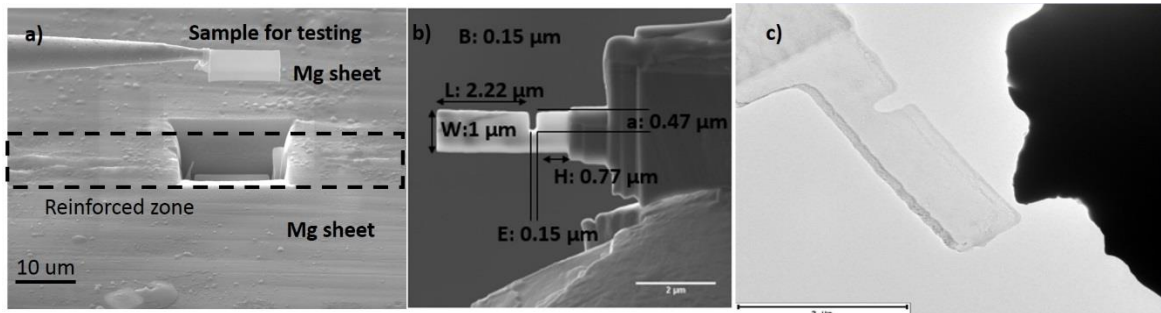


Figure 2-8: a) Sample extraction in the reinforced zone, b) cantilever bend geometry for the in situ test and c) images before in the situ test.

The nano-force sensor is a micromechanical device consisting of a thin (2-4 μm) cantilever and a piezoresistive element to measure the forces applied to the cantilever; the resolution for load and displacement are 1 nN and 1 nm, respectively. The sensor is wire bonded or soldered to a Printed Circuit Board, PCB, to form a Mechanical Part Assembly (MPA) that is mounted in the Nanofactory Instrument TEM holder. The sensor can be used for in situ TEM measurements to give mechanical (and electrical) read-out in combination with the imaging possibilities of TEM. When the cantilever is deflected, the piezo resistive material in the cantilever (doped 1-0-0 Si) changes its resistance. The resistor of the piezo resistive cantilever is part of a Whetstone-bridge and the change of resistance is registered as a change in voltage read-out of the bridge. Finally, the voltage read-out is correlated to the cantilever deflection distance and translated to a force from the cantilever spring constant (the k-value) and the electrical conversion factor (the C-value) and values for these constants were verified before testing. Figure 2-9 shows schematic and SEM images for the sensor tip.

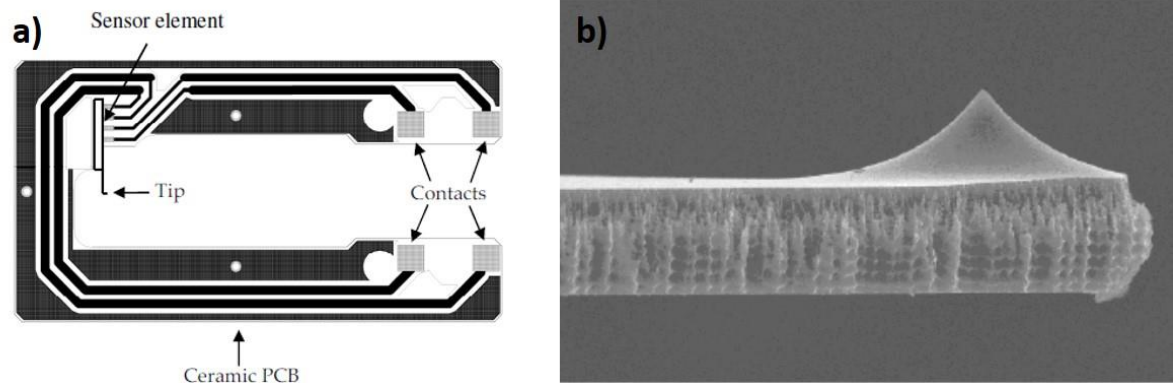


Figure 2-9: (a) Schematic AFM sensor and (b) SEM image of the sensor tip.

In order to investigate and understanding the relationship between microscale fracture toughness and bulk composite materials, in situ micro-cantilever tests on notched metal matrix composites were carried out. The macroscopic fracture toughness K_{IC} was measured using the ASTM 399-90 standard.

For testing, the cantilevers were notched using an even finer milling current (30 keV, 50 pA), at a distance of 1 μm away from the cantilever beam support. The depths of the pre-notches were measured prior to the fracture from the side view; in some cases, notches were measured after fracture as well as when the cantilever was completely fractured apart. As a consequence of the FIB-milling from the side, the crack tip was slightly rounded and not quite sharp. This might possibly lead to an overestimation of the fracture toughness. Additionally, in a conventional fracture toughness test a pre-crack is done, however in this research the pre-crack was not made. For these reasons, results are analyzed qualitatively for identifying the changes between the metal matrix composites fabricated.

The fracture toughness K_{IC} was calculated using Equation 2-3.

$$K_{IC} = \frac{F_{max}L}{BW^{\frac{3}{2}}} F\left(\frac{a}{W}\right) \quad \text{Equation 2-3}$$

where F_{max} is the fracture force and $F(a/W)$ is a dimensionless geometry factor of the tested specimens [105]. The loading span L is the distance between the notch and the loading point, a is the crack length including the pre-notch length and the initial crack length (at propagation), W is the cantilever width and B is the thickness of sample. The geometry factor $F(a/W)$ may be used for a/w -ratios between 0.05 and 0.55, according to Equation 2-4.

$$F\left(\frac{a}{W}\right) = 4 \frac{3\left(\frac{a}{W}\right)^{0.5} \left[1.23 - \left(\frac{a}{W}\right) \left(1 - \left(\frac{a}{W}\right) \right) \left(-6.09 + 13.96 \left(\frac{a}{W}\right) - 14.05 \left(\frac{a}{W}\right)^2 \right) \right]}{2 \left(1 + 2 \left(\frac{a}{W}\right) \right) \left(1 - \left(\frac{a}{W}\right) \right)^{1.5}}$$
Equation 2-4

The testing was carried out in a nanofactory holder JEOL TEM at a constant speed. Only one sample was used for each composite due to testing costs.

For crack growth analysis, conventional bright field (BF) and dark field (DF) images were recorded. Initial motion of the nanofactory holder resulted in the sequence: elastic loading and plastic loading. In the elastic regime, the stress flow was observed to occur concurrently with the application of load. This allows a stress concentration in the notch and finally, allows crack growth. In the experiments conducted in this study, plastic deformation always occurred preferentially at the tip of pre-existing cracks, which were probably introduced during the foil preparation. The presence of these cracks greatly aided the study providing valuable insight as to where to look for microstructural changes, i.e. how the crack can move across the composites and identify its path. The cracks were loaded in a predominately mode-I configuration for fracture toughness, as was shown in Figure 2-8b.

2.6.3 Corrosion characterization of the composites (additional work)

For corrosion characterization of PEO - coated composites, electrochemical impedance spectroscopy (EIS) with a GAMRY Interface 1000TM was employed to characterize the electrochemical behavior of the coated systems. A solution of 3.5 wt.% of NaCl in distilled water was used as the immersion solution, which allows to have a corrosive environment, the test was carried out at 25°C.

The electrolytic assembly setup consists of a vertical cylindrical shaped flat glass cell. A working electrode of 1 cm² at the bottom of the cell acts as an electrolyte medium exposure. A frequency between 100.000 and 0.01 Hz with an amplitude of ± 20 mV and stabilized time of 20 min and seven points logged per decade were held during the test. An Ag/AgCl reference electrode and a graphene bar like contra-electrode were used.

2.7 Experimental analysis

To perform an adequate statistical analysis it was determined to use a simple comparison method between the MWCNTs percentages added to the magnesium matrix. To represent the results obtained, a box diagram was used for each case, which describes the most important characteristics such as dispersion and symmetry. The three quartiles (Q1, Q2 or median, Q3) and the minimum and maximum values (Li, Ls) of the data are represented on a rectangle, aligned horizontally or vertically, as shown in Figure 2-10.

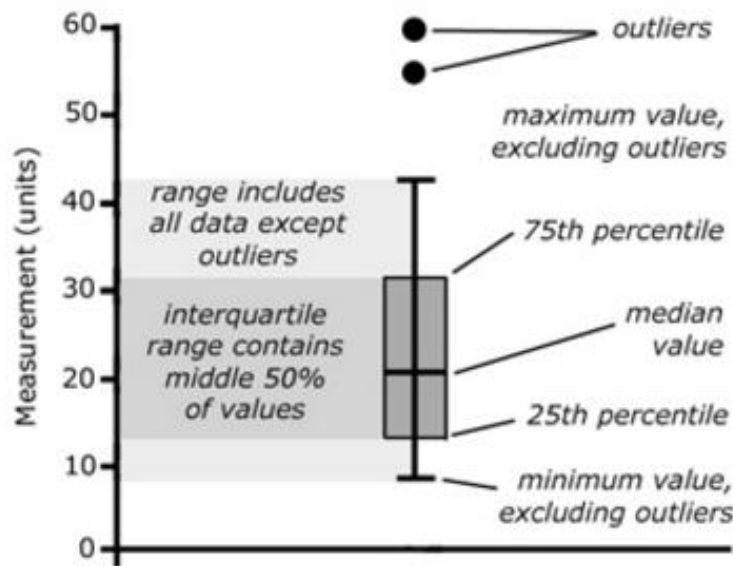


Figure 2-10: Box plot and whiskers representation.

For the statistical analysis, the simple comparison method was used in which the corresponding hypotheses are proposed that are finally rejected or accepted depending on the results obtained. For this, a hypothesis was proposed: H_0 is $\mu_1 = \mu_2$ and H_A is $\mu_1 < \mu_2$ and since the value of the variance is unknown and due to the presentation of the data it is reasonable to assume that the variance σ_1^2 and σ_2^2 are not equal. Thus, the test statistic and the rejection criterion are known as shown in Equation 2-5 and Equation 2-6.

$$t_0 = \frac{\bar{y}_1 - \bar{y}_2}{\sqrt{\frac{s_1^2}{n_1} + \frac{s_2^2}{n_2}}} \quad t_0 < -t_{\alpha, \nu} \quad \text{Equation 2-5}$$

To calculate the mean and the sample variance we use:

$$\bar{y} = \frac{1}{n} \sum_{i=1}^n y_i \qquad s^2 = \frac{1}{n-1} \sum_{i=1}^n (y_i - \bar{y})^2, \qquad \text{Equation 2-6}$$

The conclusions of the analysis are shown at the end of chapter 3 (Results and discussion).

3. Results and discussions

In this chapter, the results obtained during the research will be shown and discussed.

3.1 Multi-walled carbon nanotubes characterization

The characteristics of MWCNTs such as morphology and diameter are essential for their dispersion into the matrix. MWCNTs with a very large diameter have a small tendency to re-agglomerate after a dispersion process [106]. Contrarily, a larger aspect ratio promotes the carbon nanotubes tendency to agglomerate due to their large surface energy [107], allowing the formation of clusters which in the composite causes an inefficient load transfer from the matrix to the reinforcement.

Figure 3-1 and Figure 3-2 respectively show FESEM and HRTEM images of the as-received MWCNTs, as well as their outer and inner diameter distribution. Outer diameters of 10-40 nm and inner diameters of 10-20 nm were found.

The defects showed in Figure 3-2b include variable numbers of carbon layers and partial interior filling, amorphous carbon and “bamboo” defects, which consist of several transverse, internal walls segmenting the interior of a MWCNT into independent pods or isolated volumes. Bamboo defects are often quasi-periodic in a MWCNT [108]. Some nickel impurities were also seen.

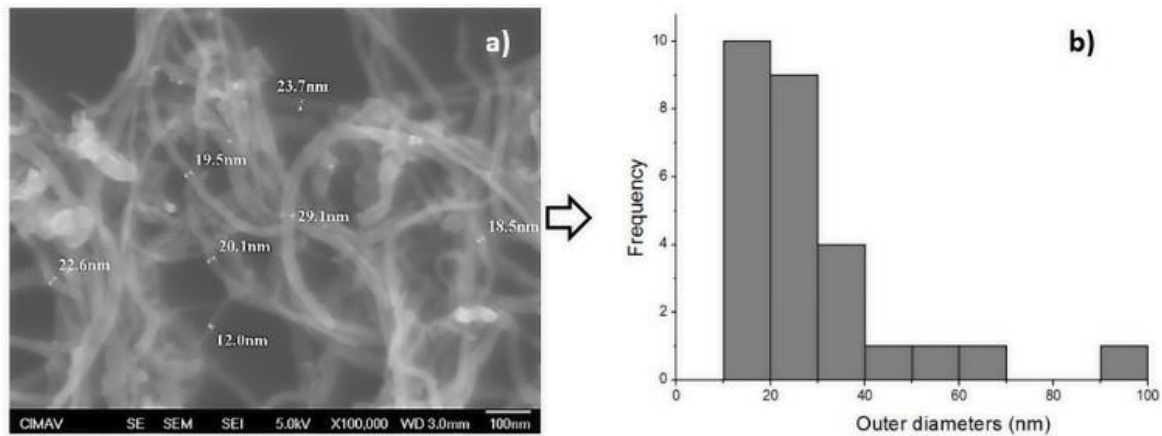


Figure 3-1: (a) FESEM images of MWCNTs and (b) outer diameter distribution.

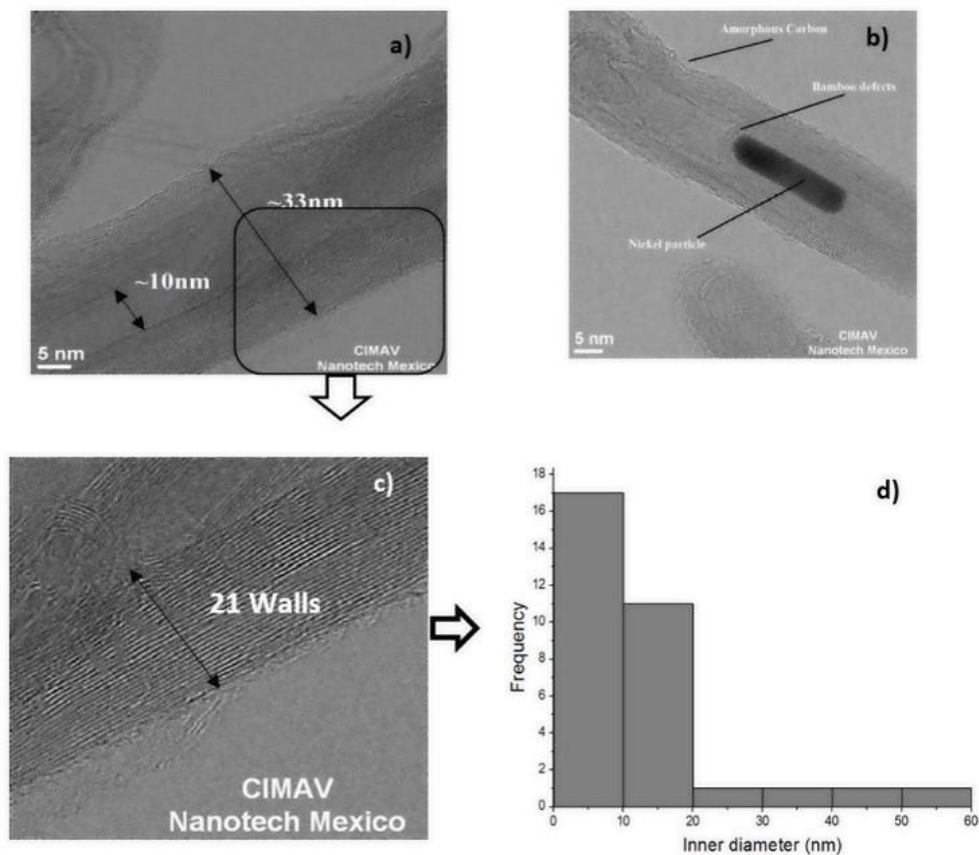


Figure 3-2: (a to c) HRTEM images of MWCNTs and (d) inner diameter distribution.

In Figure 3-2c, the presence of 21 walls in a MWCNT was observed. Although inner diameters of the MWCNTs have no direct influence on the dispersion of the CNTs in a material, outer diameters of the MWCNTs used in this work are small, which could increase

the risk of re-agglomeration. However, the use of the PVA solution allowed having a very good dispersion of MWCNTs, as well as to increase the MWCNTs percentage in the polymeric matrix as will be seen in section 3.2. The dispersing effect of the polymer was maintained even after the polymerization and curing steps, whereby the CNTs re-agglomeration was avoided, as reported by Olayo et al. [109].

3.2 Dispersion and alignment quantification in polymer matrix composites

After polymer matrix composites manufacturing (section 2.3.1), the dispersion and alignment was studied using a statistical distribution model described in section 2.4. Figure 3-3, Figure 3-4 and Figure 3-5 show TEM micrographs of the nanocomposite films with different reinforcement percentages: 0.25, 0.5 and 1.0 wt.%, respectively. Images on the left correspond to as-synthesized samples (with MWCNTs randomly dispersed), while samples on the right to those aligned by mechanical stretching; the arrows indicate the loading direction and this condition was named “aligned”. The results of the dispersion quantification are plotted below the micrographs as a histogram. R^2 and Kolmogorov-Smirnov test parameters are also shown in each figure. The Kolmogorov-Smirnov test was done for comparing the cumulative distribution function with an equivalent distribution data. The Kolmogorov-Smirnov test is a measure of the distance between the experimental and hypothetical distribution functions; for this test, it is the maximum absolute difference as the test statistic, “ $D = | \text{function equivalent} - \text{cumulative distribution function} |$ ”. For each frequency distribution the test was done and for all cases, the statistics D is less than the critical value calculated by tables with a significance value of 0.05. That means, that the hypothesis for similar distributions functions are accepted. The dispersion degree was calculated from the histograms using Equation 2-1.

Figure 3-3a presents a representative TEM image of the composite reinforced with 0.25 wt.% of MWCNTs in the as-synthesized condition. The MWCNTs are seen well dispersed into the matrix without clusters. The results show an average spacing between MWCNTs of 34.5 nm and a dispersion degree $D_{0.1}$ of 8.8%. Therefore, about 8.8% spacing data are in the range of 31.47–37.53 nm, which corresponds to the range of $0.9\bar{x}$ – $1.1\bar{x}$. The composite in the aligned condition is shown in Figure 3-3b and similar results were found: the average spacing between MWCNTs was 62.4 nm and the dispersion degree $D_{0.1}$ was

8.9%. In this case, the alignment process increased the average spacing between MWCNTs. On the one hand, the matrix in the stretching direction became highly deformed, increasing the spacing between points with respect to the as-synthesized condition, thereby increasing the spacing between MWCNTs. On the other hand, it must be recognized that because of the contraction in the direction perpendicular to the stretching direction (Poisson effect), the distance between MWCNTs was expected to be decreased. However, as an average of all directions the distance between the MWCNTs was found to be increased.

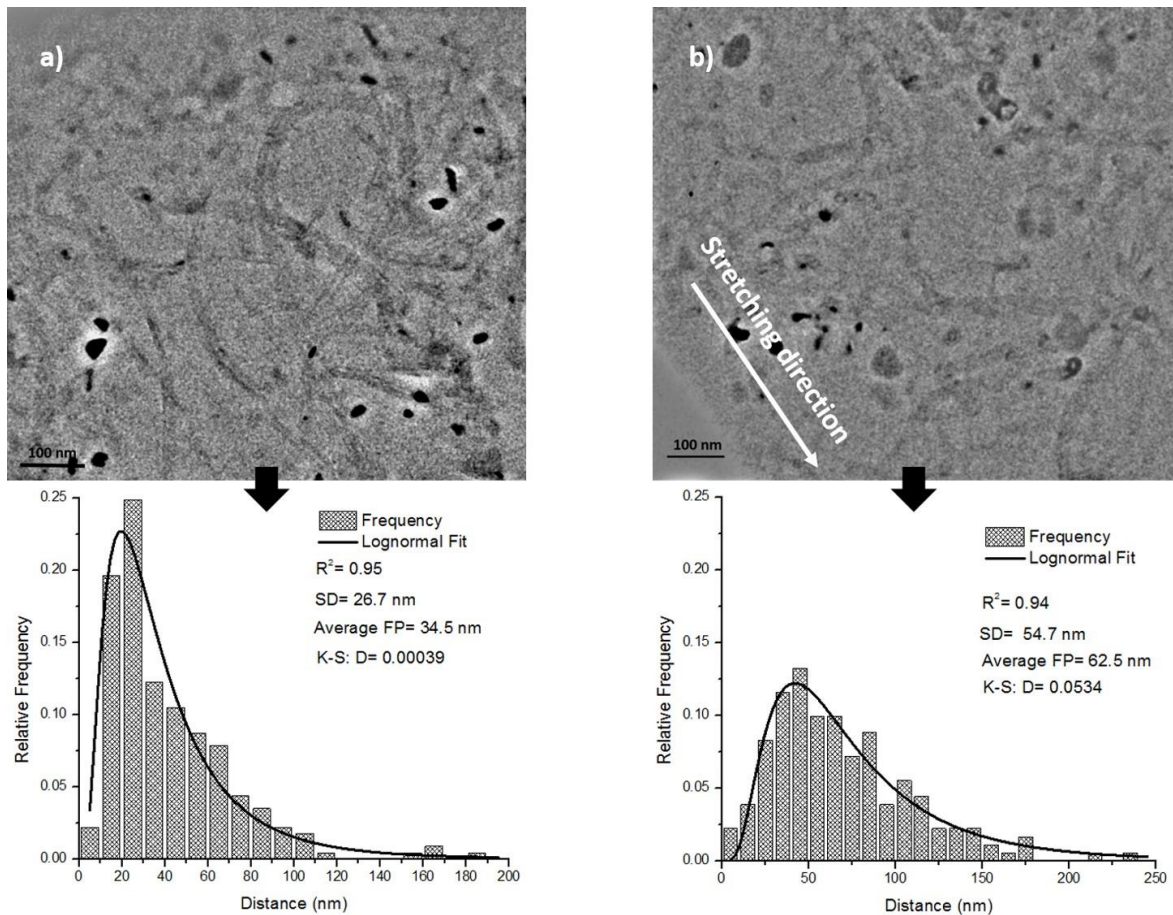


Figure 3-3. TEM images of the polymer matrix reinforced with 0.25 wt.% of MWCNTs. a) Not aligned – as-synthesized and b) aligned.

In the case of the composite reinforced with 0.5 wt.% of MWCNTs (Figure 3-4), an average distance between MWCNTs of 27.7 and 58.6 nm and a dispersion degree of 7.1 and 10.3% were calculated, for the as-synthesized and aligned composites, respectively. As shown in

Figure 3-4, the average of free-path distance and the dispersion degree increased after the alignment process, again owing to the polymer matrix deformation.

For the composite reinforced with 1.0 wt.% of MWCNTs (Figure 3-5), an average distance between MWCNTs of 22.8 and 30.0 nm and a dispersion degree of 10.4 and 10.6% were calculated, for the as-synthesized and aligned composites, respectively. For these composites, both the dispersion degree and the average distance between MWCNTs do not change significantly between the as-synthesized and aligned conditions; this can be attributed to the MWCNTs content itself: the composite becomes stiffer and constrains the deformation during the stretching process.

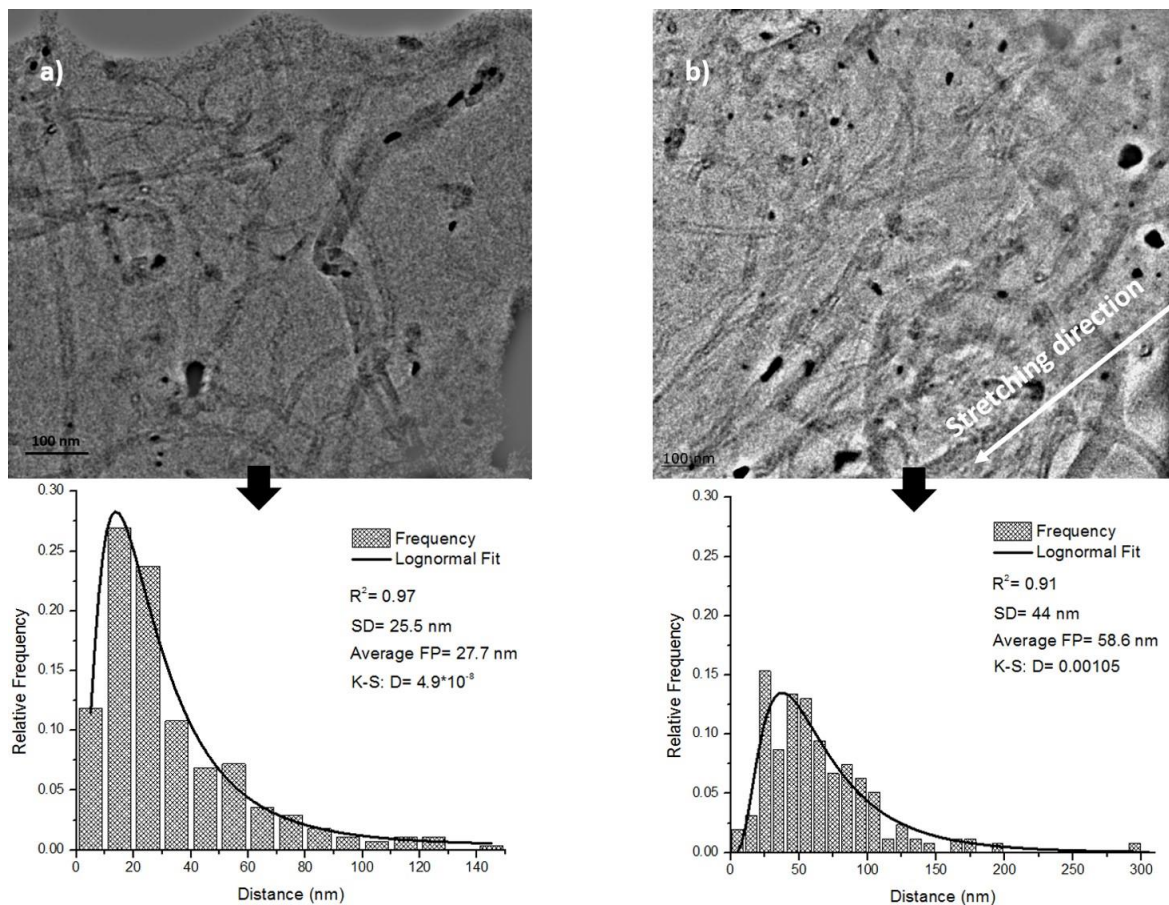


Figure 3-4: TEM images of the polymer matrix reinforced with 0.5 wt.% of MWCNTs. a) Not aligned – as-synthesized and b) aligned.

The alignment quantification is shown in Figure 3-6, where a similar log normal distribution was found for all samples. The angle frequency, measured with respect to the axis of

stretching, reveals a trend in the CNTs orientation for all composites studied. The most frequent angles were 20 degrees for all composites, which correspond to a very small angle with respect to the stretching direction after the alignment process, which means a good alignment degree. The mean values of the angles were 26.03, 22.20 and 30.60 degrees for the PVA reinforced with 0.25, 0.5 and 1.0 wt.% of CNTs, respectively. The alignment quantification was similar in all samples, although the reinforcements are not fully oriented with respect to the stretching direction.

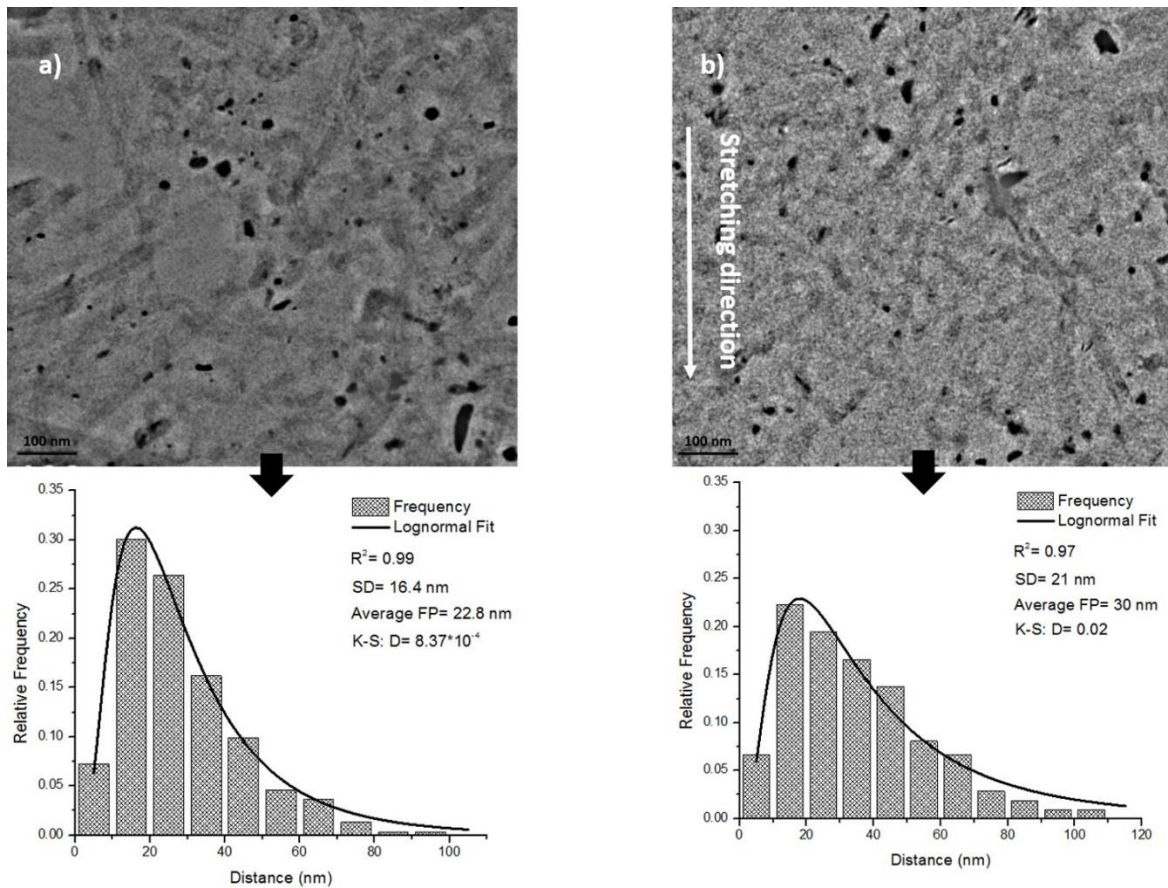


Figure 3-5. TEM images of the polymer matrix reinforced with 1.0 wt.% of MWCNTs. a) Not aligned – as-synthesized and b) aligned.

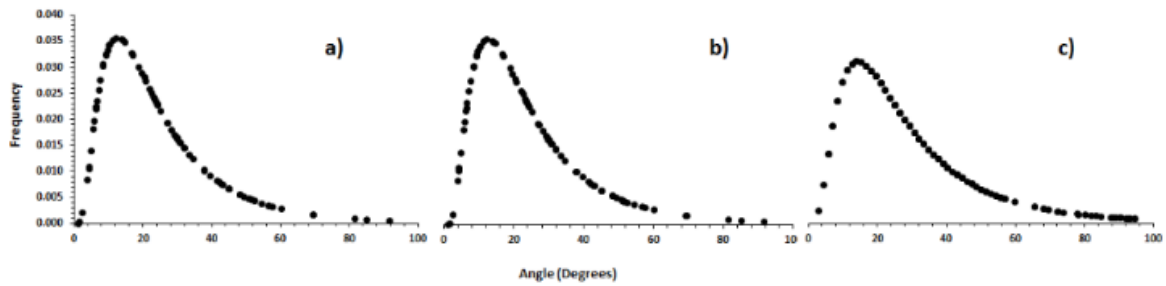


Figure 3-6. Angle frequency distribution of the alignment quantification. PVA reinforced with a) 0.25, b) 0.5 and c) 1.0 wt.% of MWCNTs.

Table 3-1 summarizes the results discussed above. Two things are clearly seen: the average free path and the dispersion degree ($D_{0.1}$) were increased by the alignment process, which was expected because the MWCNTs tried to follow the rotation of the polymeric chains thus pushing them away. This effect was lower as the concentration of MWCNTs was increased; once again this was expected since the composite becomes stiffer as the reinforcing material was added, which made the rotation of the chains difficult. In consequence, the distances between MWCNTs are shorter when the quantity of the reinforcement is increased. The quantification results for all composites showed a good dispersion degree, compared with those reported by other authors [110]. The good dispersion obtained was due to the energy ranges chosen in the sonication equipment. These energy ranges were reported elsewhere [111], where MWCNTs were dispersed in a water solution utilizing the same equipment used in this work, and both the water and PVA had a similar density. As will be discussed later, both the dispersion of MWCNTs and their alignment play a role on the mechanical properties of the composite. It is worth to noting that differences between the samples can be judged mainly based on $D_{0.1}$ values, because notwithstanding the high standard deviation of the mean free path value, the dispersion is soundly based on the probability of finding equally spaced CNTs around the mean value, the bigger this $D_{0.1}$ value the better the dispersion.

Table 3-1. Measured and calculated parameters for the PVA-MWCNTs composites.

Sample (wt.% MWCNTs)	Average free path (FP) (nm)	Standard deviation (nm)	D _{0.1} (%)
PVA-0.25	34.5	26.7	8.8
PVA-0.25 stretched	62.5	54.7	8.9
PVA-0.5	27.7	25.5	7.1
PVA-0.5 stretched	58.6	44.0	10.3
PVA-1.0	22.8	16.4	10.4
PVA-1.0 stretched	30.0	21.0	10.6

3.2.1 Mechanical properties for dispersion and alignment verification

For the measurement of the elastic modulus and hardness by nanoindentation test, a load of 100 mN was used. This load allowed reaching a high penetration depth for ensuring to sense a representative volume including matrix and MWCNTs. Figure 3-7 presents characteristic loading and unloading curves obtained from the nanoindentation test for the samples in the as-synthesized and aligned conditions. The aligned condition is clearly associated to lower penetration depths and lower initial unloading contact stiffness, i.e. the slope of the initial portion of the unloading curve, compared with the as-synthesized condition. This can be as a result of the alignment of MWCNTs and polymeric chains, as well as the subsequent increment in stiffness of the composite.

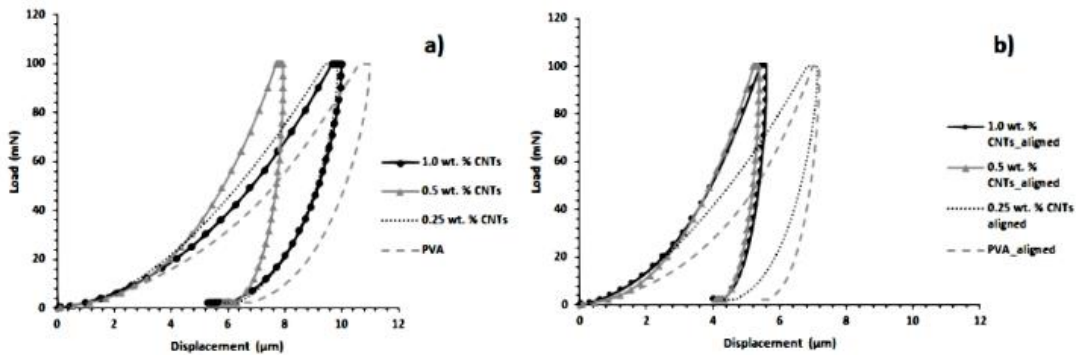


Figure 3-7. Load versus indenter displacement curves for the nanoindentation tests performed on: a) not aligned – as-synthesized and b) aligned samples.

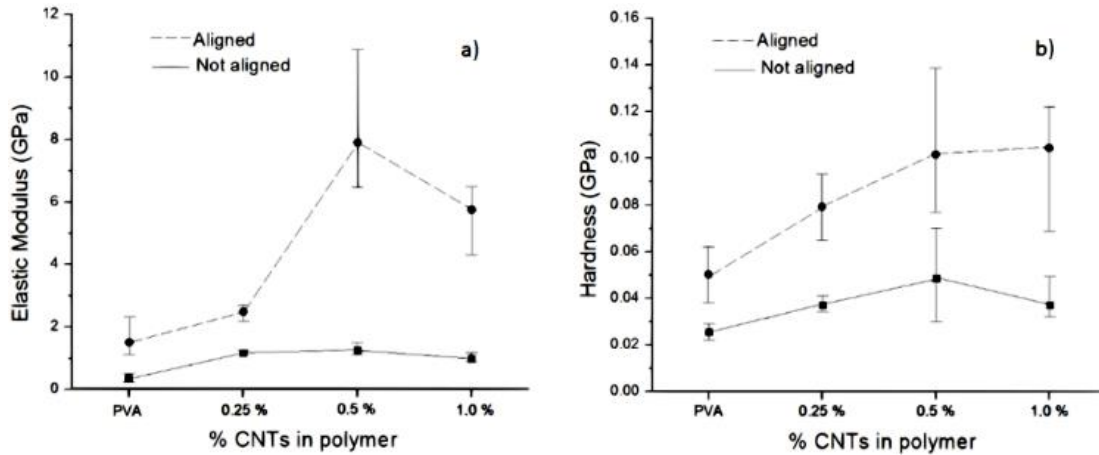


Figure 3-8. a) Elastic modulus and b) hardness measure by nanoindentation test.

The results of elastic modulus and hardness are given in Figure 3-8. When the reinforcement is added, in all cases an increase in both properties is clearly seen. It can also be seen that in general the alignment of the polymeric chains in the PVA produces an increase in those properties, even when no MWCNTs are added to the matrix. The maximum value was reached when 0.5 wt.% of MWCNTs was added to the polymer; beyond this point it was not possible to stretch the composite to the levels reached at lower reinforcement levels and, as a consequence, the elastic modulus decreases, which demonstrates that the polymeric chains alignment plays an important role in the enhancement of mechanical properties. Note that the addition of MWCNTs increases the mechanical properties with respect to the PVA polymer; however, the properties of the unstretched composites are almost constant regardless the MWCNTs content. At first glance this shows that the presence of the reinforcement is not as important as the stretching of the matrix. Nevertheless, the fact that the degree of increase in properties is much higher with 0.5 and 1.0 wt.% of the reinforcement, compared with lower levels, suggests that the alignment process and the right amount of MWCNTs play a critical role in the mechanical behavior. In this case the best results were found with 0.5 wt.% of MWCNTs. The considerable statistical dispersion of the properties seen in Figure 3-8 can be explained as follows: during the nanoindentation test the indenter is placed in zones with different microstructure, namely zones with different content or degree of alignment of MWCNTs. Note also that the unreinforced PVA produces results with small standard deviation and symmetrical confidence intervals, which is an indirect indication of the

isotropy of the material; such isotropy is lost with the addition of MWCNTs and their subsequent alignment.

The tensile stress-strain curves showed in Figure 3-9 evidence the effect of the CNTs alignment degree on the PVA and the composites, at the macro level. For these analyses all samples were stretched and then extracted in both directions. It is observed that the samples extracted from the transverse direction had low strength, elastic modulus and plastic deformation during the tensile test. On the contrary, the samples extracted from the longitudinal direction (alignment direction) showed a high enhancement in their strength, stiffness and ductility. This is, the ratio between the elastic modulus parallel (E_{\parallel}) and perpendicular (E_{\perp}) to the stretching detection, E_{\parallel}/E_{\perp} , has different values as shown by the slopes of the curves for the composite tested in both directions. DMA tests showed that the E_{\parallel}/E_{\perp} ratios were 1.75, 1.42, 2.0 and 1.014 % for the composites reinforced with 0, 0.25, 0.5 and 1.0 wt.% of MWCNTs, respectively. This strong anisotropy indicates that the stretching of PVA/CNTs films caused the alignment of CNTs. Same as found by nanoindentation test, the best tensile mechanical properties of the composites were found for the PVA reinforced with 0.5 wt.% of MWCNTs. It is highly interesting that even though the stiffness of this sample was increased in the alignment direction, its toughness was also increased and was much higher than that of the transversal direction. This phenomenon is not currently understood, but it could be suggested that in the transversal direction the reinforcement could act as a stress riser, effect that is much lower in the longitudinal direction.

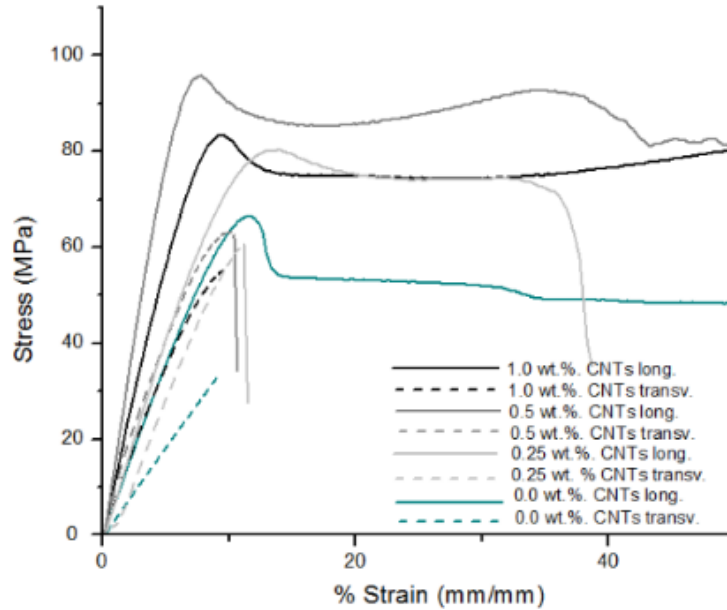


Figure 3-9. Stress versus strain curves obtained by DMA for the composites tested in two directions (longitudinal and transverse to the stretching direction).

As it was previously shown, the free-path spacing between carbon nanotubes increases after a deformation process. This increment is attributable to the chains deformation, which pushes the carbon nanotubes in the loading direction, due to this, the PVA/MWCNTs films led to a strong anisotropy, which indicates that at the nanoscopic scale, the MWCNTs are aligned into the PVA matrix along the stretching direction. Such MWCNTs orientation allows the composite mechanical properties to increase after the reinforcement was aligned into the polymer matrix. It is very important to have the MWCNTs well dispersed and well aligned into the matrix for achieving good mechanical properties in the metal matrix composites.

3.3 Bulk microstructural characterization in metal matrix composites

By convention, in this work the metal matrix composites will be named 0, 0.25, 0.5 and 1.0 wt.% for the composites reinforced with 0, 0.25, 0.5 and 1.0 wt.% of MWCNTs into the PVA, respectively. However, the true volumetric fractions for the MMCs are 0.014, 0.028 and 0.056 for the composites reinforced with 0.25, 0.5 and 1.0 wt.% of MWCNTs into the PVA, respectively.

Figure 3-10 shows optical microcopy images of the cross-section of the composites processed by the sandwich technique. The composites show a big grain size and grains

homogeneously distributed induced by the annealing and hot rolling processes performed after compaction. A good diffusion between magnesium sheets can be observed and some grains can be even seen passing through the interface between magnesium sheets. The microstructures show a grain size about $100 \pm 30 \mu\text{m}$ for the three composites. It is evident the grain twinning due to the post-processes. This twinning acts as a mechanism for plastic deformation during the tensile test.

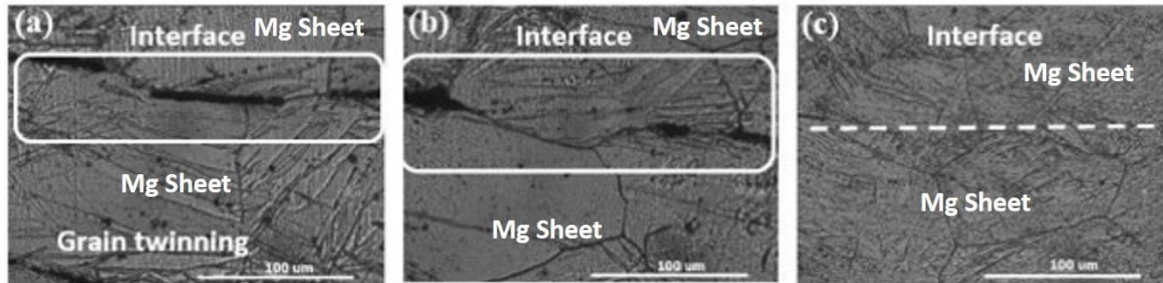


Figure 3-10: Optical microscopy images of the microstructures of magnesium reinforced with MWCNTs: a) 0.25, b) 0.5 and c) 1.0 wt.%.

Figure 3-11 shows images of the composites and a close-up of the interface between the magnesium layers, i.e. the reinforced zones or the MWCNTs-rich zones. In general, these images show a good dispersion of the MWCNTs, in addition, MWCNTs clusters were not observed, which allows promoting a good load transference between magnesium matrix and MWCNTs, which in turn produces good mechanical properties, as will be seen below. Figure 3-12 (study zone) shows some dark zones in the interface between magnesium sheets. These zones probably correspond to the formation of magnesium oxide (MgO) and aluminum oxide (Al_2O_3), as suggested by the mapping results discussed later. As it is well-known the magnesium corrodes via the oxidation with water or moisture. Then the formation of these oxides could be probably due to the hydrogen and oxygen generated during the PVA pyrolysis.

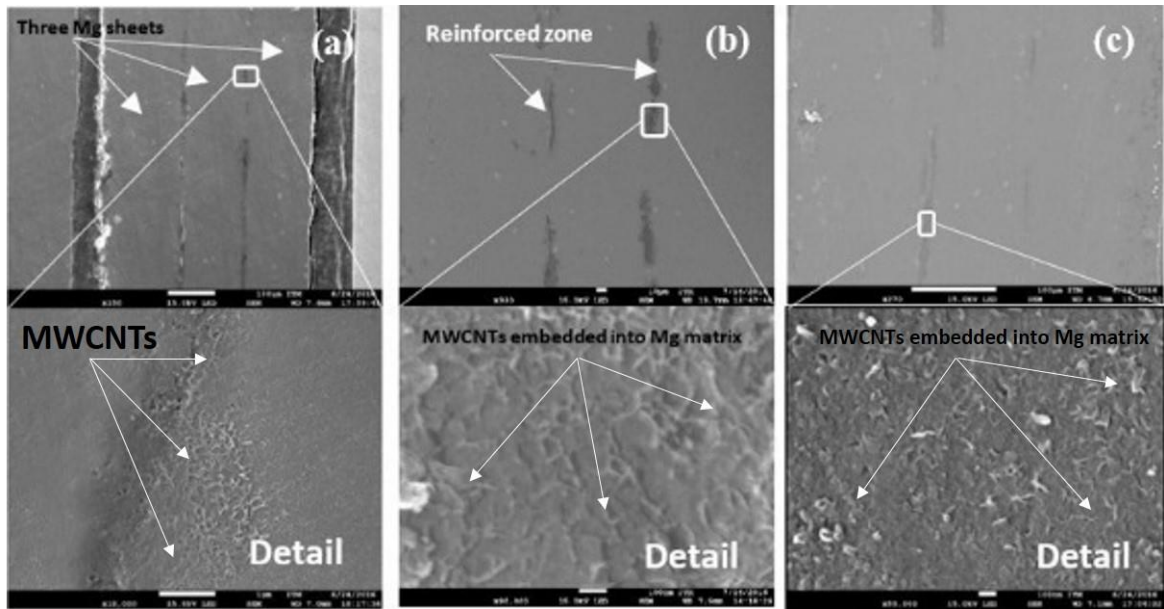


Figure 3-11: FESEM images of magnesium reinforced with MWCNTs: a) 0.25, b) 0.5 and c) 1 wt.%.

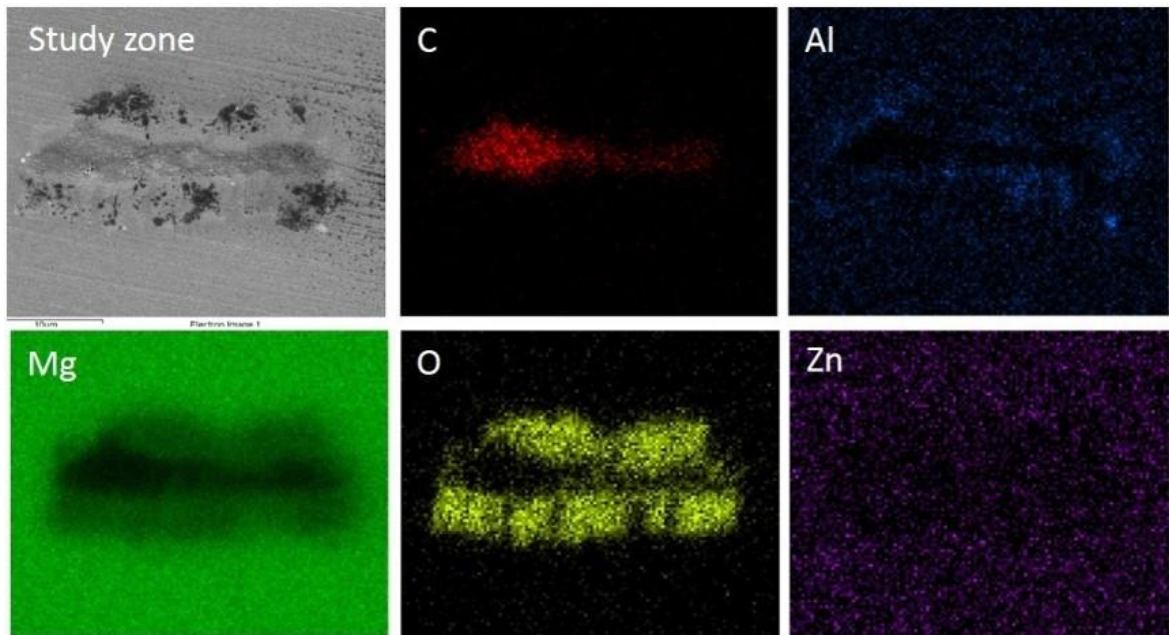


Figure 3-12: FESEM-EDS mapping analysis of the interface zone

XRD results in Figure 3-13 show the diffractograms of the composites. The results clearly show the presence of Mg and MWCNTs phases, and suggest the formation of MgO and $Mg_{17}Al_{12}$, without evidence of Al_2O_3 and carbide formation between magnesium and MWCNTs. It is probable that these phases exist, but they could not be detected due to the

equipment resolution. However, these results are in agreement with the EDS analysis showed in the images of Figure 3-12. Moreover, diffraction patterns were done by TEM in the different areas including the ones where the last EDS analysis were done, Figure 3-15 and Figure 3-16 in section 3.4 will show these results.

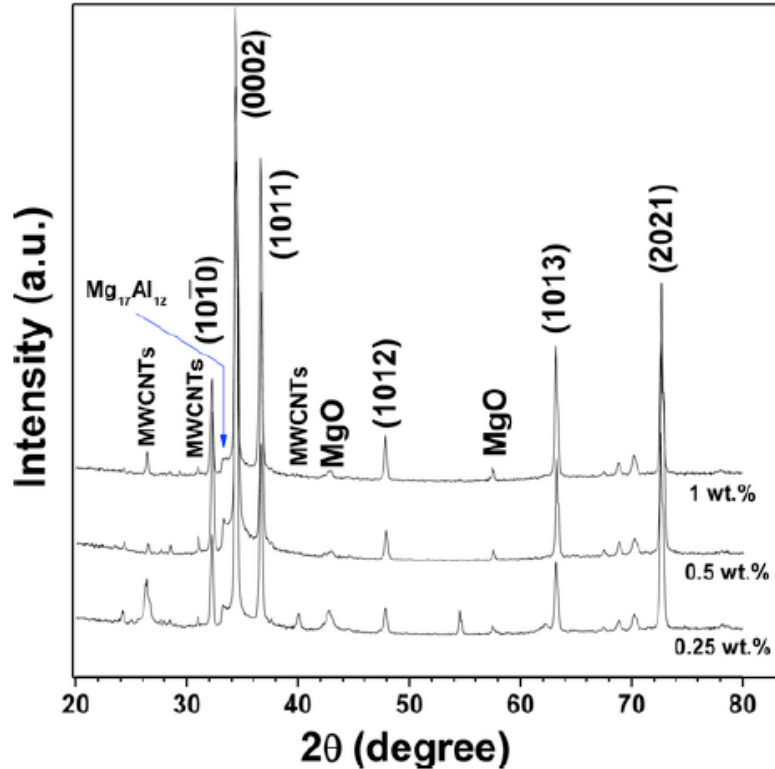


Figure 3-13: XRD patterns of magnesium reinforced with 0.25, 0.5 and 1 wt.% of MWCNTs.

3.3.1 Dispersion and alignment quantification of MWCNTs in a metal matrix

For dispersion and alignment quantification in metal matrix composites, the same methodology described in section 3.2 was used. Figure 3-14 shows FE-SEM images for all composites studied. The results of the dispersion quantification are plotted below the micrographs as a histogram, which shows a lognormal distribution. From the histograms, the dispersion degree was calculated using Equation 2-1. The Kolmogorov-Smirnov test was also done for comparing the cumulative distribution function with an equivalent distribution data. The test was done for each frequency distribution and, for all cases, the

statistics D was lower than the critical value calculated by tables with a significance value of 0.05. This means that the hypothesis for similar distributions functions are accepted.

Figure 3-14a, Figure 3-14b and Figure 3-14c, show a representative image of the composite reinforced with 0.25, 0.5 and 1% wt.% of MWCNTs, respectively. The MWCNTs are seen well dispersed into the matrix without clusters and the calculated dispersion degree $D_{0.1}$ was of 14.40 %, 8.39 % and 9.01 %, respectively.

Table 3-2 summarizes the results discussed above and shows that the dispersion degree ($D_{0.1}$) did not change (respect to the degree obtained in the MWCNTs – PVA composite) after the metal matrix composite fabrication for the composites reinforced with 0.5 and 1.0 wt.% of MWCNTs added. These results mean that after the fabrication process the MWCNTs dispersion was retained, only a low change due to the manufacturing process were evidenced.

The alignment quantification was not possible to do due to the non-alignment random found in the images; i.e. during the fabrication process, the alignment of MWCNTs was not retained because the diffusion process changed the MWCNTs orientation.

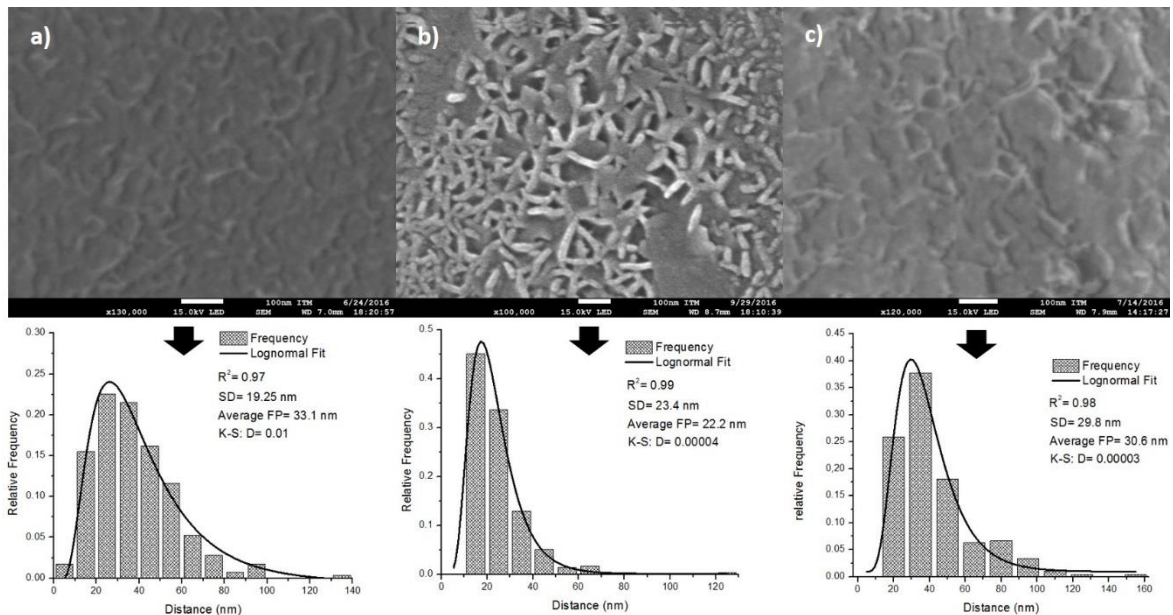


Figure 3-14: FE-SEM images of the metal matrix reinforced with MWCNTs. a) 0.25 wt.% and b) 0.5 wt.%.

Table 3-2: Measured and calculated parameters for the Mg-MWCNTs composites.

Sample (wt.% MWCNTs)	Average free path (nm)	Standard deviation (nm)	D _{0.1}
Mg-0.25 wt.%	33.1	19.25	14.40
Mg-0.5 wt.%	22.2	23.4	8.39
Mg-1 wt.%	30.6	29.8	9.01

3.4 Interface characterization between magnesium matrix and MWCNTs

In this section, the interface between magnesium sheets and between magnesium and MWCNTs will be described and discussed. For this analysis TEM, HRTEM, diffraction patterns, EDS and EELS were used.

3.4.1 Interface characterization between magnesium sheets: layer of Mg reinforced with CNTs and diffusion zone

In order to conduct a detailed study between magnesium sheets, transversal sections of the reinforced zones of some composites samples were prepared by a focused ion beam system (JEOL JEM 9320FIB); the results are shown in Figure 3-15. In this reinforced zone Mg, Al, O and C elements were detected, with no evidence of the Zn element for this particular line mapping. Results were similar for all composites (0.25, 0.5 and 1.0 wt.%).

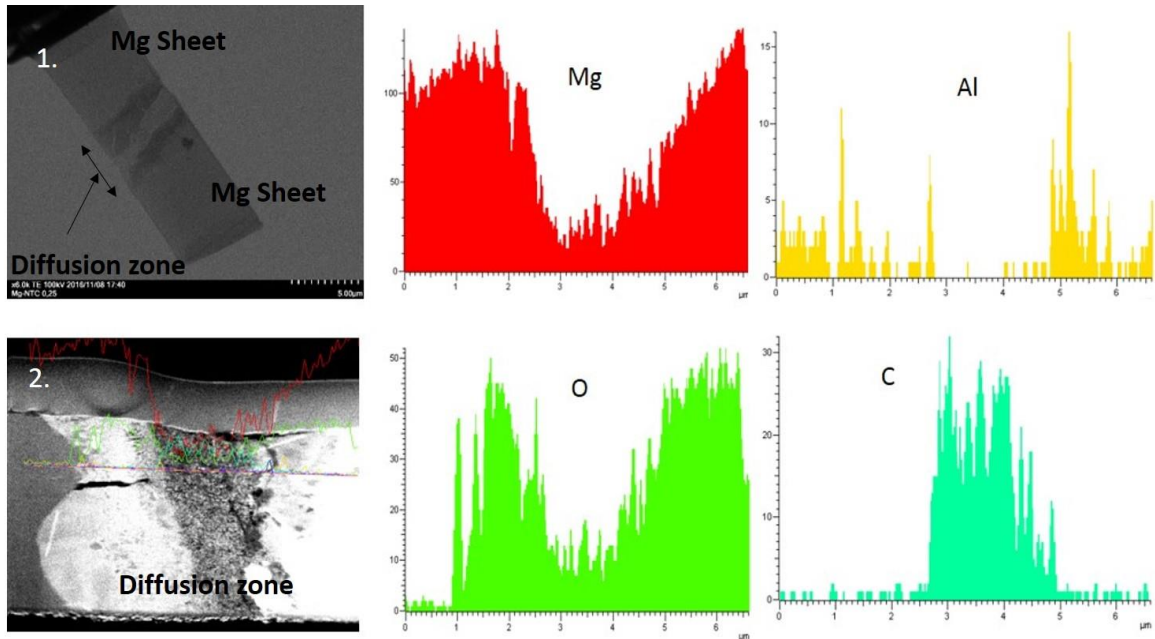


Figure 3-15: STEM EDS mapping in the study zone. 1. Lamella extracted close to the study zone (Diffusion zone). 2. Detail from diffusion zone. (see also Fig. 3-16)

An elemental analysis quantification for three different zones close to the interface between magnesium sheets was done (diffusion zone), these results are shown in Figure 3-16. Spectrum 1 (zone 1, Mg sheet) shows magnesium and aluminum as a principal element, this zone was not affected by the diffusion process during the composites manufacturing. Spectrum 2 (zone 2, transition) was acquired in the transition zone, where a high amount of oxygen was found; as will be verified below by a TEM diffraction pattern, the oxygen reacts with magnesium forming magnesium oxide (MgO). Spectrum 3 (zone 3, high MWCNTs content) was done in the interface zone between magnesium layers, where the main elements are carbon, magnesium and oxygen; the presence of Ni is due to the fact that it is used as a catalyst in the MWCNTs fabrication, as shown in Figure 3-2b.

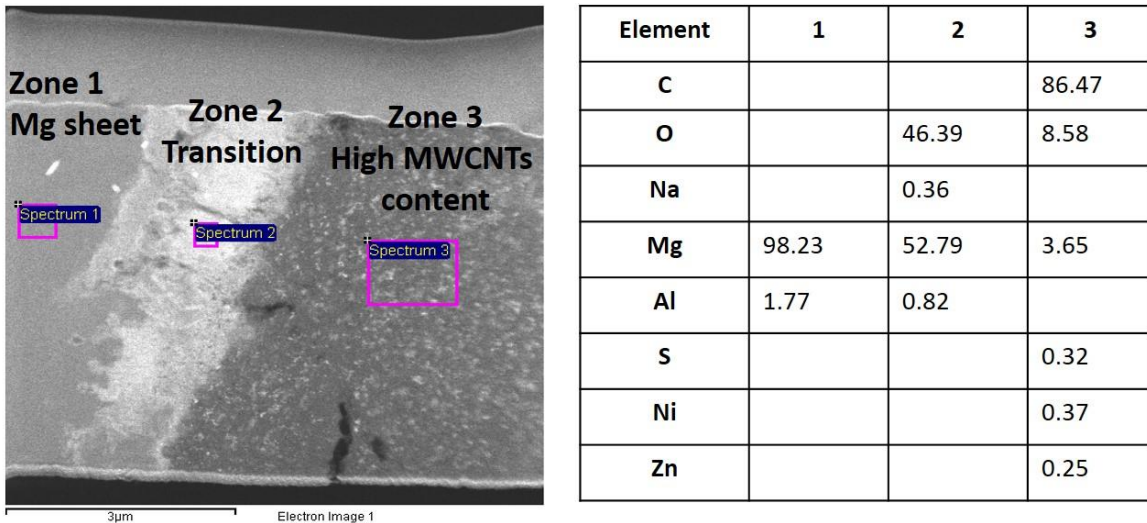


Figure 3-16: EDS analysis at the interface between magnesium sheets: Diffusion zone comprised of transition and High content CNTs zones

The crystalline structure along the interface and phases formed were obtained using HRTEM images and diffraction patterns. Zone 1 (Spectrum 1) was not affected by the diffusion process, in such a way that mainly magnesium was detected. The HCP crystalline structure of magnesium was verified in the image and pattern of Figure 3-17. The distance “d” corresponds to the basal plane (0 0 2) the HcP structure, the image was orientated in $B = z = [12\bar{1}6]$ and its planes can be seen in the diffraction pattern image of (Figure 3-17b).

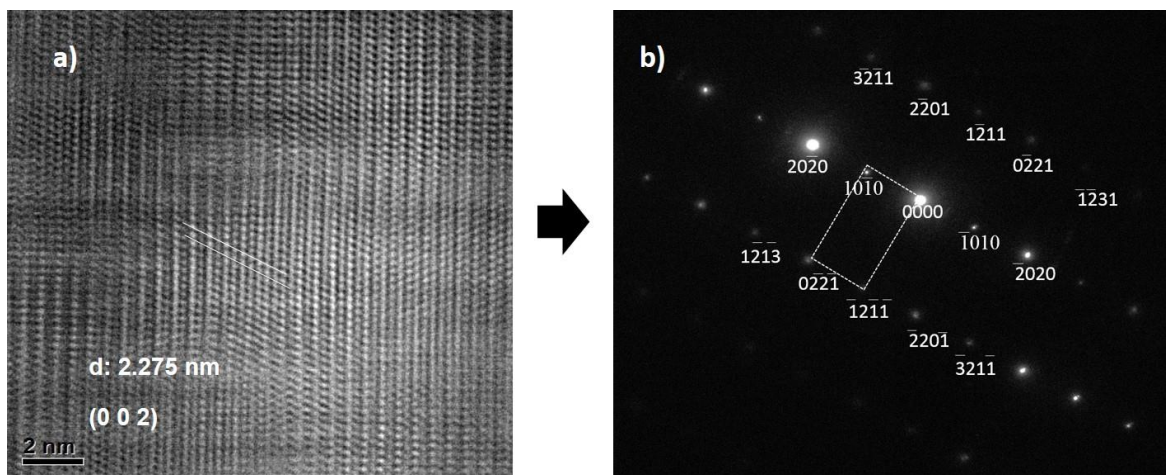


Figure 3-17: a) HRTEM image and b) diffraction pattern of the composite in zone 1 (Spectrum 1).

In the transition zone (Zone 2), where the diffusion process is very clear as was shown in Figure 3-16, it is evident the formation of magnesium oxide (MgO). This matches with what

was found by XRD (Figure 3-13), where some peaks of MgO were detected. This behavior is due to the well-known oxidation phenomenon of magnesium, via the oxidation with water or moisture, which occurs during the PVA thermal degradation in the hot compaction process. These peaks are MgO and not $\text{Mg}(\text{OH})_2$, the latter changing to MgO, which is a much more stable phase; this phase change occurs via a dehydration reaction during the hot compaction and hot extrusion [112]. In order to verify the MgO formation, a TEM image and diffraction pattern in zone 2 was obtained, (Figure 3-18). TEM bright field image (Figure 3-18) reveals the presence of MWCNTs embedded in the metal matrix as well as different grain sizes of the matrix. The TEM diffraction pattern (Figure 3-18b) reveals the presence of Mg, MWCNTs and MgO. The MgO is seen as small grains in the transition zone.

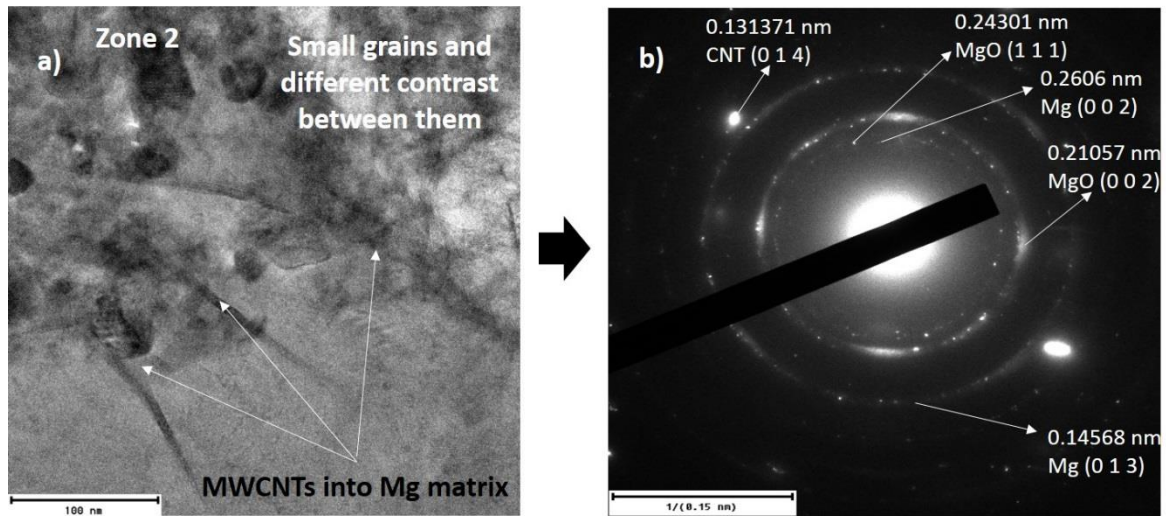


Figure 3-18: a) TEM image and b) diffraction pattern in zone 2 (spectrum 2).

Figure 3-19 shows a HRTEM image and its respective diffraction pattern for the interface between magnesium layers (Zone 3). In this zone, it is possible to see the same phases than those of the transition zone. The HRTEM image (Figure 3-19a) shows different orientated structures (polycrystalline), while the diffraction pattern (Figure 3-19b) reveals the presence of Mg, MWCNTs and MgO phases. All zones studied present a polycrystalline structure.

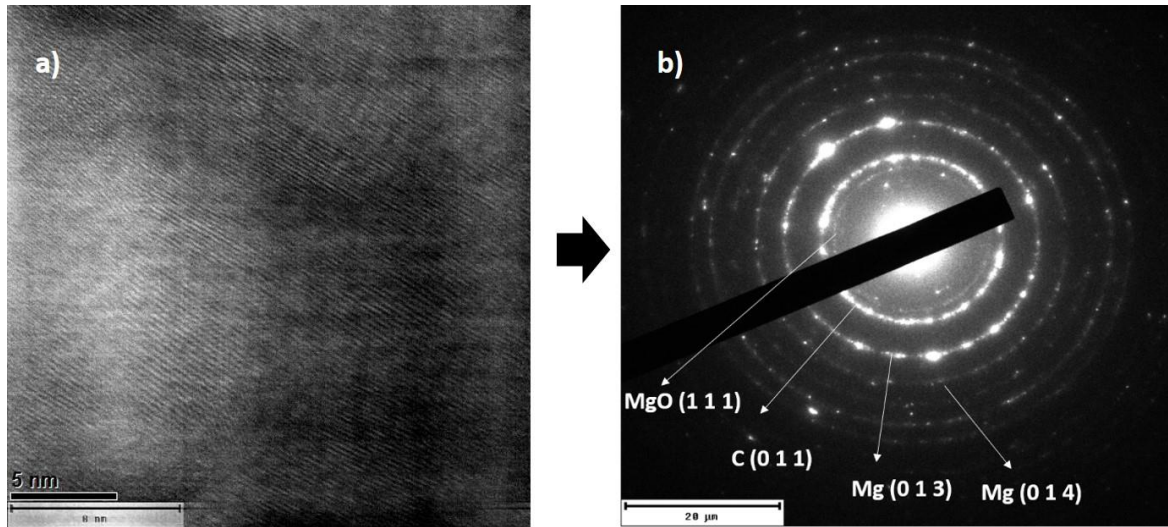


Figure 3-19: a) HRTEM image and b) diffraction pattern in Zone 3 (Spectrum 3).

Bright and dark field images in the transition zone and high MWCNTs content zone (Zone 2 and Zone 3) were taken, in order to corroborate the embedded MWCNTs in the metal matrix and the grain size reduction close to the MWCNTs. These act as important strengthening mechanisms in the metal matrix composites.

- ***Bright field and dark field images close the interface between MWCNTs and metallic matrix***

Figure 3-20 to Figure 3-22 show TEM bright field images for all composites studied, where the MWCNTs can be seen well immersed in the metallic matrix. In the transition zone (Zone 2) showed in Figure 3-20a for the composite reinforced with 0.25 wt.% of MWCNTs, it is possible to identify the MWCNTs, magnesium (bright) and magnesium oxide (dark). Figure 3-20b and Figure 3-20c show a close up of MWCNTs embedded in both Mg and Mg/MgO zones respectively, it is possible to see small grains around the MWCNTs, i.e. there was a recrystallization during the manufacturing process due to the high plastic deformation and temperature during the processing. This phenomenon is localized in the transition and final bonding zones (Zones 2 and 3); in other zones of the composites the grain size is about 100 μm, as shown in Figure 3-10.

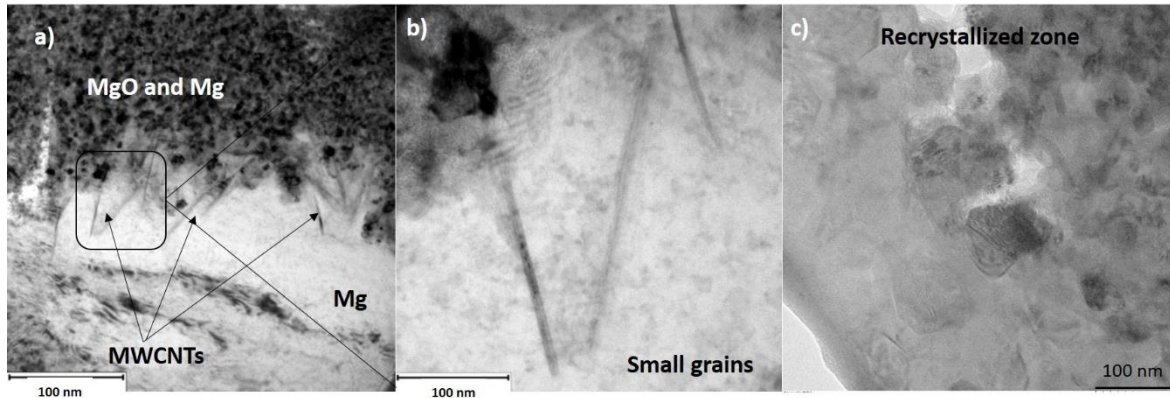


Figure 3-20: Bright field images for magnesium reinforced with 0.25 wt.% of MWCNTs. a) transition zone, b) detail of MWCNTs and c) detail of recrystallized zone.

In the case of the composites reinforced with 0.5 and 1.0 wt.% of MWCNTs, results of TEM images for regions close to MWCNTs are shown in Figure 3-21 and Figure 3-22, respectively. As can be seen, TEM bright images are similar and it is possible to identify the MWCNTs, Mg and MgO phases. On the other hand, matrix grain sizes are very small (about 60-100 nm), which increases the strength of the material, as was previously discussed. This strengthening mechanism was verified by TEM dark field images, as shown below.

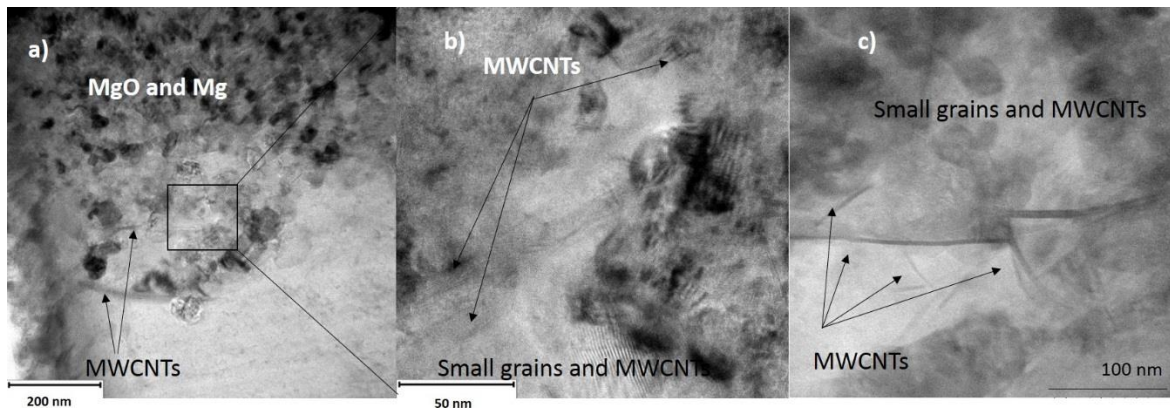


Figure 3-21: Bright field images for magnesium reinforced with 0.5 wt.% of MWCNTs. a) transition zone, b) detail of MWCNTs and c) detail of recrystallized zone.

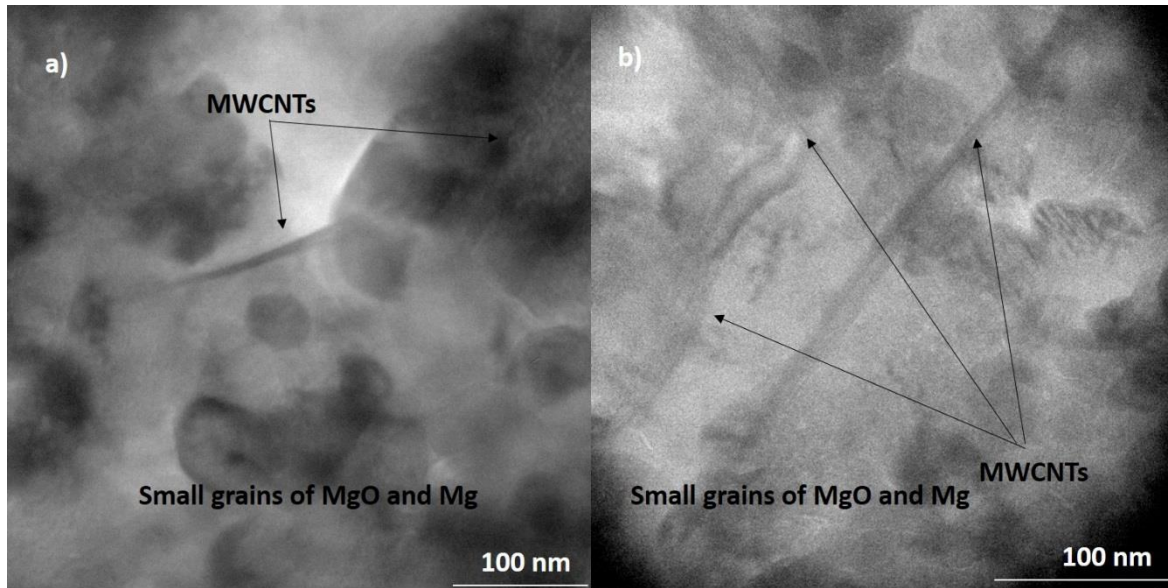


Figure 3-22: Bright field images for magnesium reinforced with 1.0 wt.% of MWCNTs. a) transition zone and b) detail of MWCNTs.

TEM dark field images consist on identifying in diffraction patterns some spots different to those coming from the central electron beam. With this selection, the electron beam passes across the sample in just one specific orientation, so the contrast in the image is associated either with different crystalline planes or different phases. Results using this technique are shown in Figure 3-23, Figure 3-24 and Figure 3-25 for the composite reinforced with 0.25, 0.5 and 1.0 wt.% of MWCNTs, respectively. These images were taken in Zones 2 and 3.

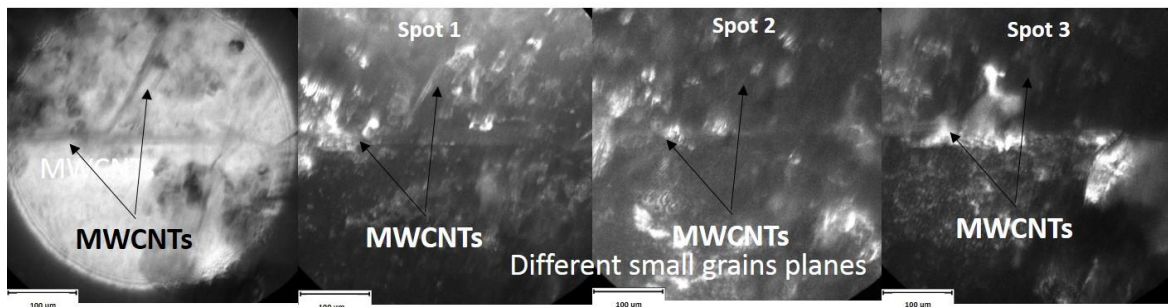


Figure 3-23: Dark field images for magnesium reinforced with 0.25 wt.% of MWCNTs.

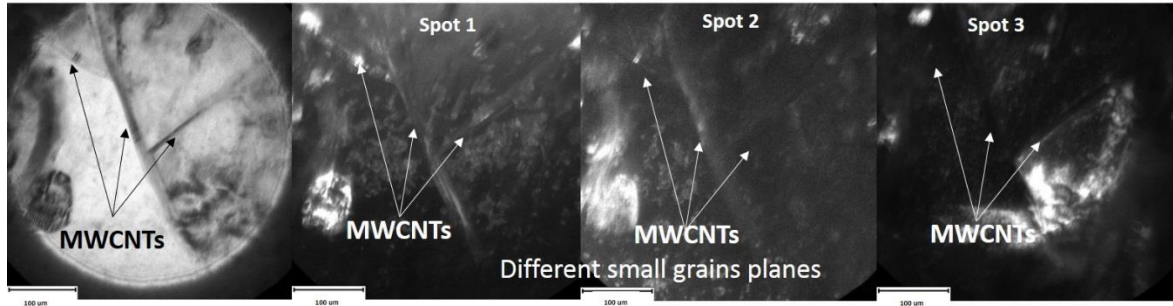


Figure 3-24: Dark field images for magnesium reinforced with 0.5 wt.% of MWCNTs.

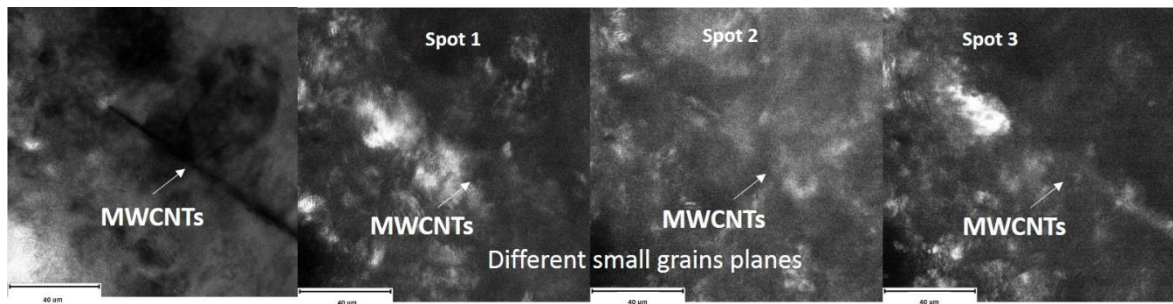


Figure 3-25: Dark field images for magnesium reinforced with 1.0 wt.% of MWCNTs.

From these images, it is easy to identify different grain orientation and size (about 10 to 60 nm in equivalent diameter for all the composites). In these dark field images it is corroborated that the recrystallization process took place during the composites manufacturing, which allow improving the mechanical properties by Hall-Petch relationship; i.e. the MWCNTs are acting as nucleation sites, restringing the grain growth by the pinning effect [113]. during the nucleation stage. The small grain sizes caused the remarkable improved yield strength, according to the Hall-Petch relationship. Thus, the load transfer mechanism and Hall-Petch relationship dominate the YS increase in the composites. The Hall-Petch equation relates grain size to yield strength and it is related as well with the deformation mechanism like dislocations. However, small grain sizes can also allow sliding between grains, which is a mechanism that enhances the plasticity in the materials. In the mechanical properties section, it will be discussed the different mechanisms for strengthening and plastic deformation.

3.4.1 Interface characterization between MWCNTs and metallic matrix

For the interface and interphase characterization between magnesium and MWCNTs several microscopy techniques were used. Dislocations stacking and coherence or semi-coherence structure between magnesium matrix and MWCNTs were found.

- ***HRTEM images at the interface between MWCNTs and metal matrix composites***

The HRTEM images were obtained close to the interface between MWCNTs and the metal matrix. Some strengthening mechanisms were identified, which allowed explaining the mechanical properties improvement with the addition of MWCNTs. TEM observation showed in Figure 3-26 to Figure 3-32 confirmed that MWCNTs were singly dispersed and completely embedded in all composites. No intermediate compounds or nanopores were detected at the interface between MWCNTs and the metal matrix, which indicates that a good interfacial bonding was achieved. Therefore, the load can be effectively transferred from the metal matrix to MWCNTs and the mechanical properties are expected to be improved; this will be corroborated in the mechanical properties section (section 3.5). For all composites studied, different zones in the composites were analyzed.

Figure 3-26 shows HRTEM images for the composite reinforced with 0.25 wt.% of MWCNTs. The well-graphitized MWCNTs structure was retained in the composite, which indicates that MWCNTs were not damaged during the fabrication process and subsequent hot rolling. It is also possible to identify the dislocation stacking in some zones of the composite at the interface between MWCNTs and metal matrix, as shown in Figure 3-26c. However, in other zones for the composite reinforced with 0.25 wt.% of MWCNTs, is it also possible to identify the dislocation generation (Figure 3-27c) due to the presence of MWCNTs reinforcement, i.e. the crystalline structure in this zone is semi-coherent. These two kind of dislocations were found and both act as strengthening mechanism that improve the composite mechanical properties.

Fast Fourier transform (FFT) images are shown as an inset in Figure 3-27b, which represent the diffraction pattern and correspond to a mixture of both magnesium and MWCNTs, as shown in the middle FFT image. This pattern shows only the diffraction

pattern for magnesium and MWCNT, i.e. at least in these images there are not compounds or interphases close to the interface between magnesium and MWCNTs. Figure 3-27c shows that the region next to the MWCNTs is comprised mainly of (0 0 2) planes and has an interplanar distance of 0.252 nm which corresponds to the magnesium phase.

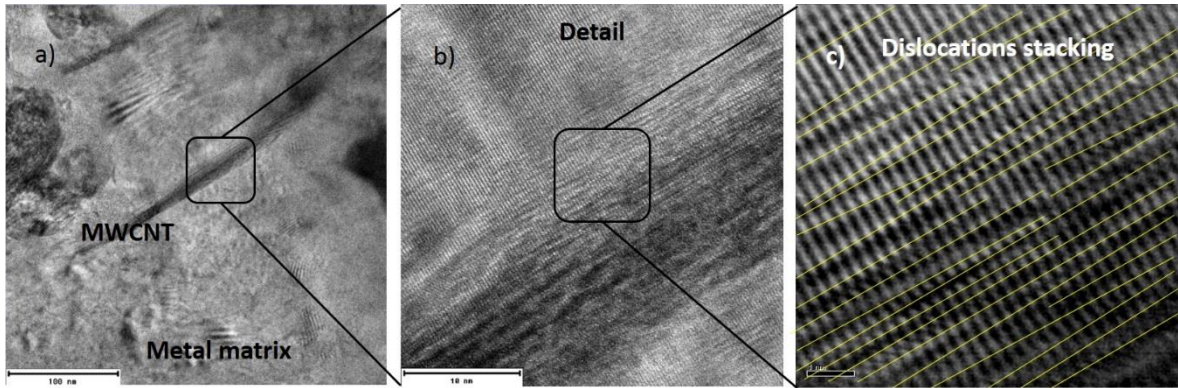


Figure 3-26: HRTEM images for the composites reinforced with 0.25 wt.% of MWCNTs. The dislocation stacking can be seen (HRTEM filter).

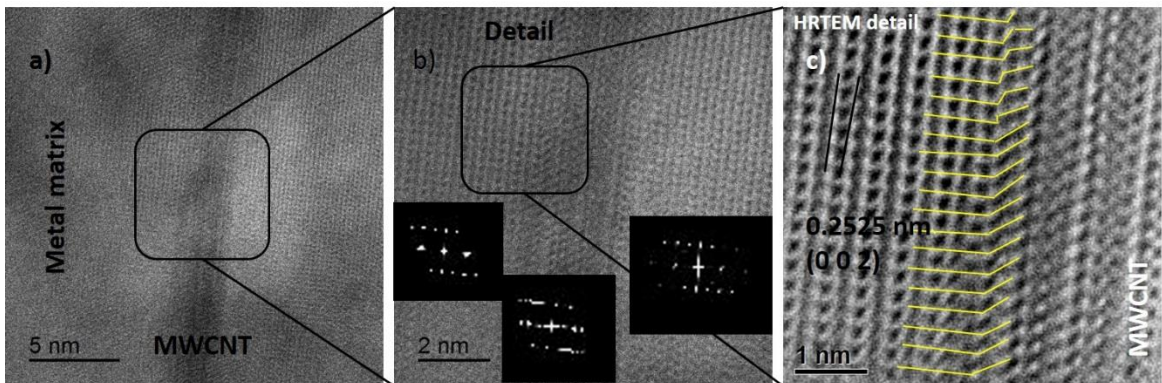


Figure 3-27: HRTEM images for the composites reinforced with 0.25 wt.% of MWCNTs. The dislocation formation can be seen (HRTEM filter).

Figure 3-28 to Figure 3-30 show HRTEM images for the composites reinforced with 0.5 wt.% of MWCNTs in two different zones. In these images, another strengthening mechanism was revealed: some MWCNTs were found in the grain boundaries as shown in Figure 3-28 and Figure 3-29. A close up shown in Figure 3-28b, reveals different crystalline orientation for different “zones”. In addition, the diffraction pattern showed in Figure 3-28c evidences the two different orientations associated to two different grains. Figure 3-29 show that these zones correspond to the planes (0 1 1) and (0 0 2) and their FFT images

corroborated such different crystalline orientation, the diffraction pattern was done in the detail image showed in Figure 3-28b. The MWCNTs located between these grains can stop the dislocation movement between grains borders, increasing the strength of the material.

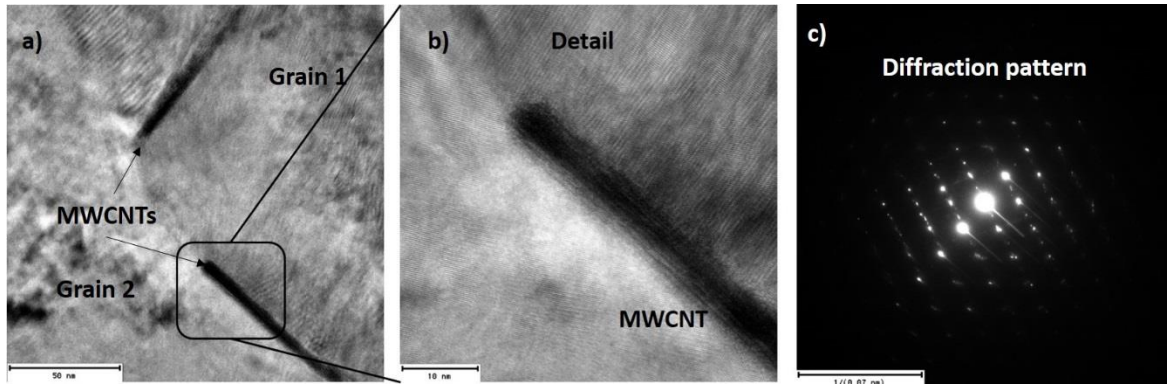


Figure 3-28: HRTEM images for the composites reinforced with 0.5 wt.% of MWCNTs. MWCNTs in grains borders can be seen (HRTEM filter).

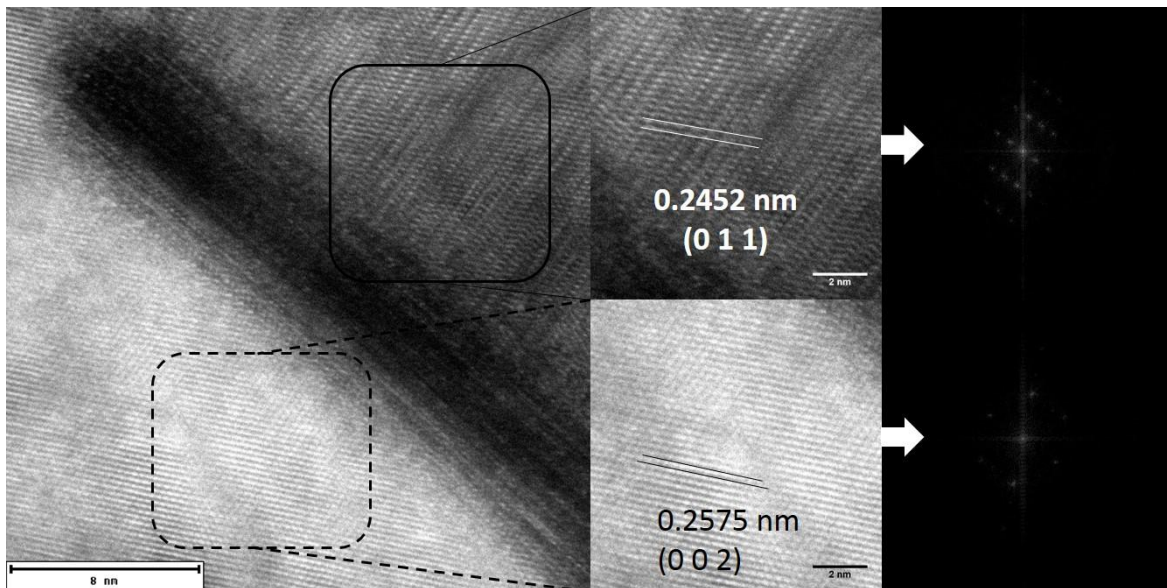


Figure 3-29: HRTEM images for the composites reinforced with 0.5 wt.% of MWCNTs. grains directions can be seen (HRTEM filter).

Figure 3-30 shows HRTEM images for the composite reinforced with 0.5 wt.% of MWCNTs in a different study zone where it is clearly seen that the MWCNT is well immersed into the metal matrix. Bright and dark field images by the annular dark-field (ADF) technique are shown in Figure 3-30a and Figure 3-30b, respectively. The close up images (Detail 1 and

Detail 2) reveal that the metal matrix and the MWCNTs are coherent at the interface in that study zone while FFT images (Detail 2) show how the crystalline structure changes between the metal matrix and the MWCNT. Because of this coherence, the load can be transferred from the metal matrix to MWCNTs, in such a way that the reinforcement effectively acts in the composite. After the indexing of the crystallographic planes in the high-resolution images, it is evident that the texture near the interface between MWCNTs and metal matrix has a preferential orientation; this analysis is detailed later.

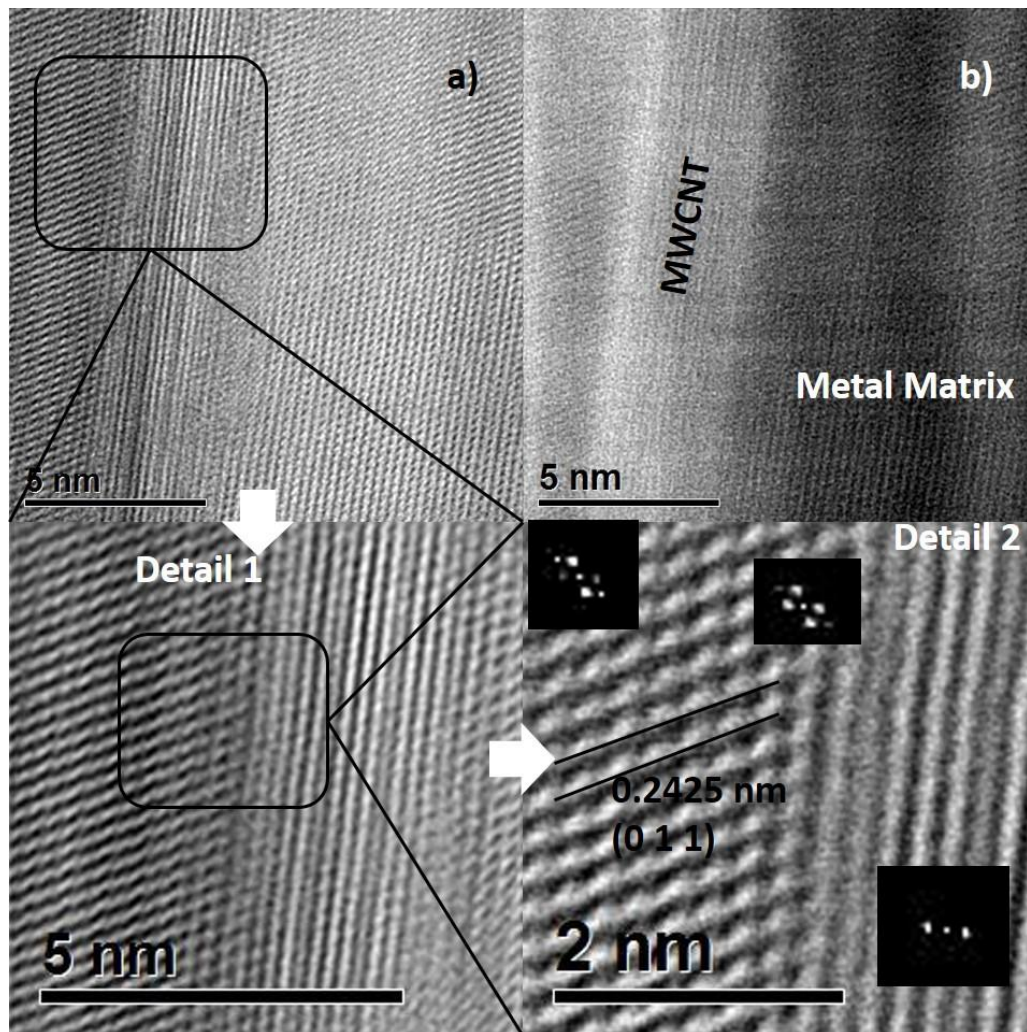


Figure 3-30: HRTEM images taken at the interface zone for the composites reinforced with 0.5 wt.% of MWCNTs (HRTEM filter).

Figure 3-31 and Figure 3-32 show HRTEM images for the composites reinforced with 1.0 wt.% of MWCNTs. A similar behavior to the 0,25 and 0,5 wt.% composites was found. Moreover, the composites zone study showed in Figure 3-31 and close up images evidence

that the family planes (0 1 1) and (0 1 0) appear at the surface of the Mg matrix and have a similar orientation to the composites 0.25 and 0.5 wt.% studied (Figure 3-32).

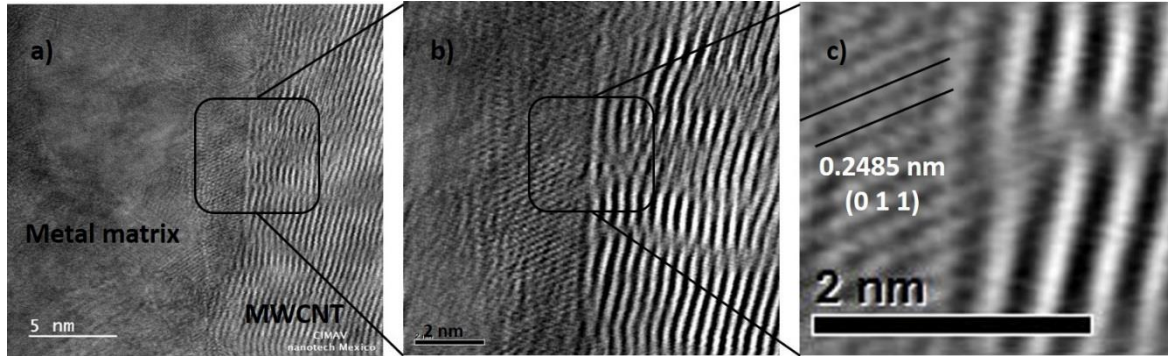


Figure 3-31: HRTEM images for the composites reinforced with 1.0 wt.% of MWCNTs, (HRTEM filter).

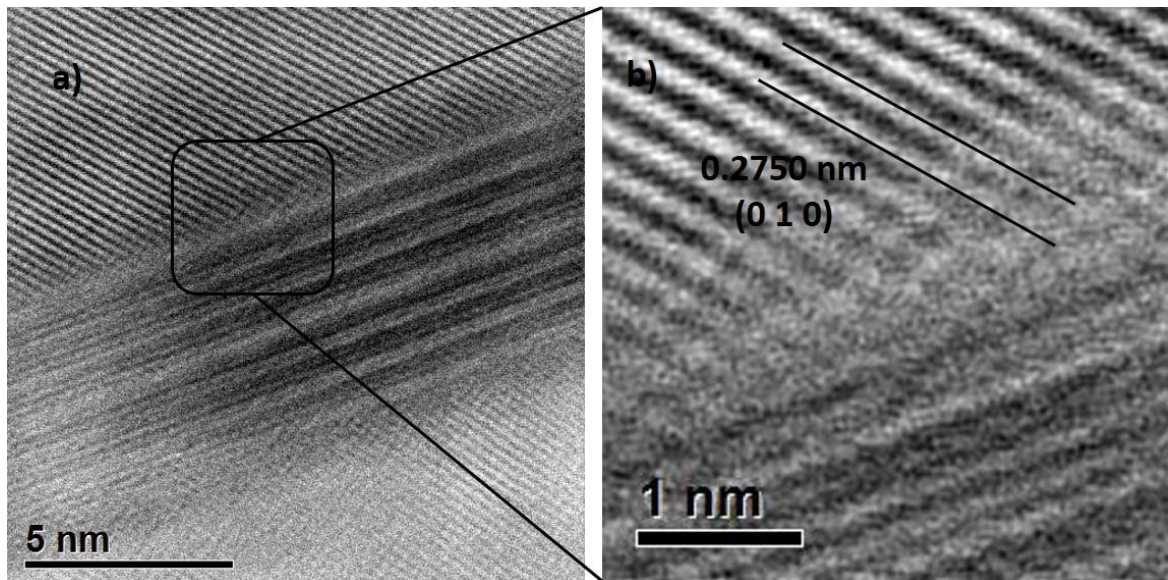


Figure 3-32: HRTEM images for the composites reinforced with 1.0 wt.% of MWCNTs, coherence of the interface between MWCNTs and metal matrix is shown (HRTEM filter).

The relative orientation of the planes near the interface respect to the CNTs surface was investigated using VESTA software (<http://jp-minerals.org/vesta/en/>). For this analysis, a unitary HcP cell was simulated in VESTA software and with the interplanar distance measured in HRTEM images the orientation of the unitary cell was identified. Figure 3-33 show the results, revealing that the basal planes $[[0002]]$ with an angle of 45° with respect

to the MWCNTs walls are the preferred ones close to the interface between MWCNTs and Mg matrix.

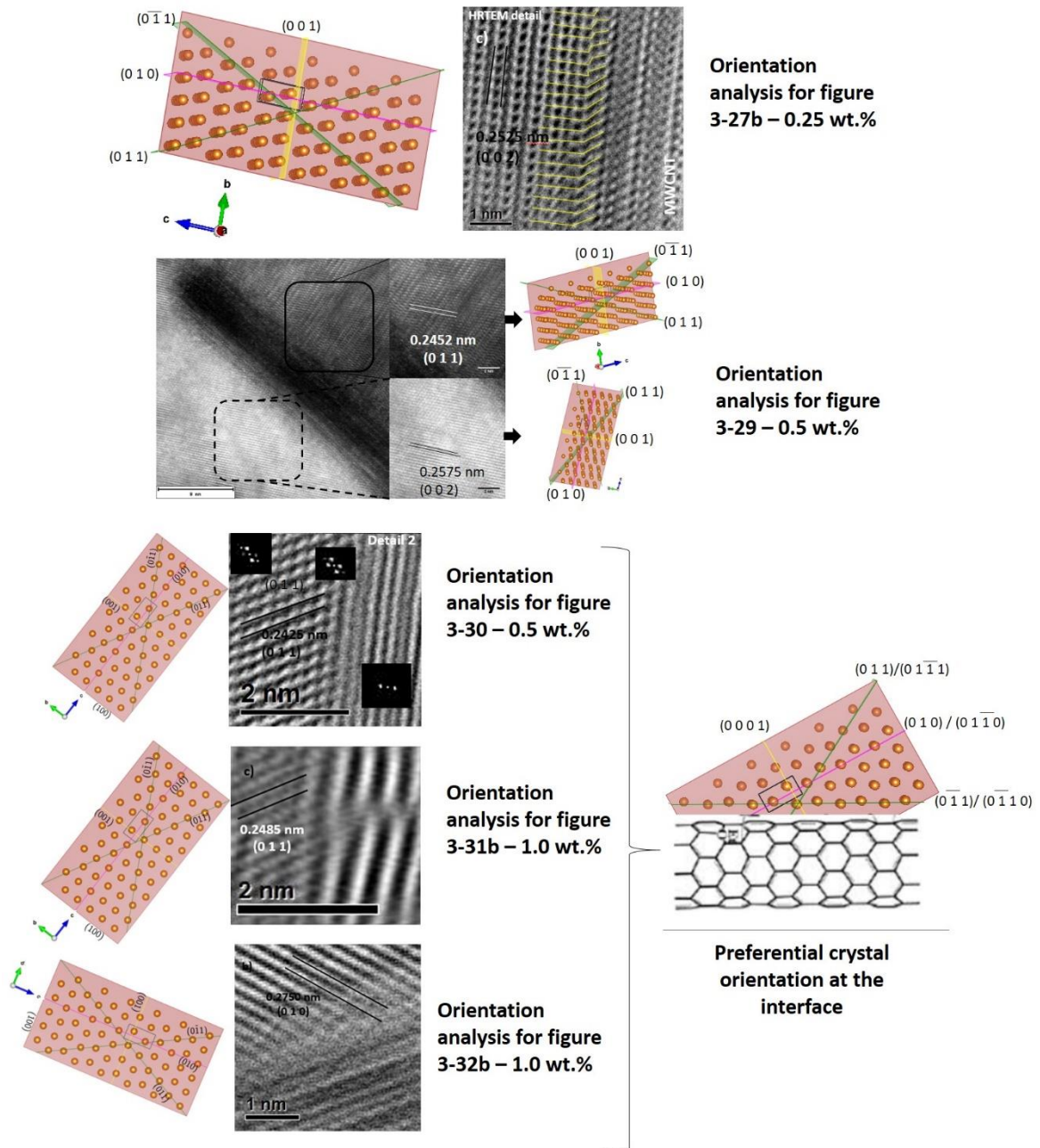


Figure 3-33: Orientation analysis at the interface between magnesium matrix and MWCNTs for images HRTEM (analysis by VESTA software).

Findings presented above are quite important because, the plastic deformation of magnesium at room temperature is limited to two main deformation mechanisms: basal

planes $[0001]$ $[11\bar{2}0]$ and mechanical twinning. Other systems such as prismatic slip $[10\bar{1}0]$ and pyramidal slip have the same $\langle a \rangle < 11\bar{2}0 \rangle$ slip direction in common but require larger critical resolved shear stresses for activation. Accordingly with the literature, under loading in directions either parallel or perpendicular to the sheet plane, basal, prismatic and pyramidal $\langle a \rangle$ slip systems fail to accommodate any deformation because they all have a slip direction parallel to the basal plane and the resulting shear strain in all slip systems is zero. For such cases, slip vectors with a component out of the basal plane are required. although for the investigated systems (MWCNT and metal matrix), the basal plane is at an angle of 45° with respect to the MWCNTs walls as is shown in Figure 3-33, due to the MWCNTs walls the plastic deformation at the interface between them is not easy and the load transfer between the metal matrix and the MWCNTs will be good. In order to activate other slide systems, is necessary a new vector acting on the pyramidal plane in the $< 11\bar{2}3 \rangle$ direction, which is referred to as pyramidal $\langle c + a \rangle$ slip. This slip mode offers five independent slip systems, thus satisfying the Von Mises criterion for an arbitrary shape change. Therefore, pyramidal $\langle c + a \rangle$ slip in magnesium usually requires substantial thermal activation, i.e. high temperatures or high shear stress for activation. With the absence of $\langle c + a \rangle$ slip at low deformation temperatures, the hexagonal crystals have no ways to accommodate the imposed strain along the sheet normal direction by crystallographic slip. This causes high stresses, modest work hardening, and, most importantly, premature brittle fracture. In magnesium, prismatic slip is not common. Furthermore, glide of $\langle c + a \rangle$ dislocations on pyramidal planes is known to be possible for this metal. The relative difficulty of these “harder” slip modes compared to the “softer” ones plays an important role in determining textures, strength and ductility.

The ease of slip on different crystal systems is usually quantified by their critical resolved shear stresses (CRSSs), which are measured in Stage I deformation on unconstrained single-crystal specimens where a unique slip system is activated. The values of stress for these planes and generate strain in the structure are 0.81 MPa for the basal plane, 45 MPa for prismatic slip planes and 80 MPa for pyramidal plane in a single crystal. These crystal orientations allow identifying the shear stress at the interface between metal matrix and MWCNTs and allows to predict the theoretical stress in the composite according with the kind of interface, i.e, according with the crystal HcP orientation. These theoretical predictions will be shown in section 3.5.8. In other hand, this preferential orientation allows

a very good load transfer between magnesium and MWCNTs due to the few plastic deformation that this direction in hexagonal structure has, during the stress flow through the interface, few dislocations could appear and the stress transfer is effective.

In summary, HRTEM analysis allowed to identify the interactions between the metal matrix composites and MWCNTs. In the HRTEM images both semi-coherent and coherent interaction between the metal matrix and MWCNTs were found. Additionally, two kind of dislocation were identified (stacking and formation of dislocations at the interface) and no intermediate interphases were found in the studied zones. Finally, the interface between metal matrix and MWCNTs have a preferential growth direction as shown in Figure 3-33 and the basal planes with 45° respect the MWCNTs walls are preferential close to the interface between them. This orientation allows knowing the shear stress at the interface between MWCNTs and metal matrix, and finally, knowing all mechanisms at the interface will be possible to predict the behavior in the composites.

- ***Elemental analysis and energy loss spectroscopy in the interface between MWCNTs and metal matrix composites***

Elemental analysis was made close to the interface between the metal matrix and MWCNTs in order to identify some chemical interactions between them. In Figure 3-34 - Figure 3-36 the results of elemental analysis done for the composite with 0.5 wt.% MWCNTs are shown. Some elements such as magnesium, aluminum, carbon, oxygen and zinc were identified at the interface, as shown in the spectrogram of Figure 3-35. The oxygen comes from the PVA thermal degradation during the hot compaction process, while the carbon from the MWCNTs. Besides the aluminum diffuses to the MWCNTs walls, and this is due to the chemical affinity between aluminum and carbon for forming aluminum carbide by hot processes. However, this Al-C diffusion pair is not enough to form some interphase at the interface between the metal matrix and MWCNTs, since just some aluminum atoms were detected in the MWCNTs walls. Further, the variation of free energy of carbide formation shows a positive value for magnesium carbide; thus, the presence of this kind of compounds are very few probably in these composites.

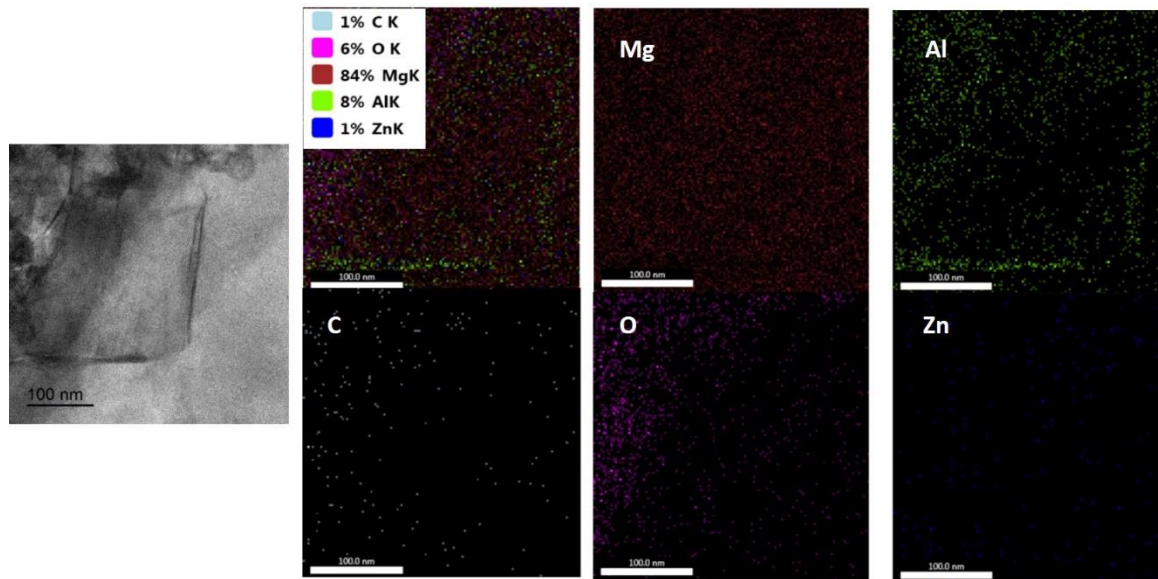


Figure 3-34: EDS mapping performed in the Mg/0.5 wt.% MWCNTs composite.

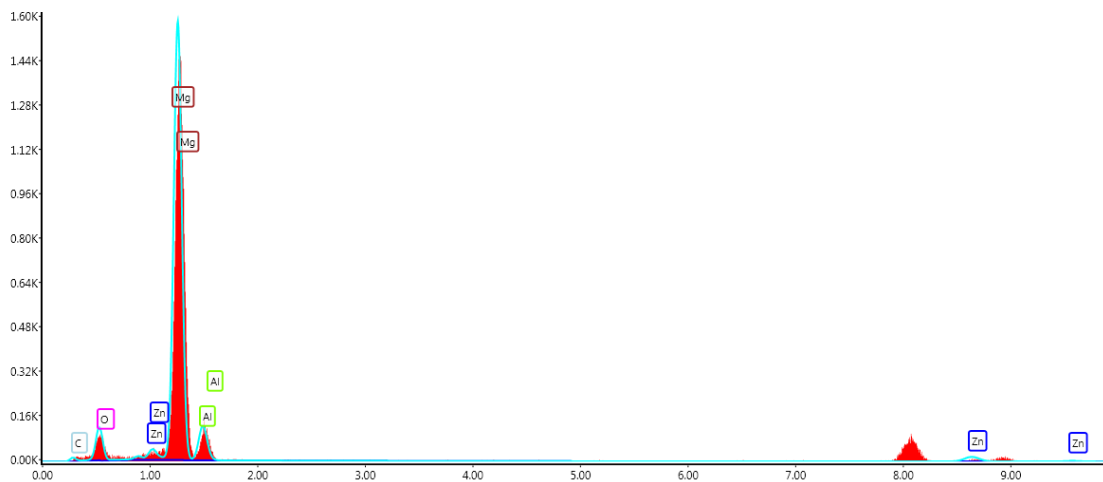


Figure 3-35: Elemental spectrogram from the study zone from the Figure 3-34.

In order to corroborate the presence of aluminum particles in the MWCNTs walls, an EELS analysis was done (Figure 3-36). The results suggest the aluminum presence close to the MWCNTs walls. As previously discussed, aluminum has chemical affinity for the carbon, which results in the formation of aluminum carbide but, in this case, no interphase was found. Similar results were found for the other composites.

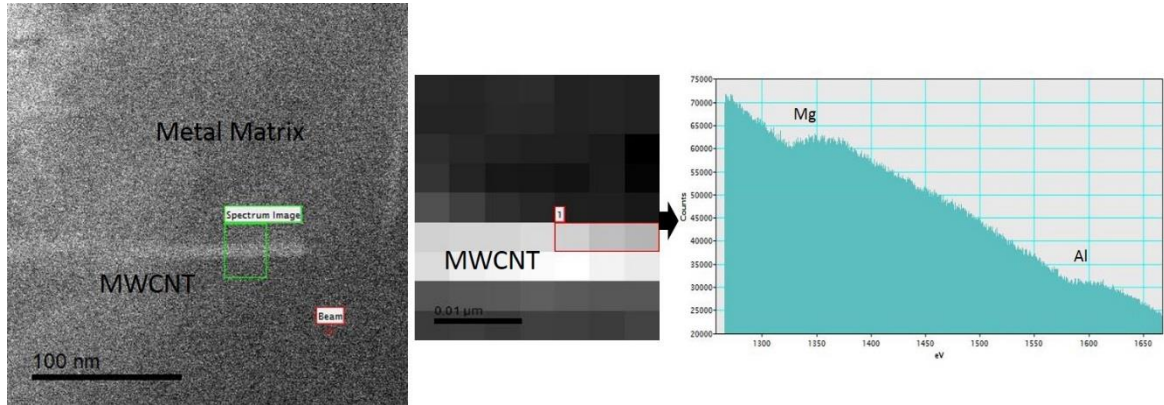


Figure 3-36: EELS analysis between MWCNTs and the metal matrix in the interface of the 0.5 wt.% of MWCNTs sample).

3.5 Mechanical properties characterization in the metal matrix composites

In this section, the mechanical testing characterization results will be described. The nanomechanical testing include nanoindentation, fracture toughness and nanoscratch technique. The bulk mechanical tests comprise tensile and microhardness testing. The results of the characterization in both scales will be correlated.

3.5.1 Nano mechanical testing characterization

The results of nanoindentation tests are shown in Figure 3-37. The elastic modulus and hardness were measured near the interfaces between magnesium sheets. All tests were made at the same load (1 mN), therefore no indentation size effect due to this factor is involved. It is worth mentioning that the value of both the elastic modulus and hardness of the Mg 0.0 wt.% of MWCNTs corresponds to the values of “bulk” magnesium reported in the literature; consequently, at this load level there is no effect at all. Both the modulus and hardness were significantly increased close to the interface for all the reinforcement contents into the magnesium matrix. The increase in elastic modulus was 66%, 88% and 90% for the composites reinforced with 0.25, 0.5 and 1.0 wt.% of MWCNTs, respectively (Figure 3-37a). The increase in hardness was between 150% and 450% compared with the magnesium sheets stacked without MWCNTs, which in turn indicates that the reinforcement is the responsible of the mechanical properties enhancement and not the potential oxides formed (Figure 3-37b). Figure 3-37c and d show the variation of the elastic modulus and

hardness as function of the distance in the test in the diffusion zone, respectively. The results showed are according with the results showed in Figure 3-15 and evidence the changes in composition in the transition zone, i.e, the mechanical properties begin to increase until the center of the diffusion zone, where the MWCNTs contents are very high as was shown in the Figure 3-15 (EDS images). Figure 3-37e and f show a representative load vs displacement curve for each composite studied and the image for the indentations done close to the interface between magnesium sheets.

Several reinforcement mechanisms might explain the improvement on the mechanical properties of the synthesized composites. One mechanism is the dislocation generation by thermal expansion mismatch between the matrix and MWCNTs. The dislocation stacking at the interface between magnesium and MWCNTs (section 3.4) plays an important role in the strengthening of Mg/MWCNTs composites; however, to achieve the theoretical value of strength prediction, a uniform dispersion of MWCNTs is necessary, which was indeed the case in this work (section 3.2). Another important mechanism is the Hall-Petch strengthening, which improves the strength of MMCs due to the grain reduction close to the interface between matrix and MWCNTs, as was previously shown by the TEM dark and bright field images (section 3.4.2). On the other hand, in the case of the Mg/MWCNTs composites studied in the present work, the carbide or other phase formation was not found at the interface, implying that there was not chemical reaction between the materials; the dislocation formation is present in the interface due to the semi-coherence behavior between magnesium and MWCNTs. Other strengthening mechanism are the grain twinning and the inhibition of dislocation motion by MWCNTs.

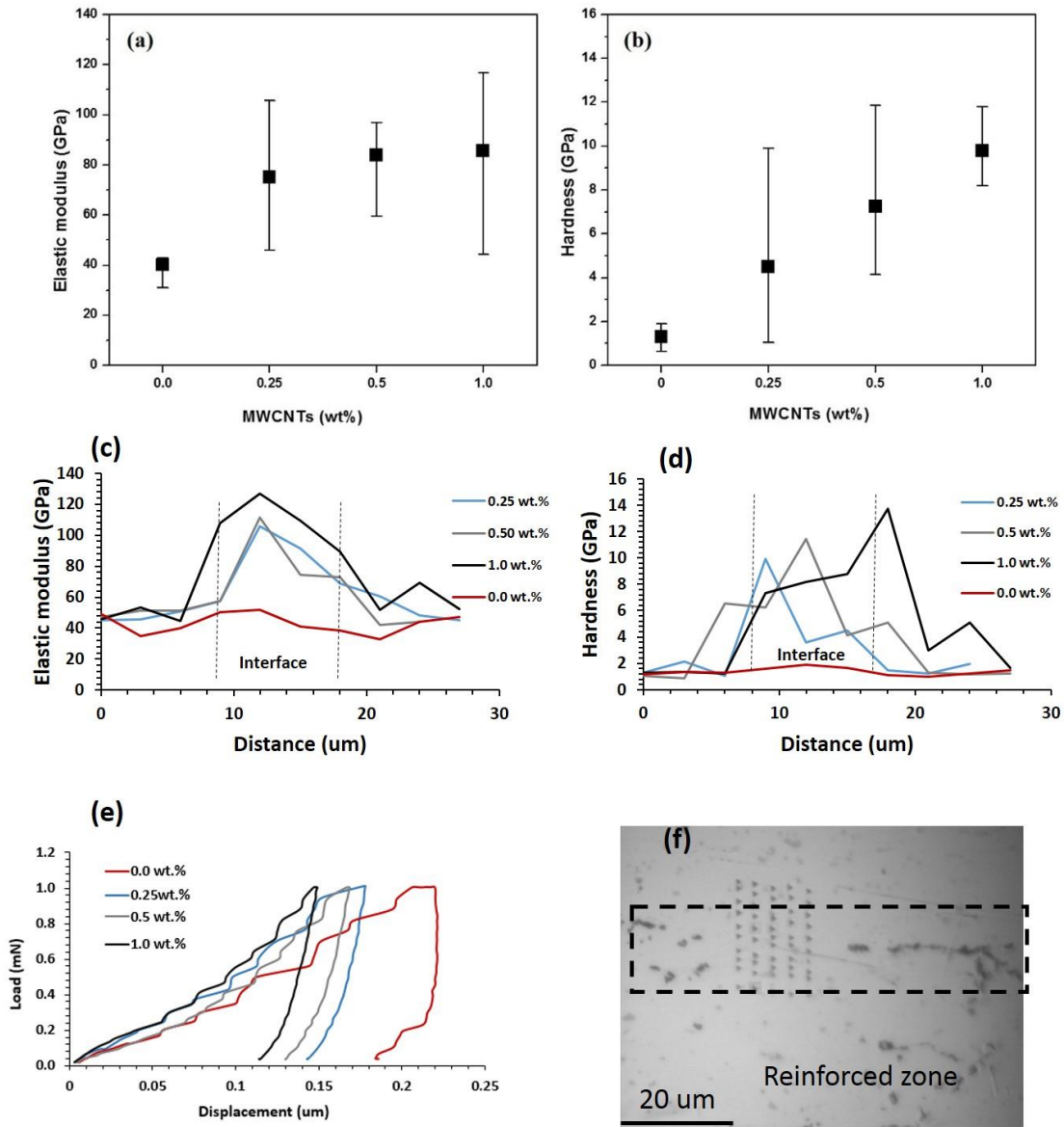


Figure 3-37: Elastic modulus, b) hardness c) load vs displacement and d) the indentations done close to the interface between Mg sheets.

3.5.2 Nano-scratch testing characterization

Due to the increasing in hardness showed in Figure 3-37b, nano-scratch tests were performed in order to verify the expected enhancement in the wear resistance of composites near the interface. Figure 3-38 shows the variation of the friction coefficient as function of the scratch length for all composites studied. Figure 3-38 resembles the behavior

of the Hardness Vs. distance to the interface shown in Figure 3-37d, although friction coefficient is less sensible compared with the nano-hardness.

Either way, the friction coefficient decreased in the study zone for the composites reinforced with 0.25 wt.% of MWCNTs from about 0.45 to 0.35 with respect to the material without reinforcement. The composite reinforced with 0.5 wt.% of MWCNTs shows a significant decreasing of its friction coefficient from about 0.45 to 0.33 with respect to the material without reinforcement, and finally, the composite reinforced with 1.0 wt.% of MWCNTs shows a decreasing of its friction coefficient in the study zone from about 0.45 to 0.28. These results are in agreement with the nanomechanical results showed in the last section. i.e. the coefficient of friction in the composites increases close to the interface between magnesium sheets (diffusion zone) which in part is due to the hardness increasing in this zones. These results are interesting for futures works for nanotribological applications. An additional scratch test was made a long the interface between magnesium sheets and the decreeing of the frictional coefficient was evidenced. These results allow exploring new engineering applications for this kind of composites. The nanogrooves for all composites are shown in Figure 3-39 and by optical microscopy was no possible to identify the wear mechanism. This research is proposed for future works.

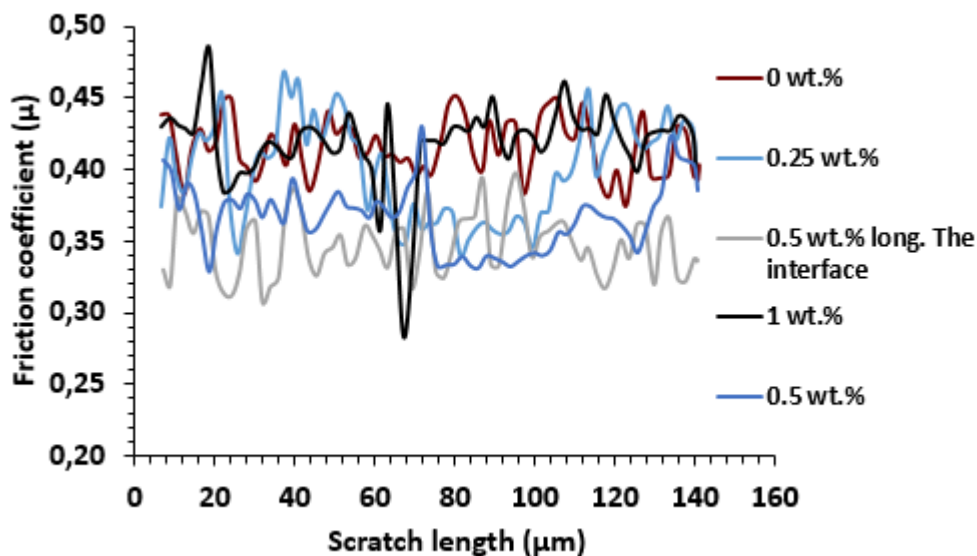


Figure 3-38: Variation of the friction coefficient as a function of scratch length for all composites studied.

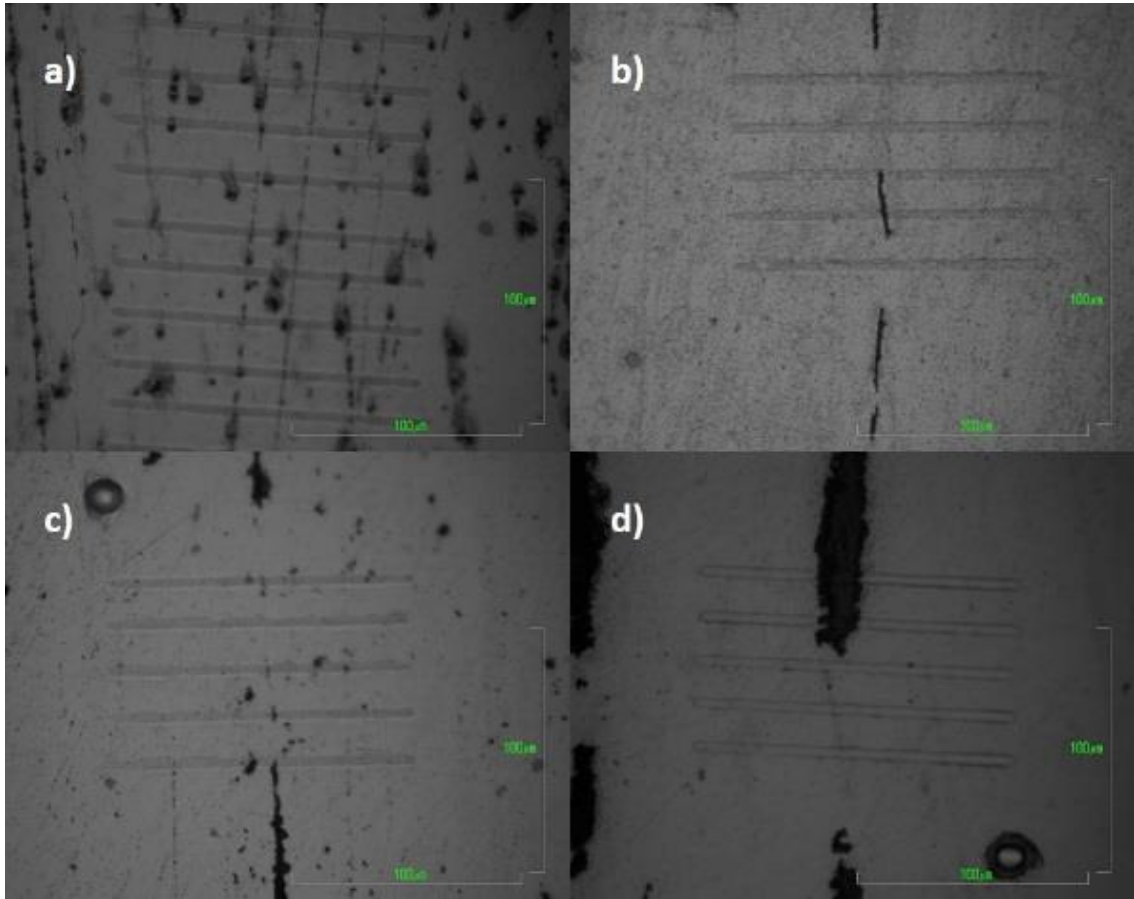


Figure 3-39: Nano-scratch tests in the study zones for all Mg composites containing a) 0.0, b) 0.25, c) 0.5 and d) 1.0 wt.% of MWCNTs.

3.5.3 In situ TEM testing characterization and crack growth

In this section, in situ TEM mechanical testing results will be discussed. Figure 3-40 shows sequence images for the micro-cantilever deformation and cracking propagation in a flexion test of a chevron type sample of a composite with 0,25 wt.% of MWCNTs. Images of the fractured TEM samples are shown in Figure 3-40, where “flow stress lines” are clearly seen as white lines, which is possible because highly stressed regions lead to change in the interplanar distance (elastic deformation) or localized dislocations movements. It is also clearly seen the regions where the stress raisers are located: both the tip-sample contact zone and the “V notch tip” are also clearly seen. In the frame 7 o Figure 3-40, the crack starts to grow at large beam deflections (beyond 200 nm) and part of the stresses are relieved because of the energy released during the crack propagation.

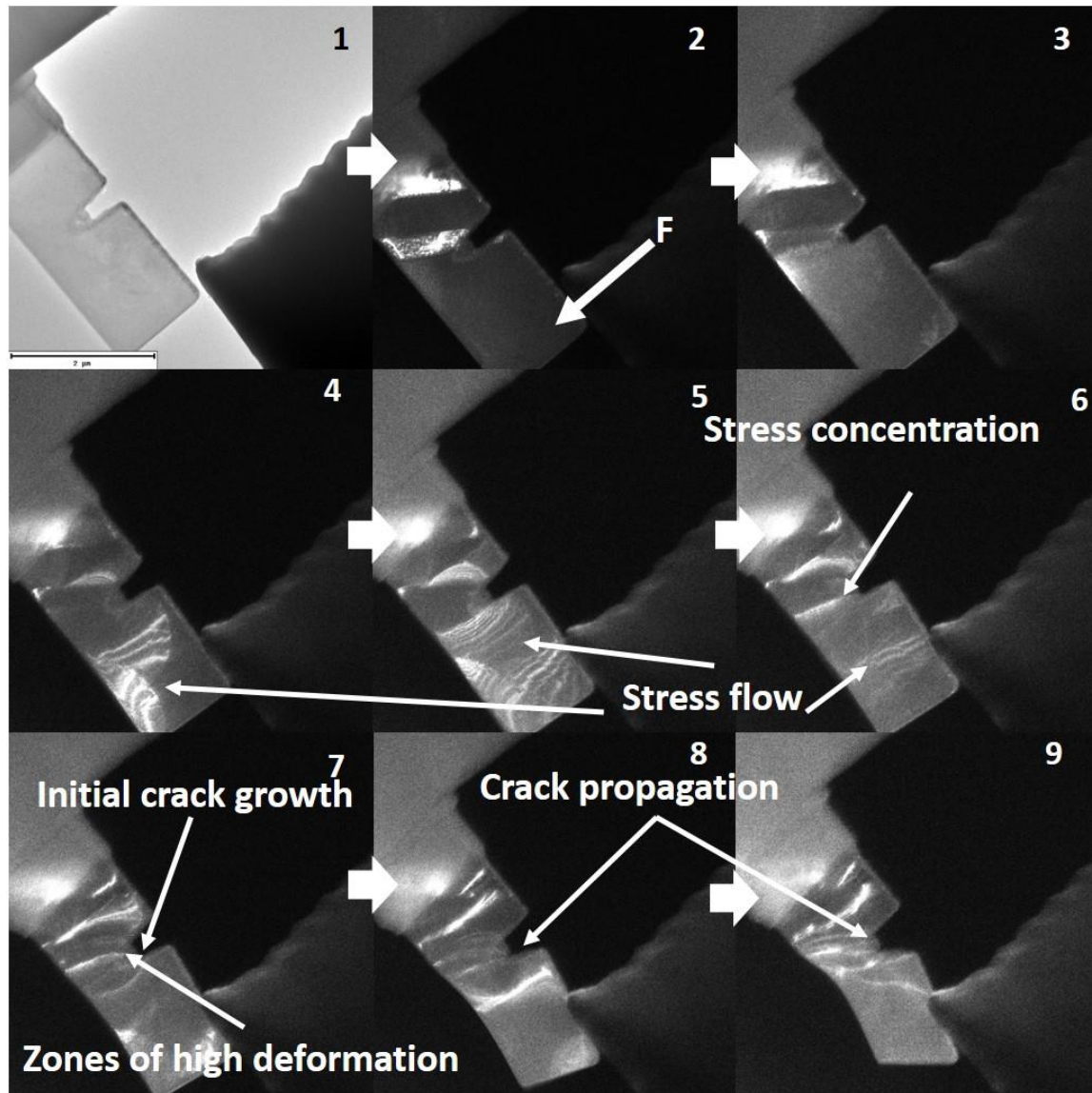


Figure 3-40: Frames images of the in situ test for the composite reinforced with 0.25 wt.% of MWCNTs

Ex situ fracture analysis, showed in Figure 3-41, allows identifying some crack growth characteristics that occurred during the micro-cantilever in situ testing. In Figure 3-41a and Figure 3-41b is clearly seen the deformation bands due to the dislocations movements concentrated near to the notch, because it acts as a strength raiser. In addition, after the initial crack started to grow, the crack continued its movement following these deformation bands. Detailed images of the failed zone (tagged as failure in Figure 3-41b), are shown in

Figure 3-41c and Figure 3-41d (These images were obtained after the cantilever was completely broken, this process was done manually), contrast image allows identifying different phases such as magnesium, magnesium oxide and some MWCNTs at the walls of the crack. The crack path was between Mg and MgO grains (intergranular fracture). This fact was verified by HRTEM images for the crack path in the composites reinforced with 1.0 wt.% (Figure 3-45), in other words, the MWCNTs had different failure behavior such as some deformed and fractured MWCNTs.

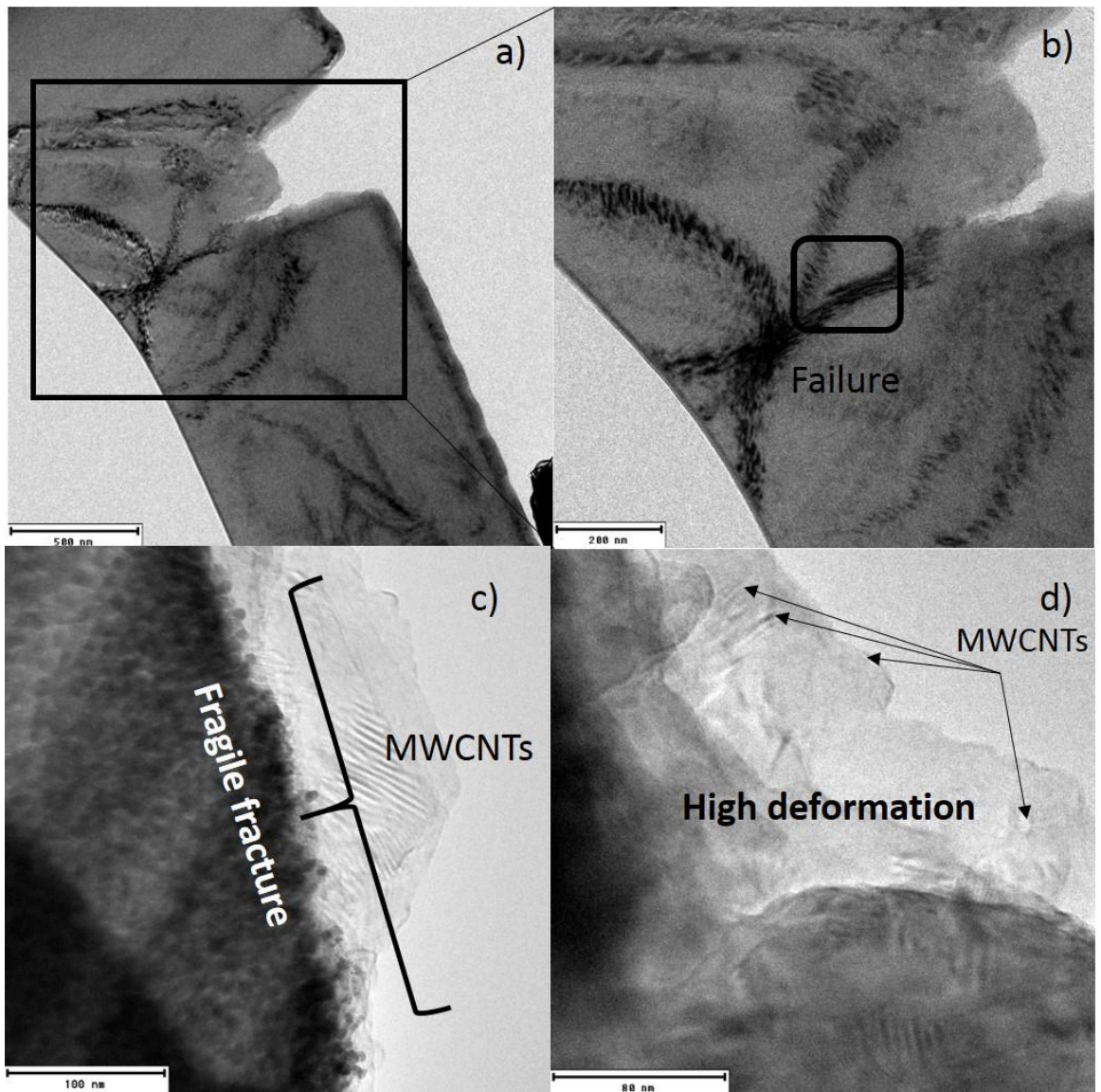


Figure 3-41: Ex situ fracture analysis for the composite reinforced with 0.25 wt.% of MWCNTs.

Dark field images of the crack evolution for the composites reinforced with 0.5 wt.% of MWCNTs are shown in Figure 3-42. As was discussed before, it is possible to identify the flow stress from the end of the micro-cantilever to the notched position. At large beam deflections (beyond 143 nm), the crack initiation took place (frame 4) and its path was parallel to the transversal section to the micro-cantilever. Note that the notch was not sharp enough to start a crack in that tip.

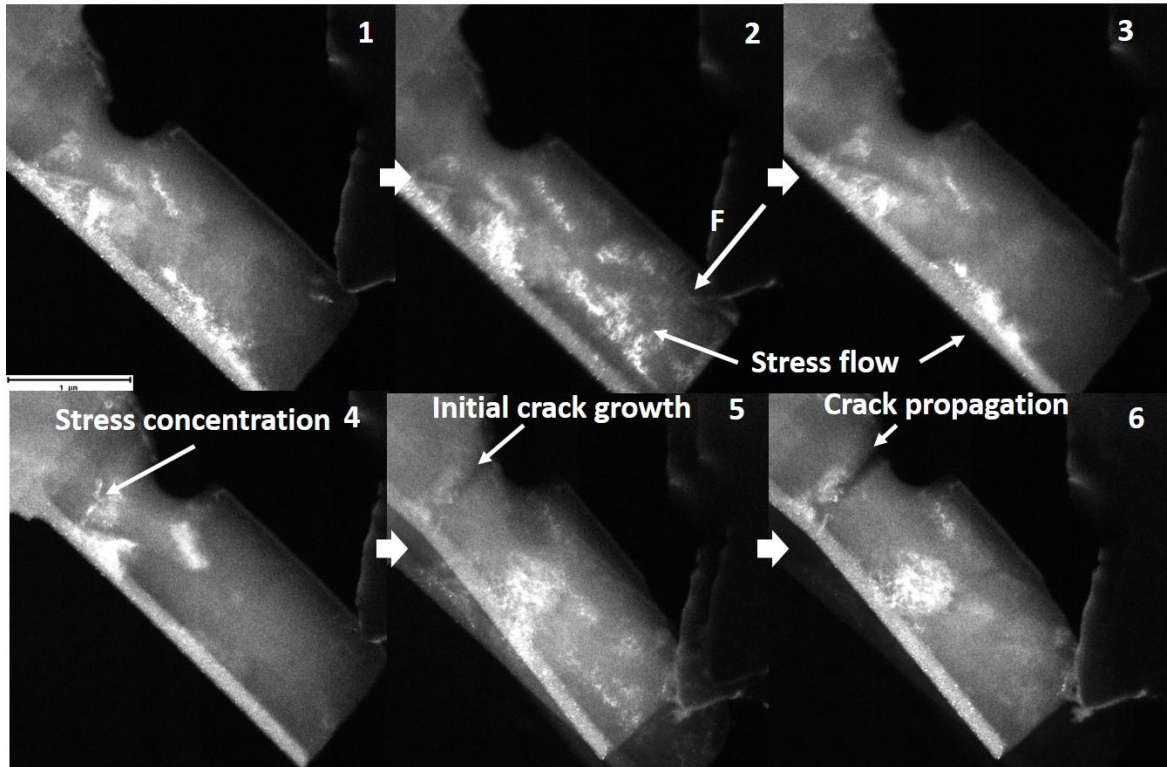


Figure 3-42: Frames images for the in situ testing for the composite reinforced with 0.5 wt.% of MWCNTs.

Ex situ fracture analysis for the composite reinforced with 0.5 wt.% is shown in Figure 3-43. Similar to the composite having 0.25 wt.% of MWCNTs, the fracture had a ductile and brittle behavior and some MWCNTs presented deformation and fracture, i.e. they were broken during the in situ testing.

The composite reinforced with 1.0 wt.% of MWCNTs (Figure 3-44 and Figure 3-45) has a similar behavior showed in the previous composites analyzed. However, dark field images show different grain sizes in the sample, which could be due to the higher MWCNTs percentage that allows a better-recrystallization process during the composite

manufacturing. At large beam deflections (beyond 189 nm), the crack propagation was sudden (Frame 5, Figure 3-44) and its path was parallel to the transversal section to the micro-cantilever.

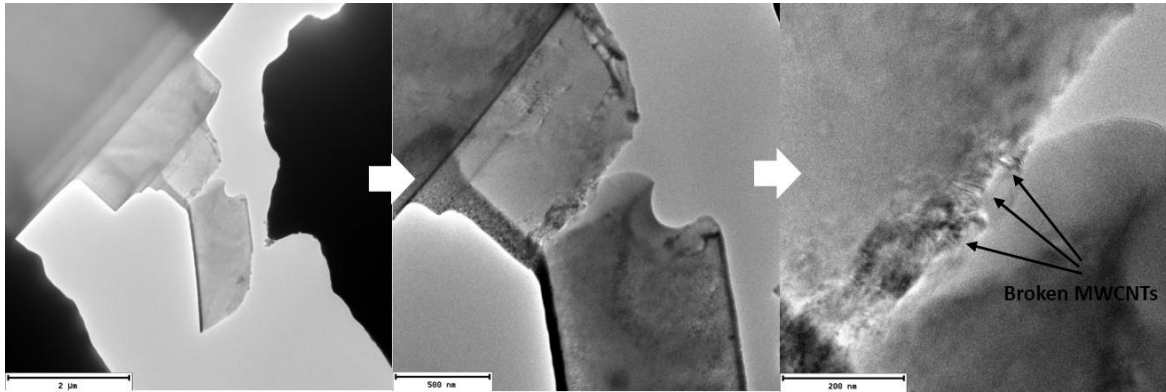


Figure 3-43: Ex situ fracture analysis for the composite reinforced with 0.5 wt.% of MWCNTs.

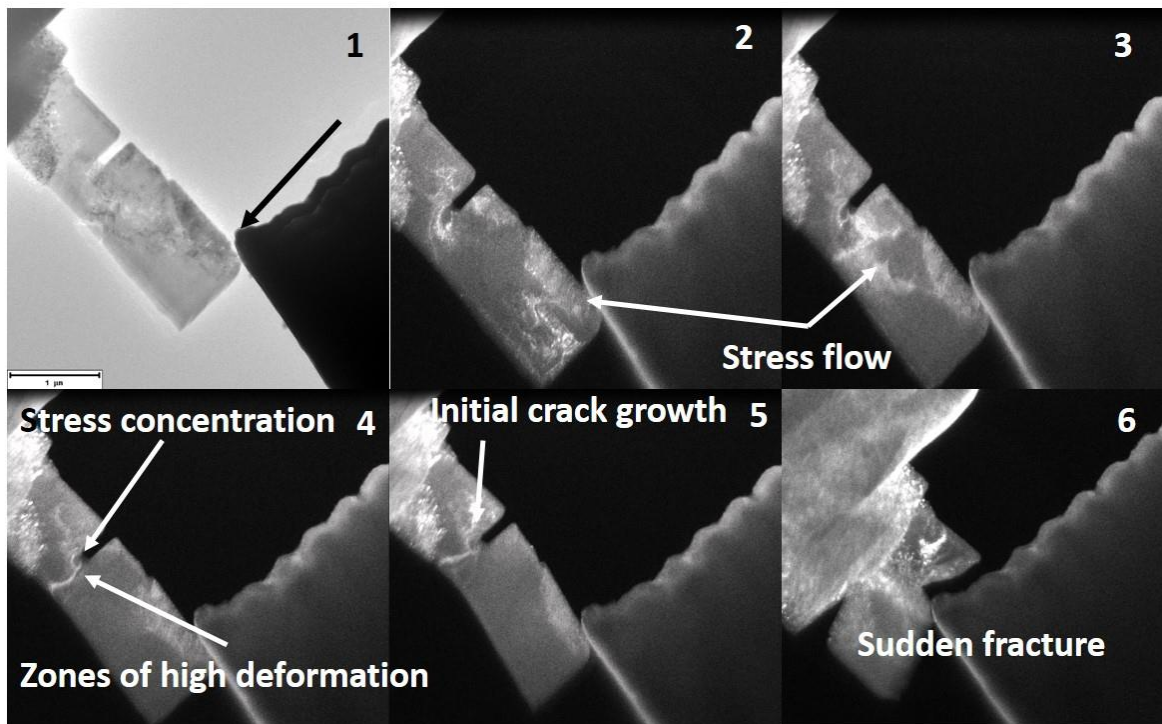


Figure 3-44: Frames images of the in situ testing for the composite reinforced with 1.0 wt.% of MWCNTs.

HRTEM images and TEM images were done in the fracture zone after in situ test for the composite reinforced with 1.0 wt.% of MWCNTs and results are shown in the Figure 3-45

shows fracture path, where it is clearly seen that the crack moved through the grains borders between Mg and MgO grains. This statement was corroborated by the diffraction patterns obtained close to the fracture zone (Figure 3-45 DP). Additionally, it can be seen some MWCNTs are damaged due to both, the FIB process and in situ bending test. (For example in Figure 3-45 DF detail 2 is possible to see the imperfect MWCNTs due to the FIB process, in that image the MWCNT is deformed and only show a one wall, and finally, in Figure 3-45 is possible to identify the damage of MWCNTs due to the bending process, in the image the MWCNTs are broken). The dark field images (DF detail 1 and Df detail 2) close to the fracture zone show the recrystallized grains and some MWCNTs sheets.

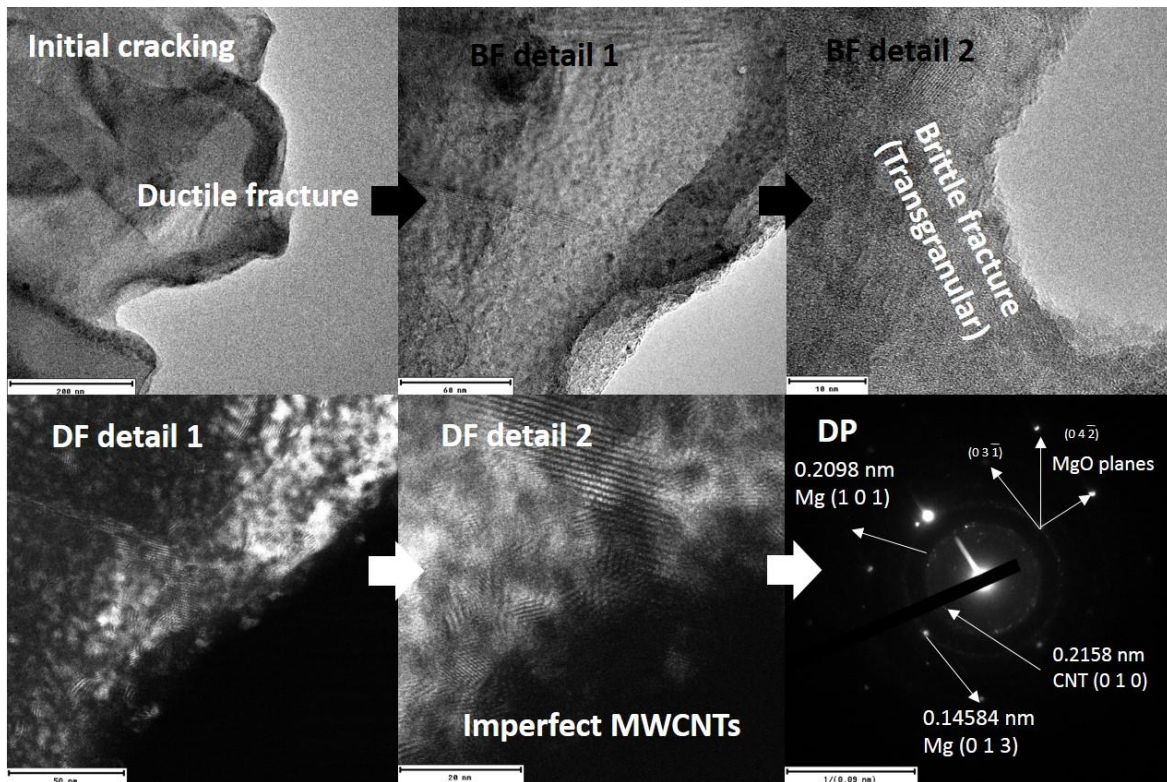


Figure 3-45: Ex situ fracture analysis for the composite reinforced with 1.0 wt.% of MWCNTs. BF: Bright field, DF: Dark field and DP: Diffraction pattern.

3.5.4 Fracture toughness analysis

Using the methodology for the fracture toughness measurement shown in section 2.6.2, the calculation for all composites studied will be presented in this section:

The fracture toughness K_{IC} was evaluated using Equation 2-3

$$K_{IC} = \frac{F_{max}L}{BW^{\frac{3}{2}}} F\left(\frac{a}{W}\right)$$

Figure 3-46 shows the sample geometry and some parameters involved in Equation 2-3, F_{max} corresponds to the maximum load when the crack growth is out of control and F is the function of the geometry of the sample and the notch (Equation 2-4).

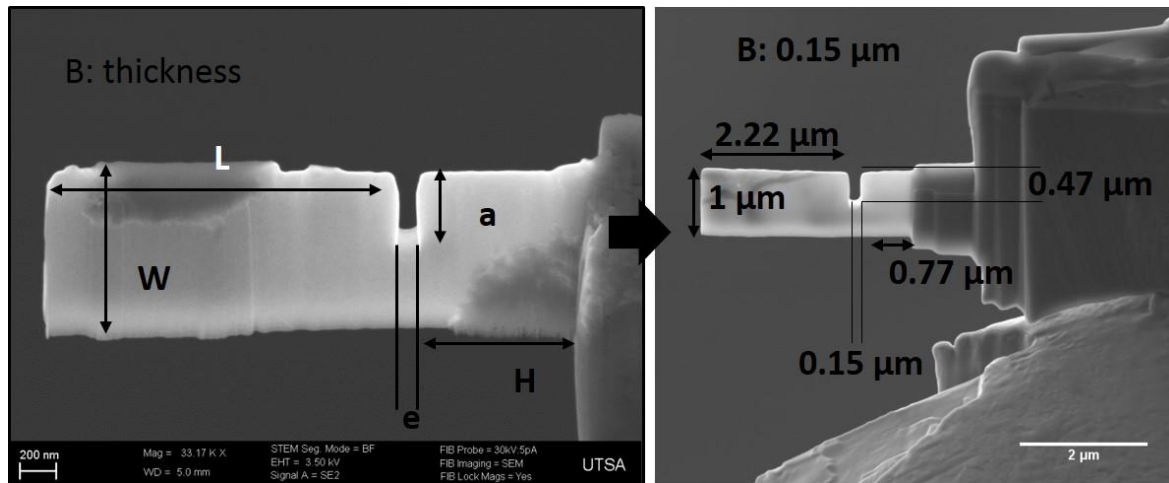


Figure 3-46: Nano-cantilever beam for the K_{IC} in situ test

In order to obtain the fracture toughness, it is required to introduce a perfectly sharp pre-crack at the sub-micrometer scale, which is a challenging task at such small dimensions. Furthermore, the FIB used for this kind of geometry could produce heterogeneous notch and thickness during the sample fabrication, which can bias the results and give overestimated values of the fracture toughness. However, a direct comparison among different composites produced can help to understand the fracture toughness changes caused by the MWCNTs added to the magnesium matrix. Here it is important to mention that the measured values correspond to the samples extracted from the MWCNTs rich region, i.e. to the interface between the magnesium sheets, and do not corresponds to the overall behavior of the composite. This last behavior will be explored in next section.

Table 3-3 summarizes the fracture toughness values for all samples, as well as the parameters used for those calculations. The value of the fracture toughness was 17.21, 21.04 and 20.13 $\text{MPa}\sqrt{m}$ for the composites reinforced with 0.25, 0.5 and 1.0 wt.% of MWCNTs, respectively. The micro-cantilever tests suggest a dependency of the fracture toughness with the MWCNTs content. This change in the fracture toughness is due to the different strengthening mechanisms such as grain size, dislocation activity and the reinforcement action. However, it is not clear if the values for fracture toughness are underestimated or overestimated because the notch does not have the correct geometry for this type of tests, there is no pre-crack as the standard stipulates, the mechanisms of plasticity are not included in the calculation (note that our case is a mixture of plastic and brittle failure) and there are no reference values for this type of material, although for Mg a value of 20 $\text{MPa}\sqrt{m}$ have been previously reported.

Table 3-3: Parameters and fracture toughness after in situ testing.

Sample	L (μm)	W(μm)	B (nm)	a(μm)	F (nN)	Fracture Toughness ($\text{MPa}\sqrt{m}$)
Mg-0.25 wt.%	1.80	0.90	151	0.50	19450	17.21
Mg-0.5 wt.% (notch without good shape)	2.22	0.90	150	0.65	17480	21.04
Mg-1.0 wt.%	2.0.	0.95	151	0.53	22000	20.13

Figure 3-47 shows a schematic illustration of the main mechanisms involved in the control of the MMCs' fracture toughness according to the literature, these include different damage mechanisms, being one of them the zone close to the notch which act ahead of the crack tip to promote crack advance (Zone with high plastic deformation, microvoid due the high stress in that zone and cleavage in some cases) and below the crack-tip-shielding mechanisms, which primarily act behind the tip to impede the crack growth.

Intrinsic toughening essentially comes from plasticity and enhances a material's inherent damage resistance. For all composites, the in situ tests (Figure 3-40, Figure 3-42 and Figure 3-44), showed evidence of plastic deformation (Figure 3-41b). Plastic zones are evidenced through the dislocations movement. The dislocation structure in notched bending samples is illustrated in Figure 3-47b, where the dislocations emitted from the

crack tip move away from the crack tip. Dislocations are expected to be piled up at the neutral axis of bending, as they perceive a repulsive force due to the existence of a region of compressive stresses in the cantilever's bottom side, thus increasing the strength of the material.

On the other hand, the nano-sized grain size (Mg and MgO) also contributes to increase the strength while MWCNTs enhances the resistance to crack propagation. In the last section, broken MWCNTs were shown after in situ testing. No debonding was detected between the metal matrix and MWCNTs allowing inferring a good interface between them. Finally, it was not detected the interphases presence between magnesium and MWCNTs.

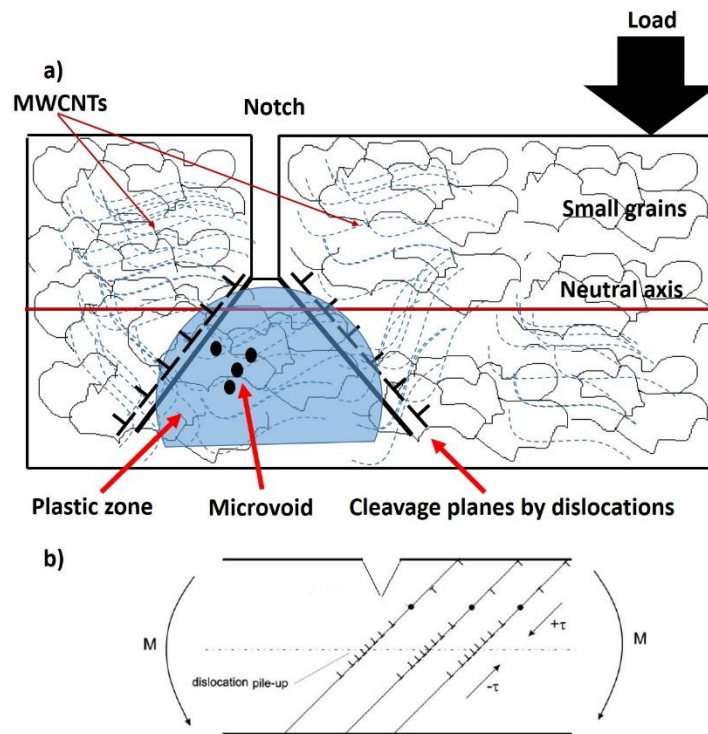


Figure 3-47: a) Schematic illustration showing how strength and fracture behavior can be considered in terms of intrinsic (plasticity) versus extrinsic (shielding) toughening mechanisms associated with crack extension and b) schematic illustration for dislocation pile up at the neutral axis.

3.5.5 Bulk mechanical testing in the composites

Results of the tensile tests using samples described in section 2.6.1 are shown in Figure 3-48. It can be observed that the addition of MWCNTs significantly improved the yield

strength, ultimate tensile strength and elastic modulus. These outstanding properties can be only explained if a good interfacial bonding between MWCNTs and matrix exists. From these findings it can be inferred that a good load transfer from the matrix to the MWCNTs was achieved, due to a good dispersion and a very good interface between magnesium and MWCNTs as was discussed in previous sections. It is also mandatory a good interaction between the magnesium layers and the “reinforced” layers, this in part is obtained because of the diffusive process, so a gradual transition of properties, especially of elastic modulus was obtained.

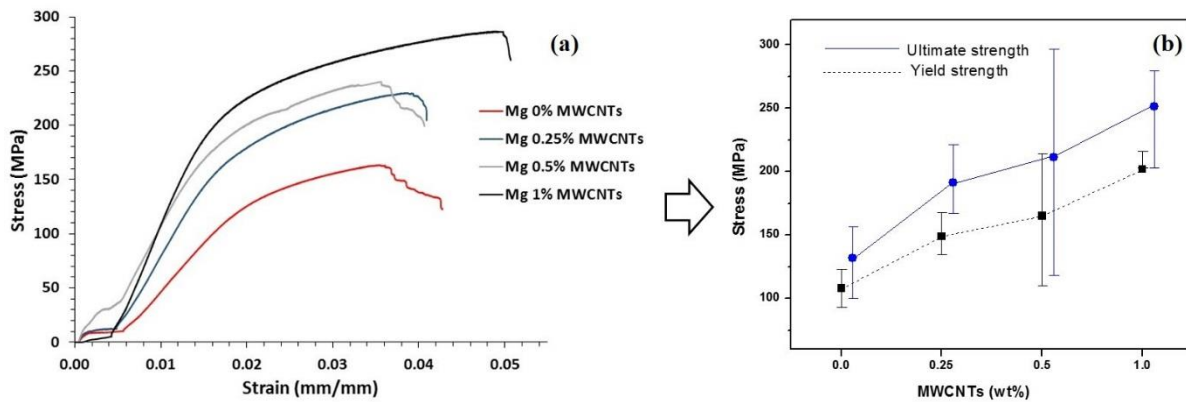


Figure 3-48: Mechanical properties by tensile test for the composites: a) stress-strain curves and b) ultimate and yield strengths.

Despite the fact that during the manufacturing process, few pores were identified the mechanical properties of the composites always increased with the addition of the MWCNTs. This shows the efficiency of the sandwich technique for producing metal matrix composites reinforced with CNTs. These results have the same behavior than those showed in Figure 3-37 by nanoindentation; i.e. the reinforced zone in the composites has the same effect on both the bulk- and nanomechanical properties.

Further, the yield (and also the ultimate tensile strength) is proportional to the hardness ($H = K\sigma_Y$). This equation is called the Tabor's relationship [114], where the constant K has not yet been established for the Mg reinforced with CNTs. However, for the reinforced layers, assuming a value of 2.71 for magnesium alloys, the mean yield stress can be estimated.

Based on these results, an additional advantage of the sandwich technique is that, it allows designing the overall behavior of this type of material, controlling both the magnesium thickness and the CNTs content. The increase in the mechanical properties with the addition of MWCNTs, at both bulk (Figure 3-48) and small-scale (Figure 3-37) levels, demonstrates once again the effectiveness of the sandwich technique for manufacturing metal matrix composites reinforced with CNTs.

3.5.6 Cracking characterization after tensile testing

SEM images analysis was done on a representative cross section (fracture in the neck zone) for all composites submitted to tensile test, in order to obtain a qualitative evaluation of damage of the samples evaluated, as well as providing a mean for measuring visible damage features. Figure 3-49 shows both interlaminar fracture between magnesium sheets and intralaminar. Figure 3-50 shows a close up to the fracture zone. This behavior was similar for all composites studied.

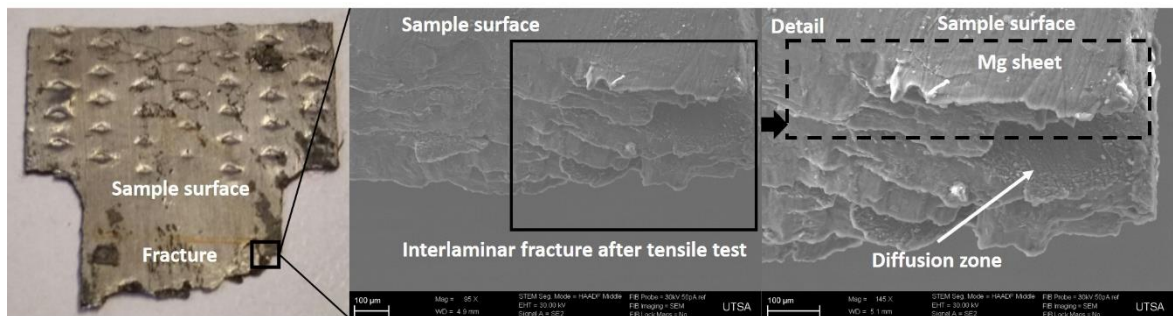


Figure 3-49: Interlaminar fracture in the composites studied.

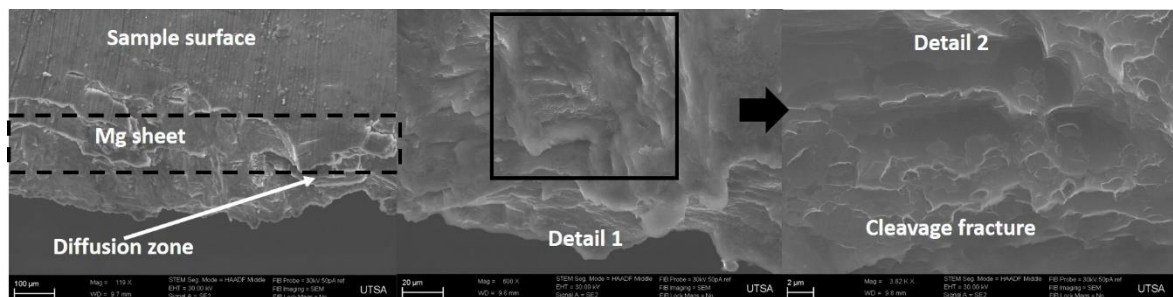


Figure 3-50: Fracture mechanism for magnesium sheets in the composites studied.

Figure 3-51 to Figure 3-53 show representative images of the fracture in the composite reinforced with 0.25, 0.5 and 1.0 wt.% of MWCNTs, respectively after tensile test. In the diffusion zone multiple cracks are shown in Figure 3-51a and its detail 2. These multiple cracks show brittle fractures as shown in Figure 3-51b and details. This phenomenon is due to the different grains size and phases found (Mg, MgO and MWCNTs). The detail 2 of Figure 3-51b, where a MWCNT was not pulled-out from the matrix, i.e. no debonding occurred between the MWCNT and the surrounding metal matrix. This implies that there is good MWCNTs/metal matrix bonding as was discussed in HRTEM section. This last fact could be in detrimental of toughness and in favor of tensile strength.

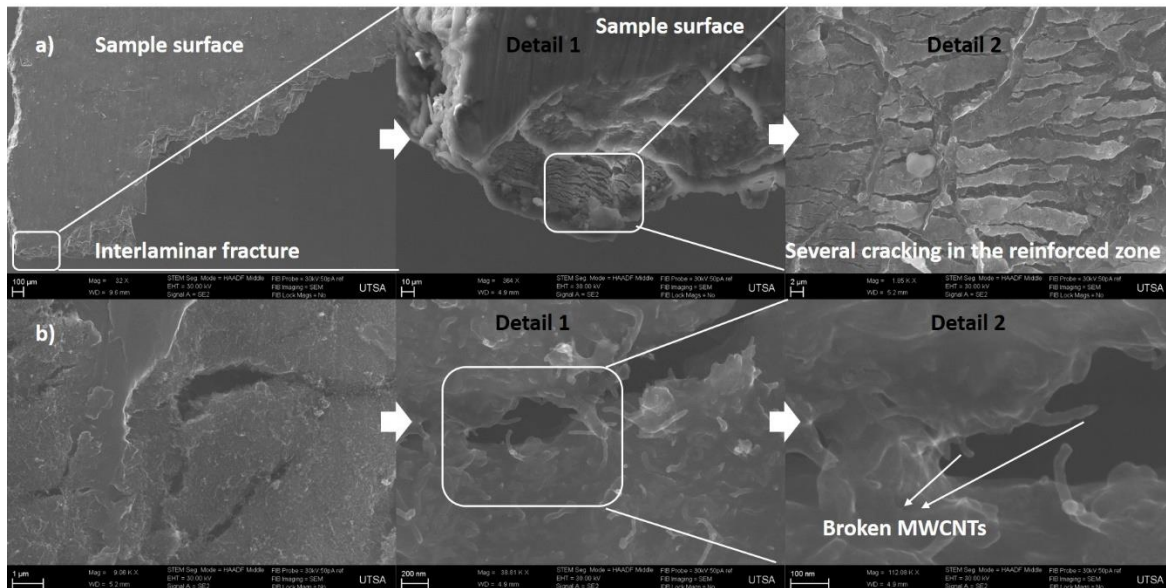


Figure 3-51: Tensile Fracture for the composite reinforced with 0.25 wt.% of MWCNTs.

Figure 3-52a and Figure 3-52b show tensile fracture images for the composites reinforced with 0.5 wt.% of MWCNTs. The behavior is similar to that of the composite reinforced with 0.25 wt.% of MWCNTs exhibiting a interlaminar failure between magnesium sheets and reinforced zones. It is possible to identify multiple fractures in the diffusion zone (detail of Figure 3-52b), in addition to broken MWCNTs close to the fracture, which allows to infer that there was a good load transition between the reinforcement and the metal matrix. Figure 3-53 shows the images for the composite reinforced with 1.0 wt.% of MWCNTs, whose fracture behavior is similar to that of the other composites analyzed. However, this composite present a good plastic deformation (Figure 3-48) due to a better recrystallization

process during the composite fabrication, i.e. there is a greater amount of small grains around the MWCNTs driven by the higher MWCNTs content.

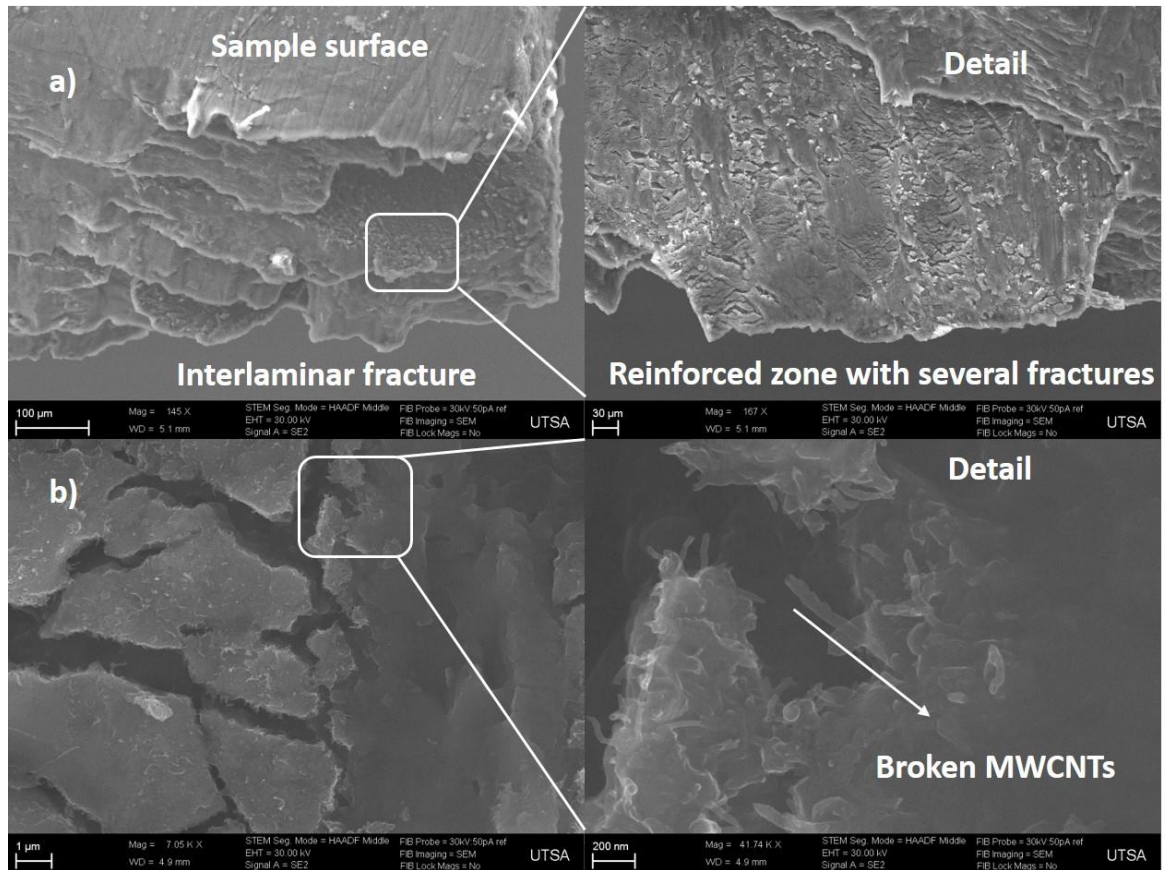


Figure 3-52: Tensile Fracture for the composite reinforced with 0.5 wt.% of MWCNTs.

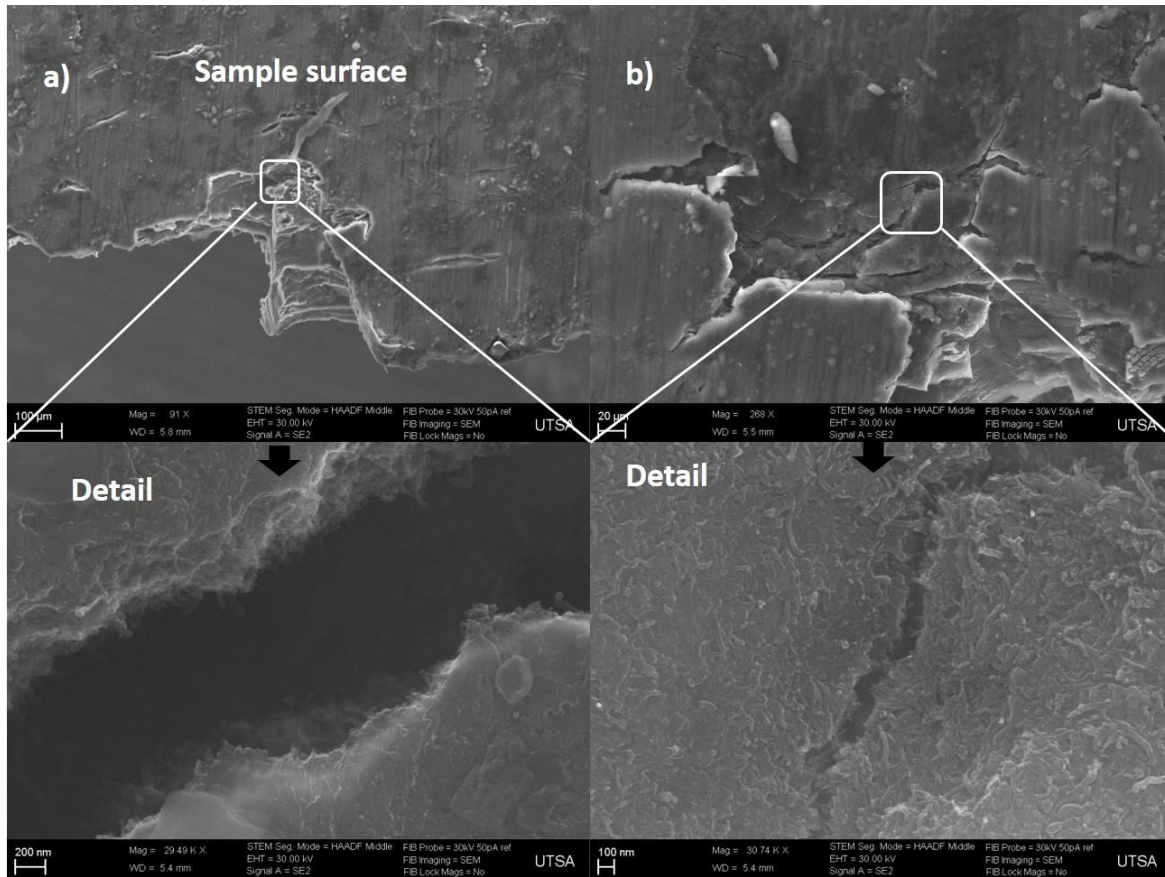


Figure 3-53: Tensile Fracture for the composite reinforced with 1.0 wt.% of MWCNTs.

In summary, according to the results of the fracture analysis achieved in this work, the composites fabricated and tested consist of a metal matrix with a brittle behavior and a reinforced zone with an elasto-plastic ductile behavior. In these materials, there are different dissipative mechanisms that influence the fracture behavior. One of these mechanisms is the sliding of planes due to the crystal structures, namely cubic and hexagonal, present close to the interface between magnesium sheets. Another mechanism is the microcracks nucleated during the deformation process in the tensile test. These different mechanisms act by changing the fracture toughness in the bulk composites.

3.5.7 Theoretical models for metal matrix composites

The elastic modulus of the MWCNTs was measured by the micro-Raman spectroscopy method, after Lourie and Wagner [115]. The method is used to monitor the cooling-induced compressive deformation of carbon nanotubes embedded in a PVA matrix. Young's modulus of multi-walled carbon nanotubes may then be derived from a concentric cylinder model for thermal stresses, using the D^* -band shift for each tube type.

Raman spectra were obtained using a Renishaw Ramascope equipped with a Linkam THMS 600 cooling cell. The incident laser beam was focused onto the specimen surface through an X50 objective lens, forming a laser spot of approximately 5 μm in diameter. PVA/MWCNTs composites were quenched for producing a compressive stress in the MWCNTs. The cooling was done by injecting nitrogen gas from a liquid nitrogen reservoir through the thermally isolated cooling cell. The temperatures used in the experiments were -180°C , -150°C and 22°C , using a cooling rate of $20^\circ\text{C}/\text{min}$.

The Raman spectra for all materials studied are shown in Figure 3-54, where the principal Raman peaks for the PVA, MWCNTs and PVA/MWCNTs are identified. The principal peak of the PVA is at a frequency of 2911.14 cm^{-1} , which does not interfere with the MWCNT D^* -band shift, whose peak is at frequency of $\sim 2700\text{ cm}^{-1}$; that is located for measuring the displacement due to the cooling process.

For the MWCNTs calculation, the displacement of the D^* -band was measured before and after the cooling process. For the PVA/MWCNTs, a shift of the D^* -band of 6 cm^{-1} to higher frequencies was observed after a quenching process at -180°C (Figure 3-55). Since the shift occurred toward higher frequencies, this is interpreted as a compression of the C–C bonds [116], which must result from the contraction of the PVA upon polymerization, which in turn reflects the cooling stresses generated by the contraction of the PVA.

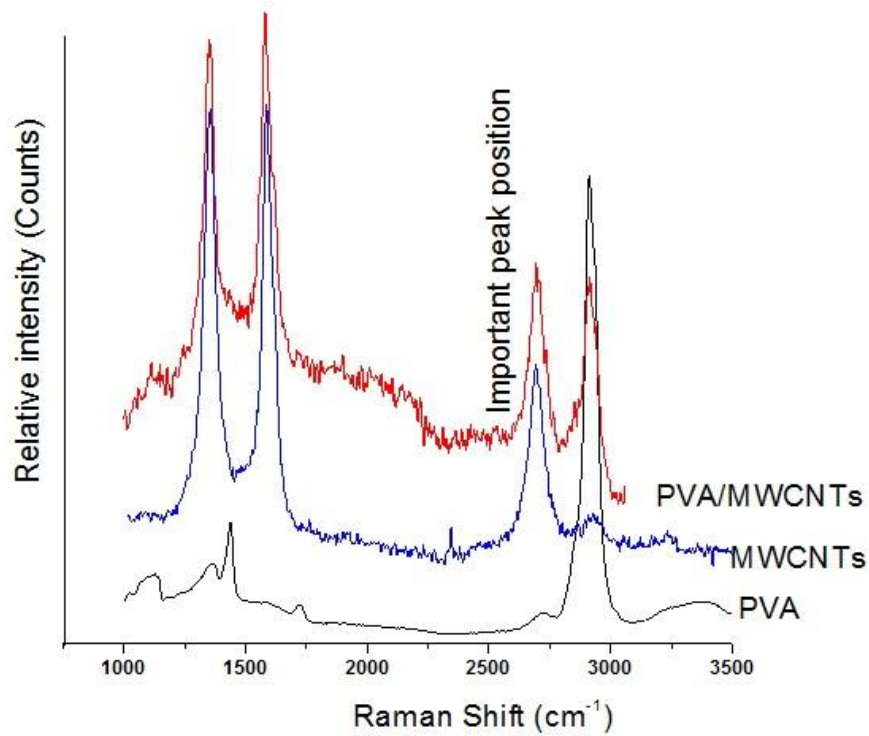


Figure 3-54: Raman spectra for PVA, MWCNTs and PVA/MWCNTs.

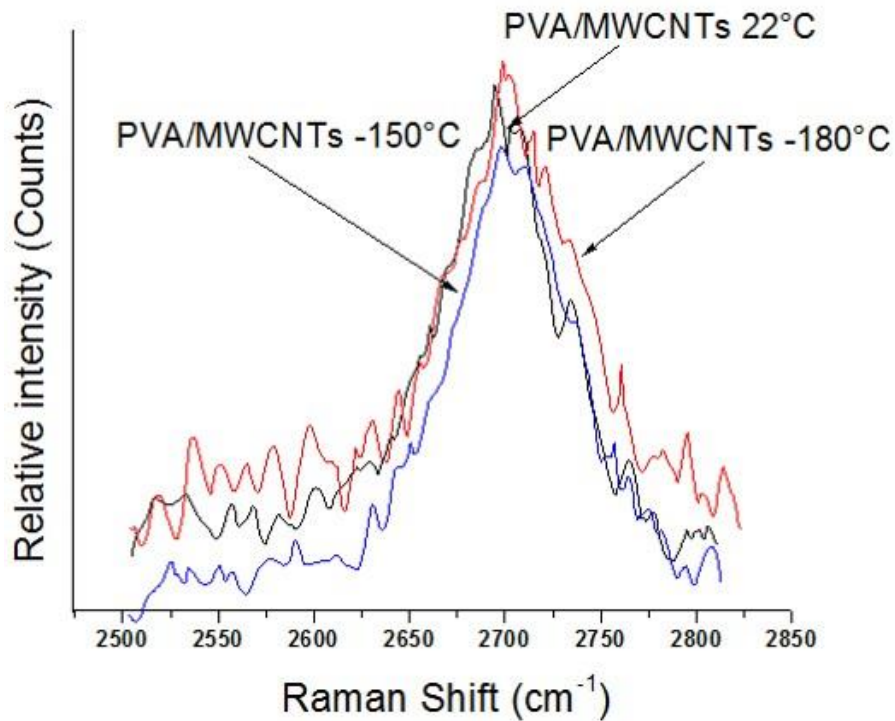


Figure 3-55: Effects of embedment and cooling on the frequency shift of the D*-band

With the information generated above and taking into account the following considerations: a) the linear dependence between the band shift and temperature explained in reference [115] and b) the correlation between the band shift and the bond length shortening [117], the compressive strain of the nanotube is $\varepsilon_{cnt} = -\frac{\Delta l}{l} = \frac{\Delta w}{w}$, (where l is the bond length and w is frequency, and this expression is an approximation). In that way, Equation 3-1 can be formulated.

$$\varepsilon_{cnt} = -\left(1 - \frac{w_o}{w_q}\right) \quad \text{Equation 3-1}$$

where, w_o and w_q are bond frequencies before and after quenching, respectively. Using a concentric cylinder model described in reference [118] the axial tube stress due to the cooling is given by Equation 3-2.

$$\sigma_{nt} = \frac{\Delta\alpha\Delta T}{1 + \frac{Vf_{cnt}(E_{cnt})}{Vf_m(E_m)}} E_{cnt} \quad \text{Equation 3-2}$$

where $\Delta\alpha$ is the difference between expansive coefficients for MWCNTs and PVA, ΔT is the difference between initial and final temperatures, Vf_{cnt} and Vf_m are the volumetric fraction in the composites for MWCNTs and PVA, respectively. Finally, E_{cnt} and E_m are the elastic moduli for the MWCNTs and PVA matrix, respectively. In that way and using the Hooke law is possible, calculate the elastic modulus for MWCNTs by Equation 3-3. whose result is given in Table 3-4. Note that the calculated value is within the range reported by others authors (Table 1-1).

$$\sigma_{nt} = \frac{\Delta\alpha\Delta T}{1 + \frac{Vf_{cnt}(E_{cnt})}{Vf_m(E_m)}} E_{cnt} \quad \text{Equation 3-3}$$

Table 3-4: Parameters and elastic modulus for MWCNTs used in this research.

ΔT K	$\Delta\alpha$ K ⁻¹	Vf_{cnt}	E_m (GPa)	E_{cnt} (GPa)
-202	0.000074	0.0021	0.3	881±105

With this result and using the elastic modulus of magnesium, the theoretical elastic modulus for the reinforced zone (equations of section 1.3.1, Equation 1-1) was calculated. These values are compared with the experimental values measured by nanoindentation (Fig. 3.37), which because of the load used during indentation are representative of a small

region (about $1 \mu\text{m}^3$), For these reason predicted values must be compared with the maximum experimental values measured by nanoindentation. Results are shown in Figure 3-56 showing a good agreement between theoretical and experimental results. The volumetric fractions were calculated using the rule of mixture in the reinforced zone and the values were 0.014, 0.028 and 0.056 for the composites reinforced with 0.25, 0.5 and 1.0 wt.% of MWCNTs in the magnesium matrix. The graphs show that the addition of MWCNTs results in an increase of the elastic modulus and stress for all MWCNTs contents, compared with the values of the AZ31B magnesium alloy. These results are in agreement with the dispersion degree measured in the PVA/MWCNTs and Mg/MWCNTs composites, i.e. a good dispersion degree allows a good strengthening in the composites fabricated.

The composite ultimate strength was also possible to be predicted by the mixture rule; however, this model does not take into account the several mechanisms (dislocation staking, interfaces and grain sizes) previously discussed (Figure 3-56b). In this case the model was applied considering three laminas of Mg and two of reinforced zones, the ultimate strength reinforced lamina was obtained using the tabor's equation ($S_u=2.7 \cdot H_v$), where S_u is the ultimate strength, H_v is the hardness and 2.7 is the Tabor factor for Mg. The predicted values were compared with those obtained in microtensile tests (Table 3-5). Result show that predicted values are overestimated, which is clearly due to the non-inclusion of hardening mechanisms and strengthening of the composite and also probably to the unsuitability of Tabors equation for the reinforced zone. For this reason, a different approach to calculate the strength of the reinforced lamina will be shown below.

Table 3-5: Results for Ultimate strength by Tabor's equation. The ultimate strength for Mg matrix is 307 MPa.

Sample	Hardness (Hv)	Su (tabor's equation)	Ultimate strength by rule mixture
0.25 wt.%	509	1374	413.7
0.50 wt.%	713	1925	468.8
1.00 wt.%	917	2475	523.6

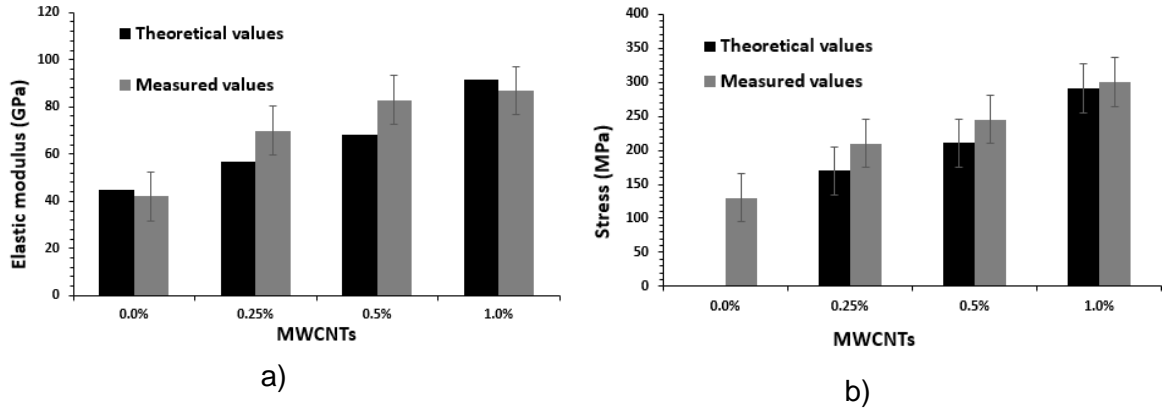


Figure 3-56: Experimental and theoretical values a) elastic modulus and b) stress for all composites studied.

The strengthening by interface described in section 1.3.1, Equation 1-8, the strength of the composites was calculated. However, in this case, the interphases between metal matrix and metal matrix were not found in TEM images. For the calculation the following assumptions were applied to perform the calculation: The shear stress for the interphase was assumed as the shear stress for the basal plane at the interface (inferred by HRTEM analysis), and the thickness of the interphase was assumed as the grain size at the interface.

As was described in section 3.4.1 the preferential crystal orientation at the interface with the basal plane with an angle of 45° with respect to the MWCNTs walls. The theoretical prediction are shown in Figure 3-57, which compared with calculated values by Tabor's equation. For these predictions, the shear stress used were 0.81 MPa for basal plane, in a single crystal.

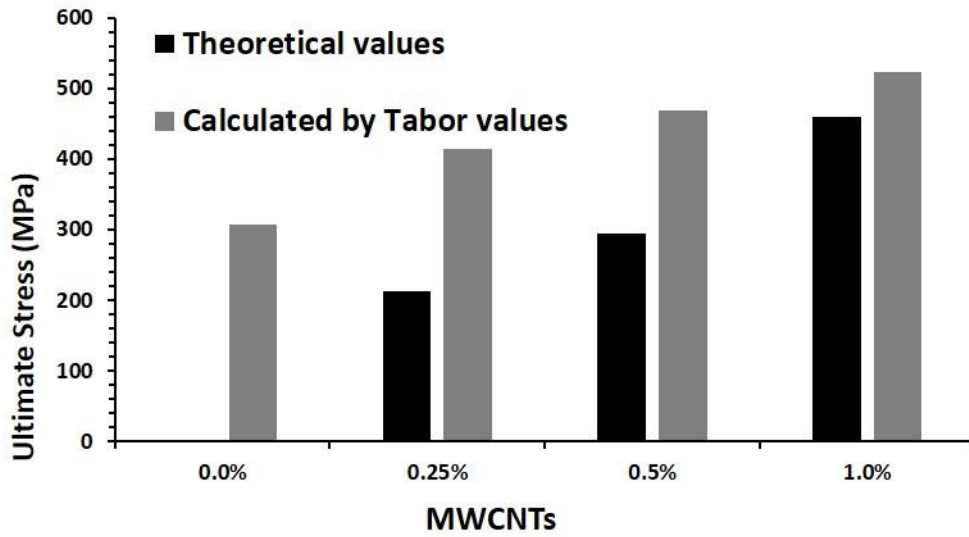


Figure 3-57: Experimental and theoretical values for ultimate stress for all composites studied in the basal crystal orientation.

The theoretical stress for the reinforced laminas are now used in conjunction with the rule of mixtures to predict the ultimate strength. Theoretical results are in agreement with experimental ones, which shows that the interface around the MWCNTs (which is just magnesium with its unitary cell oriented in a preferential direction) plays an important role in the overall mechanical behavior of the composite.

On the other hand, for ensuring a good load transfer between MWCNTs and the metal matrix, it is necessary to have a critical length of the reinforcement. In this work, the critical value was $0.46 \mu\text{m}$ and the MWCNTs used in this study are $30\text{-}40 \mu\text{m}$ in length.

The fracture stress and Young's modulus were evaluated of through the in situ test. The bending stress, σ , on the beam top surface is given by the linear-elastic bending theory stated in Equation 3-4.

$$\sigma = 6 \frac{Fl}{BW^2} \quad \text{Equation 3-4}$$

with F as the applied load, l as the bending length, W as the cantilever beam width and B was the cantilever beam thickness. The fracture stress σ is calculated using the maximum

load at fracture. The Young's modulus E can be calculated from the load versus deflection data by the Equation 3-5: where δ is the vertical deflection.

$$E = \frac{4F}{\delta B} \left(\frac{l}{W} \right)^3 \quad \text{Equation 3-5}$$

Table 3-6 shows the values for the stress and modulus calculated during the micro-cantilever in situ test. In order to verify the validity and consistency of the data determined by the cantilever deflection technique, the Young's modulus was determined and compared with the modulus measured by the nanoindentation test, as it is the most sensitive parameter for inaccuracies of the measurement. As can be seen in Table 3-6, the value are very different, i.e. the values measured by in situ testing are underestimates. This may be because the calculation does not consider the additional deflection caused by shear stresses in short and thick cantilevers. Furthermore, the deformation of the support in the region around the beam end, which leads to a small rotation of the beam as a whole, is not included in the calculation. Moreover, as discussed in section 3.5.5, the geometry does not has the accuracy that this kind of test needs. According to this, the values for fracture toughness and elastic modulus are overestimated and underestimated, respectively. However, the test shows the mechanical behavior in a qualitative way and evidence the good mechanical properties of these composites.

Table 3-6: Parameters for in situ testing and calculated mechanical properties

Sample wt. %	l (μm)	W (μm)	B (nm)	F (nN)	Fracture toughness (MPa√m)	Max. Defl. approx. (nm)	Fracture stress (MPa)	Elastic modulus (GPa) - Calculated	Elastic modulus (GPa) nano indentation
0.25	1.8	0.9	151	19450	17.21	200	1717,44	54.16 – 40 nm	90
0.50	2.2 2	0.9	150	17480	21.04	143	1916,33	66.7 30 nm	98
1.00	2	0.95	151	22000	20.13	189	1937,22	61.7 – 40 nm	110

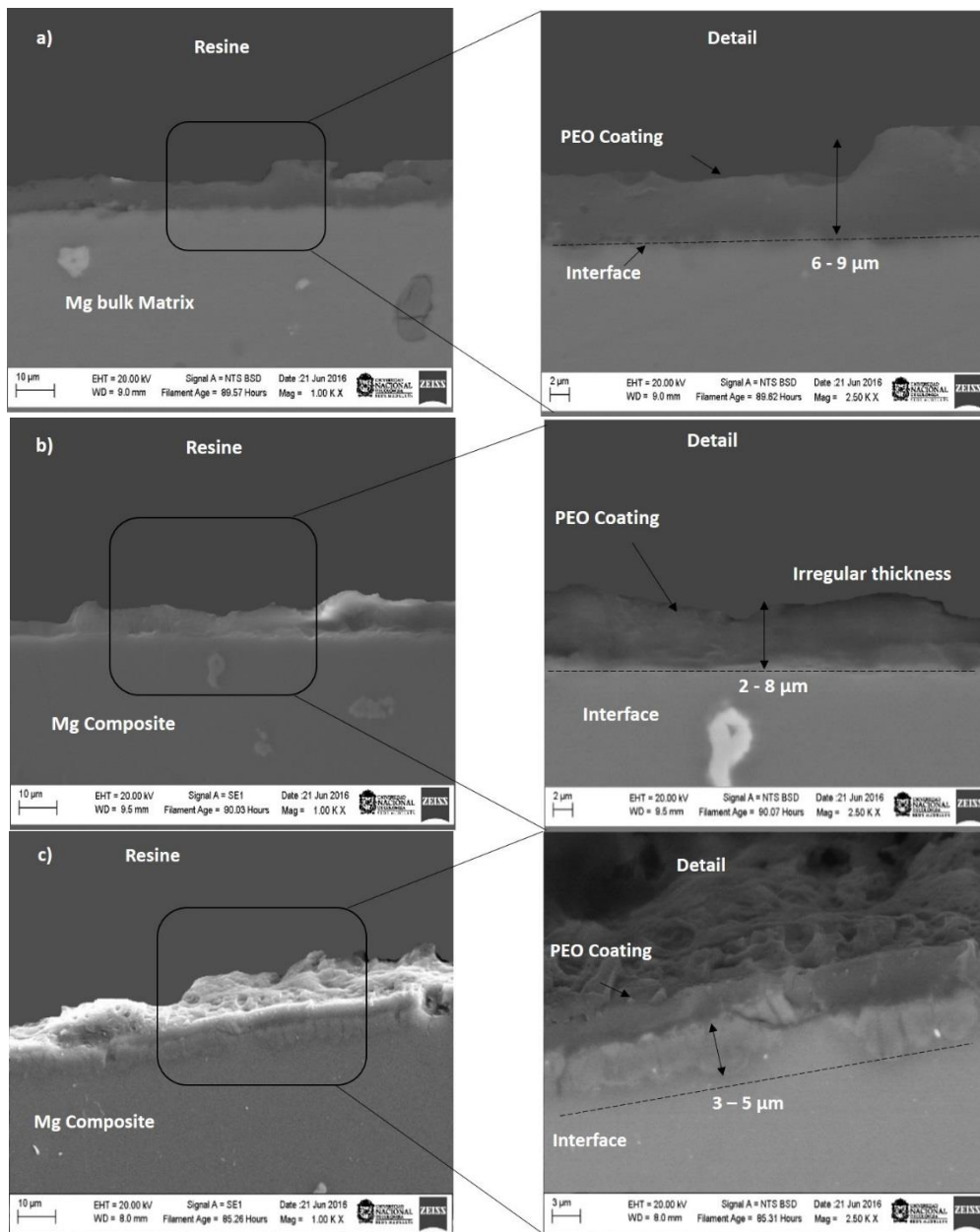
3.6 PEO coating characterization in metal matrix composites (additional work)

In this section, additional results about PEO coatings are reported and discussed, showing the possibility of using them in biomedical applications, especially for those in hard-tissue by functional coatings or films in the metal matrix composites fabricated by the sandwich technique.

3.6.1 Micros-structural and morphological PEO coating characterization

The PEO coatings deposited onto the bulk (0.0 wt.% of MWCNTs) and reinforced composites (0.25, 0.5 and 1.0 wt.% of MWCNTs) are shown in Figure 3-58; in all cases the conditions of the electrolytic process were held constant (time, concentration, pH, cell dimensions, electrode proximity and temperature), except the voltage. Coatings on both bulk material (Figure 3-58a) and the composite reinforced with 0.25 wt.% (Figure 3-58b) are quite similar, having a dense layer and a thickness between 2 and 9 μm ; besides, no noticeable micropores can be seen in the Si-O film [119]. The coatings deposited onto the composites reinforced with higher reinforcement percentages (0.5 and 1.0 wt.%) have a more porous layer, as shown in Figure 3-58a and d. Furthermore, the thickest coating was obtained for the 1.0 wt.% sample and micropores with different diameters in the Si-O film are also seen. The higher and homogenous coating thickness of the composite reinforced with 1.0 wt.% can be due to the fact that the MWCNTs percentage increases the voltage during the PEO process. It is clear that upon reaching a greater thickness of coating, the resistance increases and ohmically the voltage increases with the thickness until the coating reaches its dielectric limit, which varies with the concentration and pH of the electrolyte. However, local phenomena of dielectric rupture by the presence of defects that are generated in the layer, can be responsible for the porosity presence. At the same time, the carbon nanotubes can help to intensify the presence of these irregular pores, since they are themselves discontinuities for the diffusion of species. However, the MWCNTs, by their conductive nature, can contribute to increase the efficiency of the charge transfer in the oxide growth process, allowing ohmically that by increasing the concentration of these nanostructures, the thickness of the coatings increase [91]. Figure 3-59 shows an EDS analysis close to the coating, where a good diffusion of magnesium and aluminum in the

Si-O film is clearly seen. Notice that sodium was not detected, which may mean that it was not deposited in the coating.



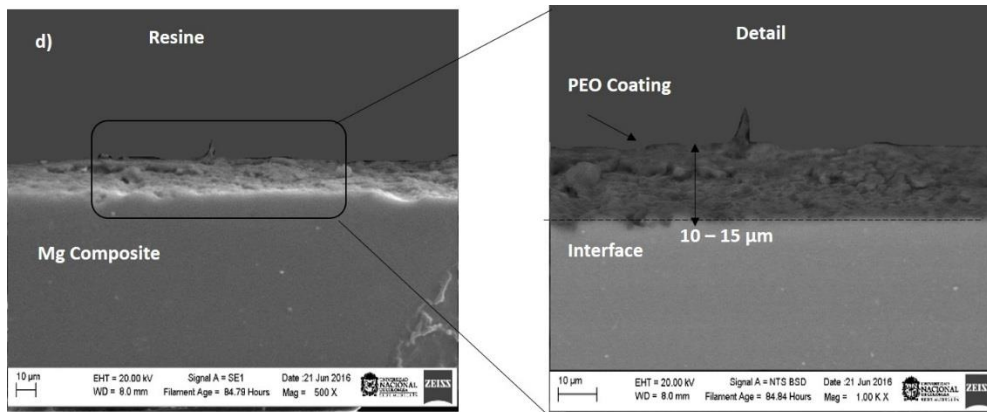


Figure 3-58: Cross-section micrographs of the PEO-film in the a) AZ31B alloy, b), c) and d) the composites reinforced with 0.25, 0.5 and 1.0 wt.% of MWCNTs, respectively.

The composition and quality of the coating layer have great influence on the corrosion resistance of the oxide films. Figure 3-59 reveals that the composition of the coating film varies through the thickness, especially for the silicon content.

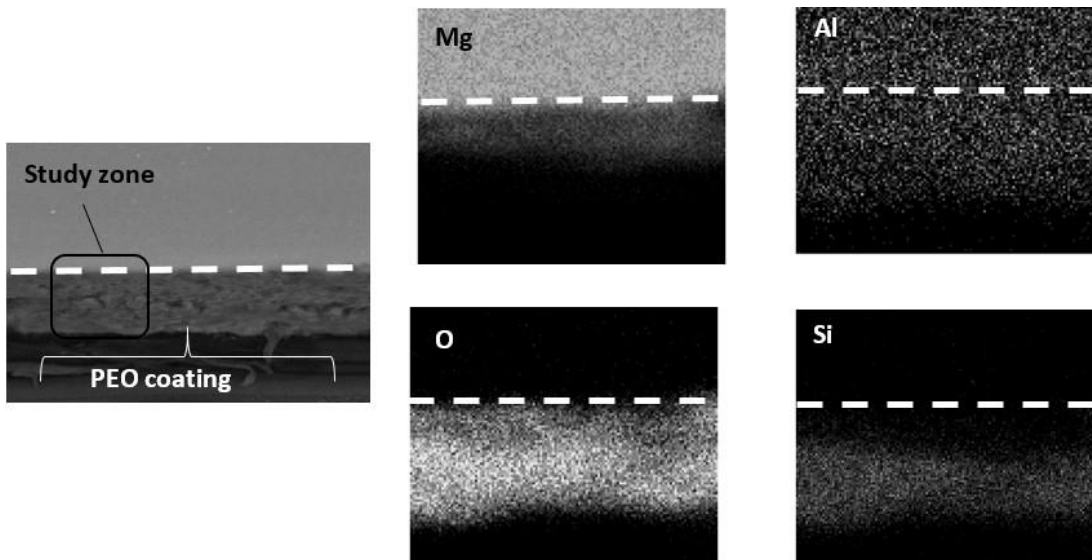


Figure 3-59: SEM-EDS mapping analysis of the interface and coating zone for the composite reinforced with 1.0 wt.% of MWCNTs.

3.6.2 Mechanical testing in the composites coating

Figure 3-60 presents the results of the nanoindentation test performed on the cross-section of the coating for all composites. The coatings deposited onto samples with 0.25 and 0.5 wt.% of MWCNTs (Figure 3-60b and Figure 3-60c) have similar mechanical properties to

those of the AZ31B alloy (0.0 wt.% MWCNTs). The coating deposited onto the 1.0 wt.% MWCNTs substrate shows a different behavior, having a lower elastic modulus and higher hardness, compared with those of the alloy with no reinforcement. As indentations were positioned at the middle of the coating cross-section and the maximum penetration depth was much lower than the coating thickness, the results were not influenced by the substrate. Moreover, a similarity in the mechanical properties allows a decreasing in the residual stresses thus promoting the adhesion of the layer to the substrate. However, as stated by Leyland et al. [120] the ratio between the hardness and the elastic modulus, H^3/E^2 , is a strong indicator of the coating's resistance to plastic deformation and then to wear. For the coatings studied here the maximum value for this parameter was obtained for the sample with 1.0 wt.% of MWCNTs owing to its low elastic modulus, which can be explained by its higher porosity as shown in Figure 3-58d. As will be seen below, this is precisely the coating with the bigger critical delamination load.

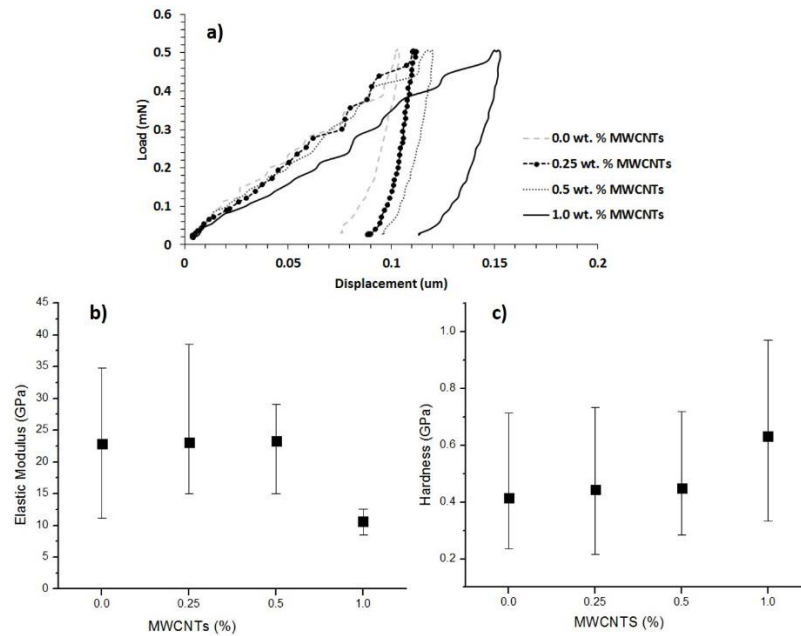


Figure 3-60: Nanoindentation results for the coating in all composites: a) load-displacement curve, b) elastic modulus and c) hardness.

Figure 3-61 presents the results of the nanoscratch test. For each test both the penetration depth and the lateral force are plotted as a function of the scratch distance. The initial contact by scratch testing is denominated by "A" It is indicated that the tip scratched into the substrate shows that the scratch response was controlled by elastic-plastic

deformation, with no delamination. The critical delamination load is labelled with the letter “B” and finally, the letter “C”, there is an abrupt change in the scratching curve, implying that the coating peeled off during this scratch process and the coefficient of friction also suddenly changed. The penetration curves show a “noisy” behavior for all composites as a result of the topographical irregularities of the surface (notwithstanding the depth signal was corrected by a surface pre-scan at a 0.2 mN). Of course, the cracking and delamination of the coatings can also increase the peak signals. In general, an increase in the load signal is accompanied by a peak in the depth signal, which allows to determine the critical load for delamination; this load was corroborated by optical microscopy. The lateral forces necessary for delamination of the coatings were: 12, 22, 35 and 45 mN for the composites reinforced with 0, 0.25, 0.5 and 1.0 wt.% of MWCNTs, respectively; such forces occurred at a penetration depth of 2, 4, 3 and 6 μm , respectively. It is clearly observed that thicker coatings have a bigger adhesion to the substrate. As the thickness of 0, 0.25, 0.5 wt.% samples is similar, and therefore their mechanical behavior, the increasing in the critical delamination loading could only be due to the microstructure and internal structure of the coatings, which can also modify the residual stresses. It is also clear that the load capacity of the 1.0 wt.% sample is much bigger than in the other samples, which determines a good delamination behavior.

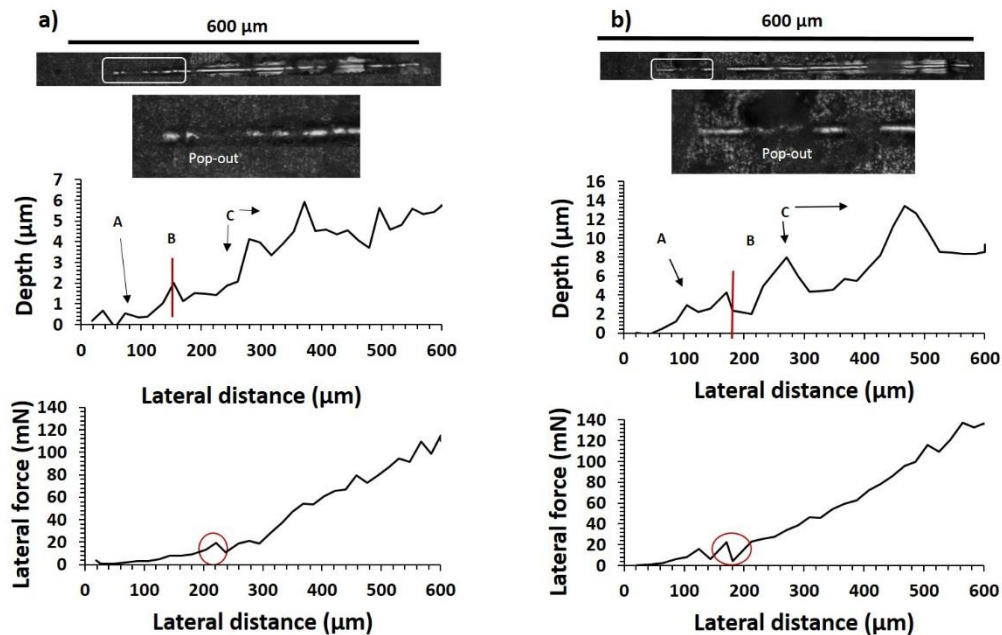


Figure 3-61: Scratch test results using a normal load from 0.5 to 100 mN. Lateral force and penetration depth as a function of the scratch distance for: a) AZ31B and b) 0.25 wt.%.

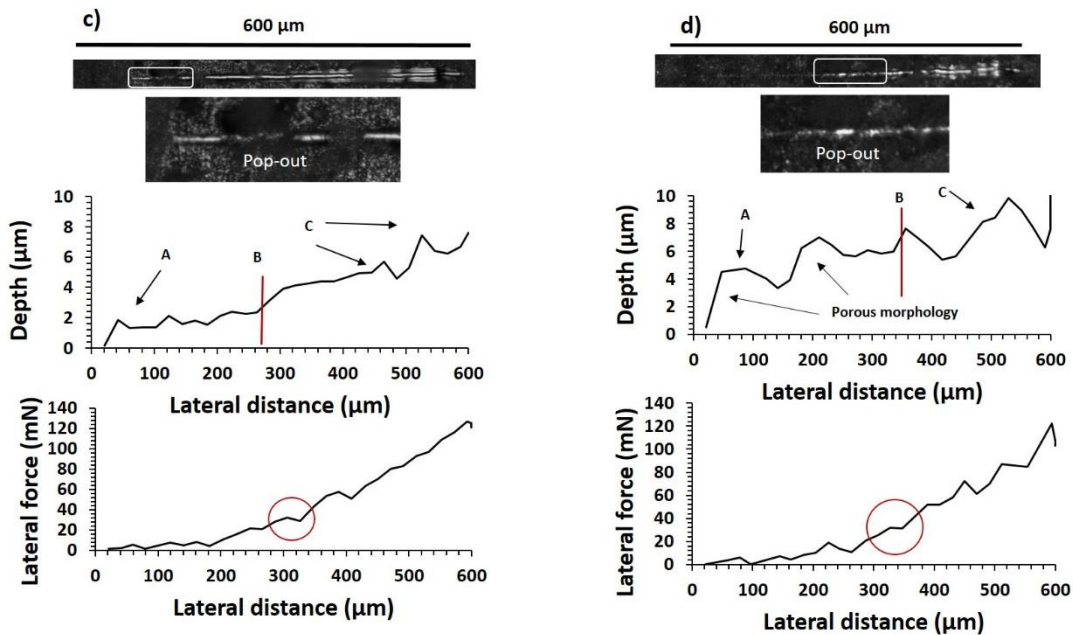


Figure 3-61 (continued): Scratch test results using a normal load from 0.5 to 100 mN. Lateral force and penetration depth as a function of the scratch distance for: c) 0.5 wt.% and d) 1.0 wt.% samples.

3.6.3 Corrosion testing in the composites coating

Electrochemical impedance spectroscopy (EIS) measurements are shown in Figure 3-62 and Figure 3-63. Experimental data of Nyquist and Bode spectra impedance are represented by dashed or dotted lines "D", while solid lines "S" correspond to the prediction obtained from the proposed equivalent circuit model shown in Figure 3-63.

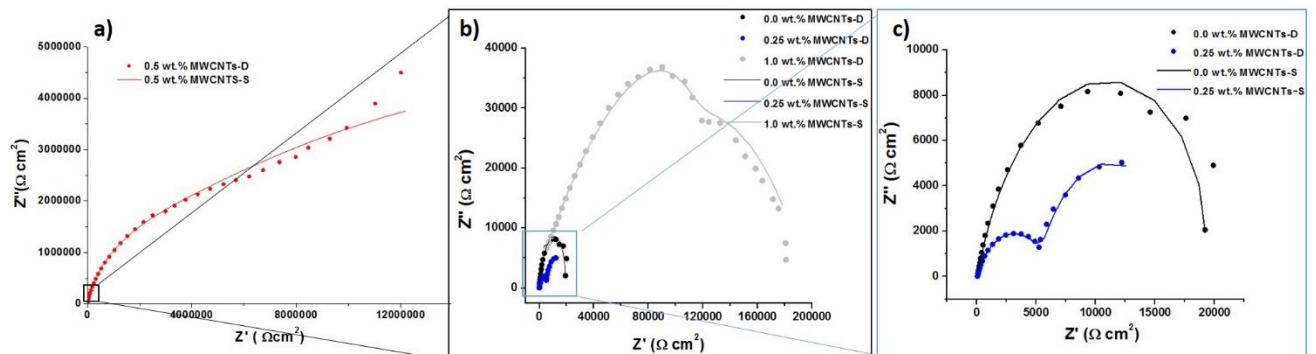


Figure 3-62: EIS (Nyquist) plots of the AZ31B alloy reinforced with MWCNTs and coated by PEO.

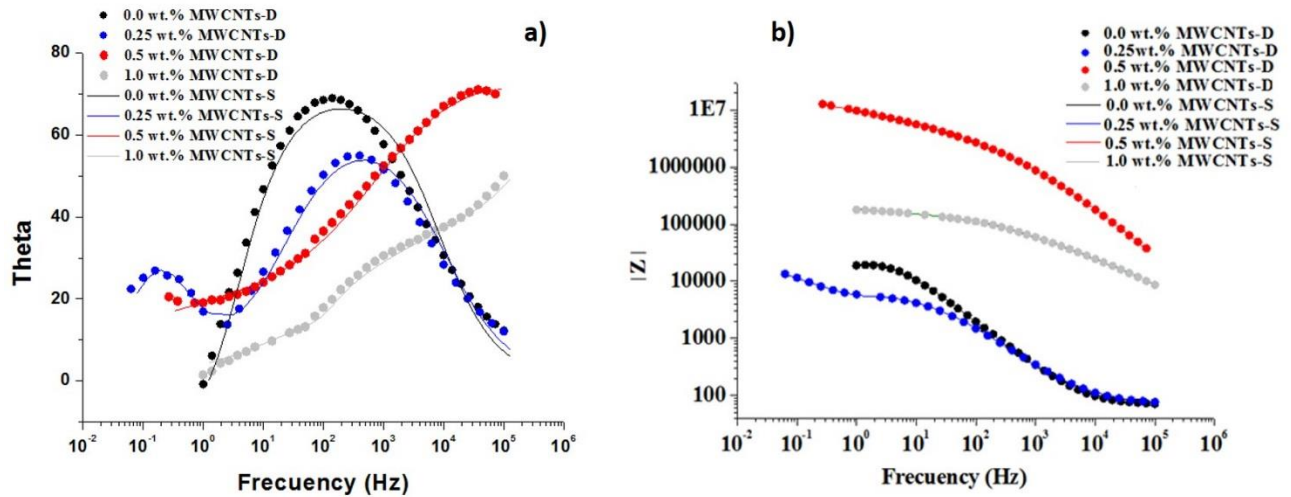


Figure 3-63: EIS (Bode) plots of the AZ31B alloy reinforced with MWCNTs and coated by PEO.

Nyquist plots obtained for samples reinforced with 0.0, 0.25, 0.5 and 1.0 wt.% show an overlap of two arcs (Figure 3-62a-c). The arc at high frequencies represents non-Faradaic processes between the working electrode and the oxide coating formed during the coating process. The arc at low frequencies represents Faradic processes between the coating surface and the electrolyte [121].

Note that as the wt.% of MWCNTs is increased the arc superposition, this is when two arcs are almost undistinguishable, is maximum at 0.5 wt.%; then the arcs starts to become distinguishable again. The overlapping in the samples reinforced with 0.5 and 1.0 wt.% of MWCNTs suggests a high adhesion between the oxide coating and the magnesium substrate, as verified by the adhesion analysis accomplished by the nanoscratch tests. On the other hand, for the 0.5 wt.% MWCNTs sample, the fact that the capacitive arc diameter is the largest one, suggests that this sample will present the best corrosion resistance of all coated systems. Figure 3-63a also suggests that the addition of MWCNTs produces an improvement of the resistance to corrosion but up to a maximum level, after which this effect starts to decrease.

Figure 3-62a shows depressed semicircles. In the case of the 0.5 wt.% MWCNTs sample this occurs at low frequencies, which indicates the presence of inhomogeneities or

restrictions [122] on the metallic ion transfer through the interface. This phenomenon is due to the presence of magnesium and silicon compounds formed at the interface between the coating and the substrate. For the 1.0 wt.% MWCNTs sample the depressed circles appear at high frequencies, phenomenon related to the presence of surface defects or inhomogeneities, which generates restrictions on the charge transfer between the electrolyte and the coating, which in turn is reflected in electrochemical instability, as will be discussed below.

The Bode plot (phase angle vs. frequency) in Figure 3-63a shows that, comparing the samples at the same frequencies, the highest value of impedance corresponds to the sample reinforced with 0.5 wt.% of MWCNTs, followed by samples reinforced with 1.0 , 0.25 and 0 wt.% of MWCNTs. Several works [96, 122] have shown that the larger the impedance the lower the corrosion rates; thus, the sample reinforced with 0.5 wt.% of MWCNTs has the lower corrosion rate, which is in line with what was found in the Nyquist plots.

However, Figure 3-63b shows that the 1.0 wt.% MWCNTs sample presents a relaxation at low frequencies (between 0.1 and 100 Hz), which is lower than the one presented by the sample reinforced with 0.5 wt.% of MWCNTs (between 0.1 and 400 Hz). This leads to the conclusion that charge transfer processes control the degradation of the 1.0 wt.% MWCNTs sample, while mass transfer processes between the substrate and the film control the degradation of the 0.5 wt.% MWCNTs sample. These findings suggest that the 1.0 wt.% MWCNTs sample, despite having a corrosion rate higher than the 0.5 wt.% MWCNTs sample, is more stable. That is, it is expected that the 0.5 wt.% MWCNTs sample has a tendency to degrade greater than 1.0 wt.% MWCNTs sample. This tendency is related to the diffusion of the species from the coating to the solution. However, results from Bode plots clearly show that this is not indeed the case and that the best behavior is precisely presented by the sample with 1.0 wt.% of MWCNTs.

Furthermore, the slope of the curves of the impedance modulus vs. frequency (Figure 3-63a), relaxations at high frequencies (between 100 and 100000 Hz), shows the resistive or capacity nature of the Faradic transfer processes of the metal. In this graph, the 1.0 wt.% MWCNTs sample shows a greater slope and relaxation than the other ones, which means that the processes occurring at the coating/solution interface are more capacitive than resistive, this suggests a decrease in the chemical activity of the metal. On the other hand,

the fact that relaxation occurs at a wide frequency range and at high frequencies for the 1.0 wt.% MWCNTs sample, means that the control of its electrochemical processes is determined by the processes of charge transfer. EIS can be contrasted with the results of an equivalent circuit model for each interface associated with charge transportation to the electrochemical double layer, as shown in Figure 3-64. R_{sln} corresponds to the electrolytic solution resistance (3.5 wt.% NaCl in distilled water), which is influenced by the mobility of the electrolytic species and the thickness of the double electrochemical layer. R_{sln} is in series with a constant phase element (CPE) named $C_{coat/sln}$. This CPE represents a non-ideal charge transfer between the coating (anodic surface) and the solution, and is associated with the phenomena in the interface between the coating surface and the electrochemical double layer. The use of this CPE was necessary because both the coating surface and the interface between the oxide and substrate have a large number of irregularities, as observed in Figure 3-58. $R_{coat/sln}$ in the equivalent circuit represents the electrochemical resistance of the coating and is in parallel to the CPE. Likewise, $C_{Mg-MWCNTs/Coat}$ is related to the chemical activity, energy and morphology at the interface between the metal matrix reinforced with MWCNTs and the internal oxide layer [92]. For the experimental data fit, it was also necessary to place one in-parallel RCPE (resistors and constant phase elements). The RCPE element represents the non-ideal capacitance behavior of the corresponding relaxation at low frequencies; such relaxation is produced by resistive and capacitive processes linked to the mass transfer between the metal substrate and the anodic PEO coating. The resistance obtained corresponds to the corrosion resistance of magnesium alloy substrate $R_{Mg-MWCNTs/Coat}$ [92] and is an important parameter to define the capacity of the coating to withstand corrosion.

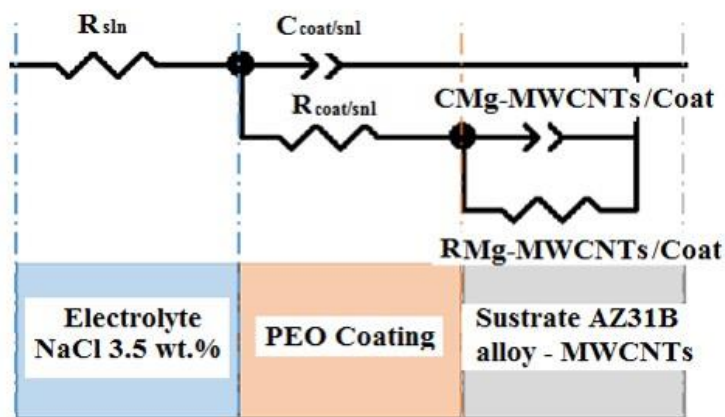


Figure 3-64: Equivalent circuit used for impedance data fitting of AZ31B magnesium alloy reinforced with MWCNTs and coated by PEO.

SEM-EDS images (Figure 3-58 and Figure 3-59) show a dense structure, which is associated with a single relaxation between capacitance and resistance [122], according to the information of the impedance spectra obtained. Besides, because of the shared metallic nature between the substrate and magnesium-silicon compounds at the interface, the model using RCPE in parallel is justified and works properly to predict the electrochemical behavior of the coated samples.

It is worth noting that the model used in the present study differs from that proposed by other authors [92]. The difference is because they have obtained a different coating microstructure: a mixture of a dense and amorphous oxide layer and a surface with pores and irregular morphology; this means that two relaxations (RCPEs) associated to the charge and mass transfer are needed to properly model the electrochemical behavior of those samples.

Table 3-7. EIS fitting results for the AZ31B alloy with different content of MWCNTs and coated by PEO (T stands for charge transfer and P for phase).

Sample	R _{sln} (Ωcm^2)	R _{coat/sln} (Ωcm^2)	R _{Mg-MWCNTs/Coat} (Ωcm^2)	C _{coat/sln-T} (F cm^2)	C _{coat/sln-P}	C _{Mg-MWCNTs/Coat-T} (F cm^2)	C _{Mg-MWCNTs/Coat-P}	Chi-Square
0.0 wt. %	68.84	2.87 E+04	1.92 E+04	2.96E-06	0.79728	1.81E-05	0.58632	0.0082404
0.25 wt. %	71.12	5.92 E+03	1.13 E+04	5.93E-06	0.71813	1.52E-04	0.90145	0.0014692
0.50 wt. %	1723.00	4.11E+05	3.93E+07	3.95E-10	0.84610	4.50E-08	0.26762	0.0006899
1.0 wt. %	3292.00	2.33E+05	3.03 E+04	3.20E-07	0.41978	2.27E-08	0.99999	0.0006522

The fitting results of the equivalent circuit for EIS are shown in Table 3-7, where it can be seen that the phase of the capacitance (C_{Mg-MWCNTs/Coat-P}) presents high values, which is due to the low amount of defects produced during the coating application process, which in turn is owing to the use of a voltage smaller than the dielectric limit voltage [123]. This is in contrast to the coatings produced at high voltages, which usually present cracks and suffer micro-cavitation, as a consequence of the hydrogen released during the plasma formation.

The C_{Mg-MWCNTs/Coat-P} value represents discontinuities in the charge transfer at the interface between the coating and the composite; accordingly, the bigger the porosity or defects in this interface the lower the values of this capacitance. Thus, the sample

reinforced with 0.5 wt.% of MWCNTs, which has the lowest phase value, will have an important amount of inhomogeneities, i.e., discontinuities in the interface, as corroborated in the cross-section SEM image shown in Figure 3-58c, where porosity and irregular morphology are clearly seen. In the case of the AZ31B sample without MWCNTs (Figure 3-58a), inhomogeneities in the interface Mg - PEO were also observed, but their size and proportion are lower compared with the 0.5 wt.% MWCNTs sample. Interfaces in samples reinforced with 0.25 and 1.0 wt.% of MWCNTs have few defects, i.e., the interface is almost a straight line, which allows an “ideal” electrochemical process transfer through this interface, then their capacitance value is high.

On the other hand, the capacitance associated with the interface between the coating and the solution ($C_{coat/sln}$) represents the transfer processes towards the electrochemical double layer. High values were found and they increased with the MWCNTs content from 0 to 0.5 wt.%, which in turn means that these samples have a low defect quantity and are energetically stable. However, the capacitance values decrease in the sample reinforced with 1.0 wt.% of MWCNTs, i.e. it has more morphological defects. Indeed, the topography and roughness in the interface and the number of cracks in this sample are bigger, which were caused by localized instability in the dielectric coating formation by the PEO technique [123]. SEM images in Figure 3-65 corroborate what it was stated above. In those images it is easy to identify a very irregular morphology with a significant presence of micro-cracks in all samples analyzed, being more evident in the surface of 1.0 wt.% MWCNTs sample.

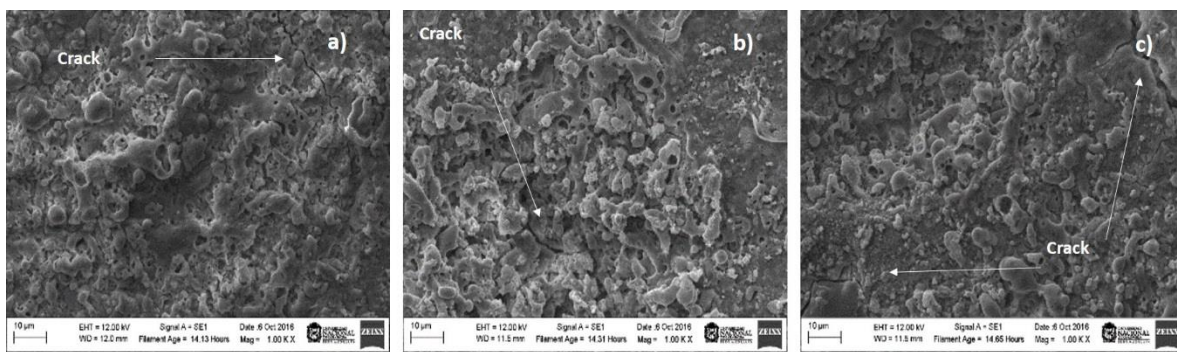


Figure 3-65: Surface morphology of the AZ31 alloy reinforced with MWCNTs and coated by PEO technique: a) 0.25, b) 0.5 and c) 1.0 wt.% of MWCNTs.

Chemical activity is defined by the value ΔG , which is related to the electrode potential E by the relationship given in Equation 3-6, where n is the number of electrons involved in the

electrochemical reaction and F is the Faraday constant. The chemical activity is also related to the capacitance by the relationship $\Delta G \propto 1/C$. Thus, with the capacitance obtained it is possible to establish a relationship with the potential difference across the interface, which was proposed by Grahame [124] and presented in Equation 3-7. Therefore, if a small capacitance value is obtained, the relative potential difference between electrode and reference electrode increases, and the ΔG will be more negative, indicating that the metal and oxygen spontaneously react by lower chemical activity. However, in this study the high capacitance values obtained could indicate a tendency of the material to degrade or become unstable producing corrosion. Thereby, the samples reinforced with 0 and 0.25 wt.% of MWCNTs had higher capacitance values than the samples reinforced with 0.5 and 1.0 wt.% of MWCNTs. These values were also obtained at the interface Mg/MWCNTs-PEO coating, indicating a strong influence of the MWCNTs content with stability and corrosion resistance of both, the metal substrate and the coating.

$$\Delta G = -nFE \quad \text{Equation 3-6}$$

$$C = \frac{\partial \sigma_s}{\partial E} \quad \text{Equation 3-7}$$

In summary, AZ31B Mg alloy reinforced with carbon nanotubes has many potential structural applications due to its mechanical properties like elastic modulus, hardness and ultimate strength. It could also have potential functional and medical applications if suitable coatings methods are developed to give it good corrosion resistance. In this aim, the purpose of the additional investigation was to explore the application of a coating by the PEO technique, which was found to have good corrosion properties in the composites fabricated by the sandwich technique.

4. Conclusions and future work

4.1 Conclusions

Several important conclusions were obtained from the work done in this research. The conclusions will be classified in terms of (a) processing technique, (b) CNT dispersion of the MWCNTs in metal matrix composites (c) mechanical properties (nano scale, micro scale and macro scale).

- **Processing technique.**

In this research work, composites of AZ31B magnesium alloy reinforced with MWCNTs were synthesized by a new process named "Sandwich technique". The technique is particularly interesting because it produces a substantial increase in all mechanical properties due to the dispersion and in some cases the alignment of the MWCNTs in a metal matrix without damage to the reinforcing material. Different strengthening mechanisms were identified that corroborate the mechanical properties improvement. The major parameters that affect strengthening are MWCNTs dispersion, the deformation during processing, and the interface between MWCNTs and magnesium matrix.

- ***MWCNTs dispersion into a metal matrix.***

The effect of MWCNTs dispersion and alignment have a direct effect on the elastic modulus and their properties as was shown in the mechanical properties characterization section by different technique testing. The dispersion directly depends on the polymer processing (PVA/MWCNTs) and hot compaction processing during composite manufacturing. The dispersion degree for both, PVA/MWCNTs and Mg/MWCNTs were good and the hot compacted processing does not affect the dispersion in the final composites. The literature review shows the problems when a good dispersion degree is not achieved and clusters

can be appear and acts as a stress concentration and do not allows a very good load transfer under external loads.

- **The deformation behavior during processing (microstructure).**

Processing techniques used for producing this kind of composites have a strong deformation process that have an impact on its properties (hot compacted and hot rolled process), however MWCNTs damages were not identified and dense composites were obtained, thus a good load transfer between the metal matrix and the MWCNTs were evidenced. On the other hand, higher degree of deformation is expected to increase the extent of alignment of MWCNTs along the hot rolling direction; however, the MWCNTs alignment is decreased during hot compaction processing.

Another behavior that allowed an strengthening of the composites was the grain size reduction due to the processing. In addition, the presence of MWCNTs into the metal matrix left to grain refinement in a number of ways. MWCNTs into the metal matrix, increase the work hardening and thermal conductivity, and act as second phases. All these lead to increased nucleation rates during recrystallization processes leading a fine grain structure as was shown by dark field TEM images. That behavior is denominated Hall Petch strengthening, and it is based on the observation that grain boundaries impede dislocation movement and that the number of dislocations within a grain have an effect on how easily dislocations can traverse grain boundaries and travel from grain to grain. On the other hand, strengthening by dislocation was possible due to the dislocation piled up against the MWCNTs external walls. Other factors can also increase the dislocation or dislocation formation during the fabrication processing such as thermal expansion mismatch as was shown in HRTEM images for dislocations formation allowing a semi-coherent interface between MWCNTs and metal matrix. However, in some study zone a coherent interface also was found, this result allows conclude about the good mechanical properties found in the different testes done.

- **Interphase between MWCNTs and metal matrix composites.**

A strong and good interface between the MWCNTs and the metal matrix was achieved in the composites done by the sandwich technique. Interphases were not evidenced in the studied zones. However, some reaction between MWCNTs and some aluminum particles were evidenced, but this reaction was not enough for interphase formation between the

metal matrix and the MWCNTs. In other hand, due to the Gibbs free energy for forming carbides, the formation of magnesium carbide is less probably than aluminum carbide, but during this process the condition processing and the aluminum percentage into the AZ31 B alloy were not enough for forming this kind of interphases.

- **Mechanical properties**

The nanoindentation and tensile tests showed the mechanical properties for the composites studied, in both the nanoindentation tests and the tensile tests, the mechanical properties increased. These results corroborated the very good interfacial behavior between magnesium and MWCNTs how was shown in HRTEM section. These behaviors are coherent with the nanoscratch results and evidence the mechanical properties increase at the interface between magnesium sheets, i.e. the tribological behavior in that zone evidence the very good hardness and yield strength.

The in situ tests in the composites done in the reinforced zone (diffusion zone) showed the changes in the fracture toughness for all composites studied. The results for fracture toughness show an increase with the MWCNTs percentage added in the metal matrix; however, the specific values can be underestimated or overestimated due to the variables that were not controlled such as the notch geometry, the cantilever geometry and the energy dissipation due to the MWCNTs for the fracture toughness calculation.

The crack path was identified by HRTEM analysis and show that the crack has incidence with the Mg, MgO and MWCNTs. These result evidenced that the fracture toughness are good and was demonstrated by tensile testing done in bulk composites.

- **PEO coating in the magnesium composites**

AZ31B Mg alloy reinforced with carbon nanotubes has potential functional and medical applications if suitable coatings methods are developed to give it good corrosion resistance. In this aim, the purpose of the additional investigation was to explore the application of a coating by the PEO technique, which was found to have good corrosion properties in the composites fabricated by sandwich technique.

The electrochemical results showed that the coating has a better behavior with the addition of MWCNTs to the magnesium matrix. This finding is very interesting because it is possible to make new light composites with very good mechanical and corrosion properties.

The PEO coatings developed in this work have good mechanical properties like elastic modulus and hardness, which are similar to those of the magnesium composites. This similarity in properties between the coating and composites can be beneficial during the service time of components fabricated from these materials. The MWCNTs content has an influence on the morphology of the PEO coating obtained. Samples with higher MWCNTs percentage have more inhomogeneities in the PEO coating, as a result of the dielectric localized instability.

Data fitting by equivalent circuit model made possible to identify the relationship between the PEO electrical properties and chemical activity when samples are in contact with saline environmental. It was clearly seen that the capacitance values obtained are influenced by the MWCNTs content, affecting the stability and strength of the coating. Thus, for high MWCNTs percentages there is no spontaneous chemical reaction, but a degradation tendency. On the contrary, samples with low MWCNTs content are thermodynamically more stable because the chemical reaction occurs spontaneously.

4.2 Future works


The next step for this kind of composite is to do a prototype of metal matrix composite reinforced with MWCNTs by the alternative technique. The prototype must be bigger (10x10 cm) like plates and trying to verify the mechanical properties under aeronautical standards. This works would be in order to create a new technological product for aeronautical or automotive industries.

Other important aspect is the medical applications that this kind of composite can become in the implants industry or surgical instruments, for this a serious research in these fields must be proposed

A. Annex: Publications in this dissertation

- Journal Publications

Journal of Alloys and Compounds 707 (2017) 257–263




ELSEVIER

Contents lists available at [ScienceDirect](#)

Journal of Alloys and Compounds


journal homepage: <http://www.elsevier.com/locate/jalcom>



Metal matrix composites reinforced with carbon nanotubes by an alternative technique

Cesar A. Isaza Merino ^{a, b}, J.E. Ledezma Sillas ^b, J.M. Meza ^a, J.M. Herrera Ramirez ^{b, *}

^a Universidad Nacional de Colombia, Facultad de Minas, Departamento de Materiales y Minerales, Cl 75 No 79A 51, 050032, Colombia
^b Centro de Investigacion en Materiales Avanzados (CIMAV), Laboratorio Nacional de Nanotecnología, Miguel de Cervantes 120, 31136, Chihuahua, Chih., Mexico

 CrossMark

ARTICLE INFO

Article history:
 Received 27 July 2016
 Received in revised form 8 November 2016
 Accepted 24 November 2016
 Available online 24 November 2016

Keywords:
 Metal matrix composites
 Reinforcement
 Mechanical properties

ABSTRACT

The metal matrix composites (MMCs) have been used in several applications where high specific resistance and temperature are required for some uses in the aerospace and aeronautic industry. In general, these composites are manufactured using as reinforcing material particles or some fibers like glass, ceramic and carbon fibers. Recently a new manufacturing process for the production of MMCs reinforced with carbon nanotubes, known as sandwich technique has been proposed. This technique produces materials comprised of a metallic matrix and banded structured-layers of multiwall carbon nanotubes (MWCNTs). However, among other issues, the matrix-reinforcement interface and the reinforcement dispersion degree are still open questions. The present study has been aimed on the reinforcement of magnesium sheets with MWCNTs by the sandwich technique. Field emission scanning electron microscopy was used to demonstrate that the method is capable of producing a good dispersion of the MWCNTs with no evidence of damage. The mechanical properties were measured by tensile and nanoindentation tests; yield and ultimate strengths, elastic modulus and hardness were increased with respect to the unreinforced material.

© 2016 Elsevier B.V. All rights reserved.

Article



Journal of Composite Materials
0(0) 1–10
© The Author(s) 2017
Reprints and permissions:
sagepub.co.uk/journalsPermissions.nav
DOI: 10.1177/0021998317731151
journals.sagepub.com/home/jcm



Dispersion and alignment quantification of carbon nanotubes in a polyvinyl alcohol matrix

Cesar A Isaza M^{1,2}, JM Herrera Ramirez¹, JE Ledezma Sillas¹ and JM Meza²

Abstract

In recent years, due to their high specific mechanical properties, polymer matrix composites have been widely used. In particular, carbon nanotubes have been used as reinforcement because of their exceptional properties. In this work, the degree of dispersion and alignment of multiwalled carbon nanotubes into polyvinyl alcohol was quantified, which is a key information to optimize the mechanical properties of composites. For the dispersion of the multiwalled carbon nanotubes into the solution, a magnetic stirring and ultrasonic agitation were used. Finally, the mixture was dried to obtain a multiwalled carbon nanotubes reinforced polymer. The composites were mechanically stretched to obtain sheets with multiwalled carbon nanotubes aligned in the stretching direction. The layers obtained were prepared for transmission electron microscopy analysis. A dispersion quantification method based on the statistical distribution of horizontal and vertical separation distance between carbon nanotubes was used; a lognormal distribution was obtained. The angle of carbon nanotubes with respect to the stretching direction was used to quantify the alignment degree of carbon nanotubes. The bulk mechanical properties of the composites were measured by nanoindentation test; tensile test allowed to measure the mechanical properties of the composites in both the stretching and perpendicular directions to the stretching direction. Multiwalled carbon nanotubes showed a good dispersion and alignment degree and this, in conjunction with stretching, produced a high increase of both the stiffness and strength in the stretching direction, which allowed an increment of the mechanical properties measured by nanoindentation test; the best properties of the composites were reached with 0.5 wt% of MWCNTs.

Keywords

Polymer matrix composites, carbon nanotubes, polyvinyl alcohol, dispersion and alignment

Characterization of Metal Matrix Composites Reinforced with Carbon Nanotubes by High Resolution Transmission Electron Microscopy

Cesar A. Isaza M¹, J. M. Meza¹, J. E. Ledezma Sillas² and J. M. Herrera-Ramirez².

¹ Universidad Nacional de Colombia, Facultad de Minas, Departamento de Materiales y Minerales Cl 75 No 79A 51, Colombia.

² Centro de Investigacion en Materiales Avanzados (CIMA), Laboratorio Nacional de Nanotecnologia, Miguel de Cervantes 120, Chihuahua, Chih., Mexico.

Since their discovery by Iijima [1], carbon nanotubes have been considered as an ideal reinforcing material to improve the mechanical properties in polymeric, ceramic and metallic materials [2-4]. The need to find high-strength lightweight materials in transportation industries has driven the development of new materials and manufacturing methods to reduce CO₂ emissions into the atmosphere.

Recently, a new manufacturing process for the production of metal matrix composites reinforced with carbon nanotubes, known as sandwich technique, has been proposed [5-7]. This technique produces materials comprised of a metallic matrix and banded structured-layers of multiwalled carbon nanotubes (MWCNTs).

The composites fabricated, both pure aluminum and AZ31 magnesium reinforced with MWCNTs, were characterized and studied by FESEM, TEM and HRTEM techniques for identifying the interaction between aluminum or magnesium matrix and MWCNTs. Figure 1a shows the MWCNTs used in this study, which have outer diameters of 10–40 nm and inner diameters of 10–20 nm, with a length of 30–50 μm. Some imperfections, including variable numbers of carbon layers and partial interior filling, amorphous carbon, and “bamboo” defects, are showed. These defects consist of several transverse, internal walls segmenting the interior of MWCNTs into independent pods or isolated volumes.

In both aluminum and magnesium composites a good dispersion of the MWCNTs into the metal matrix is clearly seen (Figures 1b and 1c), which proves the success of the sandwich technique to synthesize these kind of composites. Figures 2 shows TEM and HRTEM images for both composites, where the MWCNTs can be observed embedded into the aluminum matrix (Figure 2a) and the magnesium alloy matrix (Figure 2b). The details in Figure 2 let see a good and homogeneous interface between both metal matrices and the MWCNTs, with no evidence of the formation of carbides or any other phase.

A Novel Technique for Production of Metal Matrix Composites Reinforced With Carbon Nanotubes

Cesar Isaza, G. Sierra and J. M. Meza

[\[+\] Author and Article Information](#)

J. Manuf. Sci. Eng 138(2), 024501 (Sep 09, 2015) (5 pages)

Paper No: MANU-14-1641; doi: 10.1115/1.4030377

History: Received November 28, 2014

[ARTICLE](#) | [REFERENCES](#) | [FIGURES](#) | [CITING ARTICLES](#)

Abstract

[Abstract](#) | [Introduction](#) | [Experimental Procedure](#) | [Results and Discussion](#) | [Conclusions](#) | [Acknowledgements](#) | [References](#) ▲

The metal matrix composites (MMCs) have been widely used where high specific properties and temperature resistance are required, particularly in aerospace applications. In this work, an ASTM-1100 aluminum alloy in the form of sheets was reinforced with multiwalled carbon nanotubes (MWCNTs) by a novel technique which we have called sandwich technique. Carbon nanotubes (CNTs) are dispersed in a polyvinyl alcohol (PVA) solution; this solution is poured into a container and dried to obtain a reinforced polymer, which is then stretched to obtain a sheet with CNTs aligned in the stretching direction. These composite sheets were stacked with aluminum sheets, and then these stacks were hot compacted in a die using an argon atmosphere to prevent the damage of the CNTs. During this process, most of the polymer evaporates and aluminum diffusion allows obtaining a consolidated matrix with a banded structure of CNTs. The mechanical properties of the composite were measured by tensile and nano-indentation tests, showing increases of up to 100% in the elastic modulus and significant increases in yield and ultimate strength with respect to unreinforced material. Field emission scanning electron microscopy (FESEM) analyses showed a good dispersion of the CNTs within the bands with no evidence of CNTs' damage. No harmful phases were found in the composite after micro X-ray diffraction (XRD) tests. The results showed that the proposed technique is promissory to solve some of the problems in the nano-MMCs manufacturing such as dispersion and alignment of the reinforcing phase.

Article



Journal of Composite Materials
0(0) 1-11
© The Author(s) 2016
Reprints and permissions:
sagepub.co.uk/journalsPermissions.nav
DOI: 10.1177/0021998316658784
jcm.sagepub.com



Mechanical properties and interfacial phenomena in aluminum reinforced with carbon nanotubes manufactured by the sandwich technique

Cesar A Isaza M^{1,2}, JE Ledezma Sillas¹, JM Meza² and JM Herrera Ramirez¹

Abstract

Recently, a new manufacturing process for the production of metallic matrix composite materials reinforced with carbon nanotubes, known as sandwich technique has been proposed. This technique produces a material comprised of a metallic matrix and a banded structures-layers of multi-walled carbon nanotubes. However, among other issues, the matrix-reinforcement interface and the reinforcement dispersion degree are still open questions. The present study uses field emission scanning electron microscopy and high resolution transmission electron microscopy to probe that the method is capable to achieve a good dispersion of the multi-walled carbon nanotubes with no evidence of carbon nanotubes' damage. The mechanical properties were measured by tensile and nanoindentation tests; improvements in the elastic modulus, yield and ultimate strengths were found, with respect to the unreinforced material.

Keywords

Metal matrix composites, interfacial phenomena, carbon nanotubes, mechanical properties

Mechanical and thermal behavior of polyvinyl alcohol reinforced with aligned carbon nanotubes

Sergio Alonso Medina Escobar¹, César Augusto Isaza Merino¹
Juan Manuel Meza Meza¹

¹Tribology and Surfaces Group, Universidad Nacional de Colombia - Medellín
Escuela de materiales y minerales, Calle 75 No 79 A -5, Bloque M17 Medellín, Antioquia, Colombia, 050034.
e-mail: samedinae@unal.edu.co, cesarisaz@gmail.com, jmmezam@unal.edu.co

ABSTRACT

In recent years, due to their high specific mechanical properties, the polymer matrix composites have been widely used. In particular, carbon nanotubes (CNTs) have been used as reinforcement due to its exceptional mechanical and electrical properties. In this work the mechanical behavior of polyvinyl alcohol (PVA) reinforced with different percentages of mechanically oriented CNTs was studied. The composite material was made starting with a solution of PVA+ distilled water, and then the CNTs were added to the solution and dispersed by magnetic stirring and ultrasonic agitation. During this step, a surfactant was added to help with the CNTs dispersion. This mixture was poured into a container and dried using a heat source to accelerate its polymerization and curing. The layers obtained were subjected to mechanical stretching at controlled temperature to align the CNTs in the loading direction. The mechanical properties were measured by tensile testing and nanoindentation. The results show a large increase in modulus and hardness compared with non-reinforced polymeric material, it was also found a significant increase in the tensile strength. The composite with the best properties was subjected to thermal stabilization by ethanol, obtaining an increase in the degradation temperature of about 100°C approximately, although in this case the mechanical stiffness and hardness were decreased compared to unstabilized material, the usefulness of this material is enhanced.

Keywords: Mechanical properties, Polymer matrix composites, Carbon nanotubes, Polyvinyl alcohol.

References

1. Iijima, S., *Helical microtubules of graphitic carbon*. Nature, 1991. 354(6348): p. 56-58.
2. Jiang, L., et al., *An approach to the uniform dispersion of a high volume fraction of carbon nanotubes in aluminum powder*. Carbon, 2011. 49(6): p. 1965-1971.
3. Schwartz, M.M., *Composite materials: processing, fabrication, and applications*. Vol. 2. 1997: Prentice Hall.
4. Desai, A. and M. Haque, *Mechanics of the interface for carbon nanotube-polymer composites*. Thin-walled structures, 2005. 43(11): p. 1787-1803.
5. Wang, X., et al., *Processing, microstructure and mechanical properties of micro-SiC particles reinforced magnesium matrix composites fabricated by stir casting assisted by ultrasonic treatment processing*. Materials & Design, 2014. 57: p. 638-645.
6. Luo, D., et al., *Microstructure and mechanical properties of SiC particles reinforced Mg-8Al-1Sn magnesium matrix composites fabricated by powder metallurgy*. Powder Metallurgy, 2015. 58(5): p. 349-353.
7. Mounib, M., et al., *Reactivity and microstructure of Al₂O₃-reinforced magnesium-matrix composites*. Advances in Materials Science and Engineering, 2014. 2014.
8. Jiang, Y., et al., *Particles reinforced magnesium alloy produced by friction stir processing*. Rev. Adv. Mater. Sci, 2013. 33: p. 29-32.
9. Hassan, S. and M. Gupta, *Development of nano-Y₂O₃ containing magnesium nanocomposites using solidification processing*. Journal of Alloys and Compounds, 2007. 429(1): p. 176-183.
10. Goh, C., et al., *Simultaneous enhancement in strength and ductility by reinforcing magnesium with carbon nanotubes*. Materials Science and Engineering: A, 2006. 423(1): p. 153-156.
11. Li, Q., et al., *Improved processing of carbon nanotube/magnesium alloy composites*. Composites Science and Technology, 2009. 69(7): p. 1193-1199.
12. Li, Q., C.A. Rottmair, and R.F. Singer, *CNT reinforced light metal composites produced by melt stirring and by high pressure die casting*. Composites Science and Technology, 2010. 70(16): p. 2242-2247.
13. Rashad, M., et al., *Use of high energy ball milling to study the role of graphene nanoplatelets and carbon nanotubes reinforced magnesium alloy*. Journal of Alloys and Compounds, 2015. 646: p. 223-232.
14. Tjong, S.C., *Recent progress in the development and properties of novel metal matrix nanocomposites reinforced with carbon nanotubes and graphene nanosheets*. Materials Science and Engineering: R: Reports, 2013. 74(10): p. 281-350.
15. Paramsothy, M., et al., *Simultaneous enhancement of tensile/compressive strength and ductility of magnesium alloy AZ31 using carbon nanotubes*. Journal of nanoscience and nanotechnology, 2010. 10(2): p. 956-964.
16. Bakshi, S.R., et al., *Aluminum composite reinforced with multiwalled carbon nanotubes from plasma spraying of spray dried powders*. Surface and Coatings Technology, 2009. 203(10): p. 1544-1554.

17. Esawi, A., et al., *Effect of carbon nanotube (CNT) content on the mechanical properties of CNT-reinforced aluminium composites*. Composites Science and Technology, 2010. 70(16): p. 2237-2241.
18. Morsi, K. and A. Esawi, *Effect of mechanical alloying time and carbon nanotube (CNT) content on the evolution of aluminum (Al)-CNT composite powders*. Journal of Materials Science, 2007. 42(13): p. 4954-4959.
19. Rozhin, A.G., et al., *Anisotropic saturable absorption of single-wall carbon nanotubes aligned in polyvinyl alcohol*. Chemical physics letters, 2005. 405(4): p. 288-293.
20. Oberlin, A., M. Endo, and T. Koyama, *Filamentous growth of carbon through benzene decomposition*. Journal of crystal growth, 1976. 32(3): p. 335-349.
21. Vishalli, et al. *Production of carbon nanotubes by AC arc discharge method*. in *AIP Conference Proceedings*. 2013. AIP.
22. Berkman, A.J., et al., *Aligning carbon nanotubes, synthesized using the arc discharge technique, during and after synthesis*. Carbon, 2013. 55: p. 185-195.
23. Singhal, S., et al. *Effect of Magnetic Field on the Growth of Aligned Carbon Nanotubes Using a Metal Free Arc Discharge Method and their Purification*. in *Solid State Phenomena*. 2013. Trans Tech Publ.
24. Jeong, M.S., J.H. Han, and Y.C. Choi, *Influence of the purification process on the semiconducting content of single-walled carbon nanotubes synthesized by arc discharge*. Carbon, 2013. 57: p. 338-345.
25. Niu, K.-Y., et al., *The synthesis of carbon nanotubes by pulsed-laser ablation of a nickel/carbon composite target in ethanol or ambient air*. Science of Advanced Materials, 2012. 4(3-4): p. 463-466.
26. Yuan, D., et al., *The fabrication of vertically aligned and periodically distributed carbon nanotube bundles and periodically porous carbon nanotube films through a combination of laser interference ablation and metal-catalyzed chemical vapor deposition*. Nanotechnology, 2012. 23(21): p. 215303.
27. Amendola, V., S. Polizzi, and M. Meneghetti, *Laser ablation synthesis of silver nanoparticles embedded in graphitic carbon matrix*. Science of Advanced Materials, 2012. 4(3-4): p. 497-500.
28. Rouleau, C.M., et al. *Catalytic nanoparticles for carbon nanotube growth synthesized by through thin film femtosecond laser ablation*. in *SPIE LASE*. 2014. International Society for Optics and Photonics.
29. Thurakitseree, T., et al., *Diameter controlled chemical vapor deposition synthesis of single-walled carbon nanotubes*. Journal of nanoscience and nanotechnology, 2012. 12(1): p. 370-376.
30. Chiodarelli, N., et al., *Correlation between number of walls and diameter in multiwall carbon nanotubes grown by chemical vapor deposition*. Carbon, 2012. 50(5): p. 1748-1752.
31. Yang, H., et al., *Precise control of the number of walls formed during carbon nanotube growth using chemical vapor deposition*. Nanotechnology, 2012. 23(6): p. 065604.
32. Treacy, M.J., T. Ebbesen, and J. Gibson, *Exceptionally high Young's modulus observed for individual carbon nanotubes*. Nature, 1996. 381(6584): p. 678.
33. Qian, D. and E. Dickey, *In-situ transmission electron microscopy studies of polymer-carbon nanotube composite deformation*. Journal of Microscopy, 2001. 204(1): p. 39-45.

34. Poncharal, P., et al., *Electrostatic deflections and electromechanical resonances of carbon nanotubes*. science, 1999. 283(5407): p. 1513-1516.
35. Yu, M.-F., et al., *Strength and breaking mechanism of multiwalled carbon nanotubes under tensile load*. Science, 2000. 287(5453): p. 637-640.
36. Salvetat, J.-P., et al., *Elastic and shear moduli of single-walled carbon nanotube ropes*. Physical review letters, 1999. 82(5): p. 944.
37. Lu, X. and Z. Hu, *Mechanical property evaluation of single-walled carbon nanotubes by finite element modeling*. Composites Part B: Engineering, 2012. 43(4): p. 1902-1913.
38. Stein, J., et al., *Mechanical reinforcement of a high-performance aluminium alloy AA5083 with homogeneously dispersed multi-walled carbon nanotubes*. Carbon, 2012. 50(6): p. 2264-2272.
39. Li, H., et al., *Mechanical properties and interfacial analysis of aluminum matrix composites reinforced by carbon nanotubes with diverse structures*. Materials Science and Engineering: A, 2013. 577: p. 120-124.
40. Jeyasimman, D., et al., *Fabrication and consolidation behavior of Al 6061 nanocomposite powders reinforced by multi-walled carbon nanotubes*. Powder Technology, 2014. 258: p. 189-197.
41. Singhal, S., et al., *Fabrication and characterization of Al-matrix composites reinforced with amino-functionalized carbon nanotubes*. Composites Science and Technology, 2011. 72(1): p. 103-111.
42. Li, H., et al., *Alumina powder assisted carbon nanotubes reinforced Mg matrix composites*. Materials & Design, 2014. 60: p. 637-642.
43. Sun, F., et al., *In situ synthesis of CNTs in Mg powder at low temperature for fabricating reinforced Mg composites*. Journal of Alloys and Compounds, 2013. 551: p. 496-501.
44. Habibi, M., et al., *Using integrated hybrid (Al+ CNT) reinforcement to simultaneously enhance strength and ductility of magnesium*. Composites Science and Technology, 2011. 71(5): p. 734-741.
45. Habibi, M., A. Hamouda, and M. Gupta, *Enhancing tensile and compressive strength of magnesium using ball milled Al+ CNT reinforcement*. Composites Science and Technology, 2012. 72(2): p. 290-298.
46. Liu, Z., et al., *Singly dispersed carbon nanotube/aluminum composites fabricated by powder metallurgy combined with friction stir processing*. Carbon, 2012. 50(5): p. 1843-1852.
47. Kwon, H., et al., *Dual-nanoparticulate-reinforced aluminum matrix composite materials*. Nanotechnology, 2012. 23(22): p. 225704.
48. Kwon, H., et al., *Effect of milling time on dual-nanoparticulate-reinforced aluminum alloy matrix composite materials*. Materials Science and Engineering: A, 2014. 590: p. 338-345.
49. Shin, S., H. Choi, and D. Bae, *Micro-alloying assisted consolidation of aluminum/carbon nanotubes powder*. Materials Science and Engineering: A, 2014. 599: p. 46-50.
50. Goh, C., et al., *Development of novel carbon nanotube reinforced magnesium nanocomposites using the powder metallurgy technique*. Nanotechnology, 2005. 17(1): p. 7.
51. Shimizu, Y., et al., *Multi-walled carbon nanotube-reinforced magnesium alloy composites*. Scripta materialia, 2008. 58(4): p. 267-270.

52. Liao, J. and M.-J. Tan, *Mixing of carbon nanotubes (CNTs) and aluminum powder for powder metallurgy use*. Powder technology, 2011. 208(1): p. 42-48.
53. Jiang, L., et al., *Strong and ductile carbon nanotube/aluminum bulk nanolaminated composites with two-dimensional alignment of carbon nanotubes*. Scripta Materialia, 2012. 66(6): p. 331-334.
54. Kwon, H. and M. Leparoux, *Hot extruded carbon nanotube reinforced aluminum matrix composite materials*. Nanotechnology, 2012. 23(41): p. 415701.
55. Paramsothy, M., et al., *Addition of CNTs to enhance tensile/compressive response of magnesium alloy ZK60A*. Composites Part A: Applied Science and Manufacturing, 2011. 42(2): p. 180-188.
56. Paramsothy, M., et al., *Carbon nanotube addition to simultaneously enhance strength and ductility of hybrid AZ31/AA5083 alloy*. Materials Sciences and Applications, 2011. 2(01): p. 20.
57. Fukuda, H., et al., *Fabrication of magnesium based composites reinforced with carbon nanotubes having superior mechanical properties*. Materials Chemistry and Physics, 2011. 127(3): p. 451-458.
58. Kwon, H., et al., *Combination of hot extrusion and spark plasma sintering for producing carbon nanotube reinforced aluminum matrix composites*. Carbon, 2009. 47(3): p. 570-577.
59. Morsi, K., et al., *Spark plasma extrusion (SPE) of ball-milled aluminum and carbon nanotube reinforced aluminum composite powders*. Composites Part A: Applied Science and Manufacturing, 2010. 41(2): p. 322-326.
60. Morsi, K., et al., *Characterization and spark plasma sintering of mechanically milled aluminum-carbon nanotube (CNT) composite powders*. Journal of composite materials, 2010.
61. Liao, J.-z., M.-J. Tan, and I. Sridhar, *Spark plasma sintered multi-wall carbon nanotube reinforced aluminum matrix composites*. Materials & Design, 2010. 31: p. S96-S100.
62. Das, A. and S.P. Harimkar, *Effect of graphene nanoplate and silicon carbide nanoparticle reinforcement on mechanical and tribological properties of spark plasma sintered magnesium matrix composites*. Journal of Materials Science & Technology, 2014. 30(11): p. 1059-1070.
63. Wu, Y. and G.-Y. Kim, *Carbon nanotube reinforced aluminum composite fabricated by semi-solid powder processing*. Journal of Materials Processing Technology, 2011. 211(8): p. 1341-1347.
64. Li, C., et al., *Effect of solidification on microstructures and mechanical properties of carbon nanotubes reinforced magnesium matrix composite*. Materials & Design, 2014. 58: p. 204-208.
65. Zhou, S.-m., et al., *Fabrication and tribological properties of carbon nanotubes reinforced Al composites prepared by pressureless infiltration technique*. Composites Part A: Applied Science and Manufacturing, 2007. 38(2): p. 301-306.
66. Park, Y., et al., *Fabrication and mechanical properties of magnesium matrix composite reinforced with Si coated carbon nanotubes*. Procedia Engineering, 2011. 10: p. 1446-1450.
67. Srivatsan, T., et al., *Influence of nano-sized carbon nanotube reinforcements on tensile deformation, cyclic fatigue, and final fracture behavior of a magnesium alloy*. Journal of Materials Science, 2012. 47(8): p. 3621-3638.

68. Paramsothy, M., et al., *Carbon nanotube addition to concentrated magnesium alloy AZ81: enhanced ductility with occasional significant increase in strength*. Materials & Design, 2013. 45: p. 15-23.
69. Hassan, S.F., et al., *Effect of carbon nanotube on high-temperature formability of AZ31 magnesium alloy*. Journal of materials engineering and performance, 2014. 23(8): p. 2984-2991.
70. Keshri, A.K. and A. Agarwal, *Wear behavior of plasma-sprayed carbon nanotube-reinforced aluminum oxide coating in marine and high-temperature environments*. Journal of thermal spray technology, 2011. 20(6): p. 1217-1230.
71. Bakshi, S.R., A.K. Keshri, and A. Agarwal, *A comparison of mechanical and wear properties of plasma sprayed carbon nanotube reinforced aluminum composites at nano and macro scale*. Materials Science and Engineering: A, 2011. 528(9): p. 3375-3384.
72. Kang, K., et al., *Thermally activated reactions of multi-walled carbon nanotubes reinforced aluminum matrix composite during the thermal spray consolidation*. Materials Chemistry and Physics, 2012. 133(1): p. 495-499.
73. Izadi, H. and A.P. Gerlich, *Distribution and stability of carbon nanotubes during multi-pass friction stir processing of carbon nanotube/aluminum composites*. Carbon, 2012. 50(12): p. 4744-4749.
74. Liu, Z., et al., *Developing high-performance aluminum matrix composites with directionally aligned carbon nanotubes by combining friction stir processing and subsequent rolling*. Carbon, 2013. 62: p. 35-42.
75. Yu, S., M.N. Tong, and G. Critchlow, *Use of carbon nanotubes reinforced epoxy as adhesives to join aluminum plates*. Materials & Design, 2010. 31: p. S126-S129.
76. Merino, C.A.I., et al., *Metal matrix composites reinforced with carbon nanotubes by an alternative technique*. Journal of Alloys and Compounds, 2016.
77. Isaza, C., G. Sierra, and J. Meza, *A novel technique for production of metal matrix composites reinforced with carbon nanotubes*. Journal of Manufacturing Science and Engineering, 2016. 138(2): p. 024501.
78. Sillas, J.L., J. Meza, and J.H. Ramírez, *Mechanical properties and interfacial phenomena in aluminum reinforced with carbon nanotubes manufactured by the sandwich technique*. Journal of Composite Materials, 2016: p. 0021998316658784.
79. Cox, H., *The elasticity and strength of paper and other fibrous materials*. British journal of applied physics, 1952. 3(3): p. 72.
80. Kelly, A. and N.H. Macmillan, *Strong Solids*. Oxford University Press, Walton Street, Oxford OX 2 6 DP, UK, 1986., 1986.
81. Affdl, J. and J. Kardos, *The Halpin-Tsai equations: a review*. Polymer Engineering & Science, 1976. 16(5): p. 344-352.
82. Hashin, Z. and S. Shtrikman, *On some variational principles in anisotropic and nonhomogeneous elasticity*. Journal of the Mechanics and Physics of Solids, 1962. 10(4): p. 335-342.
83. Coleman, J.N., et al., *High performance nanotube-reinforced plastics: Understanding the mechanism of strength increase*. Advanced Functional Materials, 2004. 14(8): p. 791-798.
84. Lahiri, D., et al., *Dual strengthening mechanisms induced by carbon nanotubes in roll bonded aluminum composites*. Materials Science and Engineering: A, 2009. 523(1): p. 263-270.

85. Kassner, M., *Taylor hardening in five-power-law creep of metals and Class M alloys*. Acta materialia, 2004. 52(1): p. 1-9.
86. Jayakumar, J., B. Raghunath, and T. Rao, *Investigation on Fracture Mechanisms in Mg alloy AZ31 Nano Composites Reinforced with Multi Wall Carbon Nano Tubes*. Magnesium (Mg), 2013. 2(9).
87. Hassan, S.F., et al., *Effect of Carbon Nanotube on High-Temperature Formability of AZ31 Magnesium Alloy*. Journal of Materials Engineering and Performance: p. 1-8.
88. Laha, T., et al., *Interfacial phenomena in thermally sprayed multiwalled carbon nanotube reinforced aluminum nanocomposite*. Acta Materialia, 2007. 55(3): p. 1059-1066.
89. Ma, P.-C., et al., *Dispersion and functionalization of carbon nanotubes for polymer-based nanocomposites: a review*. Composites Part A: Applied Science and Manufacturing, 2010. 41(10): p. 1345-1367.
90. Singhal, S., et al., *Carbon nanotubes: amino functionalization and its application in the fabrication of Al-matrix composites*. Powder technology, 2012. 215: p. 254-263.
91. Pezzato, L., et al., *Effect of process parameters of plasma electrolytic oxidation on microstructure and corrosion properties of magnesium alloys*. Journal of Applied Electrochemistry, 2014. 44(7): p. 867-879.
92. Aktuğ, S.L., et al., *Effect of Na₂SiO₃·5H₂O concentration on microstructure and mechanical properties of plasma electrolytic oxide coatings on AZ31 Mg alloy produced by twin roll casting*. Ceramics International, 2016. 42(1): p. 1246-1253.
93. Gray, J. and B. Luan, *Protective coatings on magnesium and its alloys—a critical review*. Journal of alloys and compounds, 2002. 336(1): p. 88-113.
94. Guo, K.W., *A review of magnesium/magnesium alloys corrosion and its protection*. Recent Pat. Corros. Sci, 2010. 2: p. 13-21.
95. Hornberger, H., S. Virtanen, and A. Boccaccini, *Biomedical coatings on magnesium alloys—a review*. Acta biomaterialia, 2012. 8(7): p. 2442-2455.
96. Duan, H., C. Yan, and F. Wang, *Effect of electrolyte additives on performance of plasma electrolytic oxidation films formed on magnesium alloy AZ91D*. Electrochimica Acta, 2007. 52(11): p. 3785-3793.
97. Jo, J.-H., et al., *Enhancing biocompatibility and corrosion resistance of Mg implants via surface treatments*. Journal of biomaterials applications, 2012. 27(4): p. 469-476.
98. Zhang, X., et al., *Corrosion and wear resistance of AZ91D magnesium alloy with and without microarc oxidation coating in Hank's solution*. Journal of Materials Science, 2007. 42(20): p. 8523-8528.
99. Gu, X., et al., *Corrosion resistance and surface biocompatibility of a microarc oxidation coating on a Mg–Ca alloy*. Acta Biomaterialia, 2011. 7(4): p. 1880-1889.
100. Lu, K., et al., *Mechanical damage of carbon nanotubes by ultrasound*. Carbon, 1996. 34(6): p. 814-816.
101. Mukhopadhyay, K., C.D. Dwivedi, and G.N. Mathur, *Conversion of carbon nanotubes to carbon nanofibers by sonication*. Carbon, 2002. 40(8): p. 1373-1376.
102. Medina Escobar, S.A., C.A. Isaza Merino, and J.M. Meza Meza, *Mechanical and thermal behavior of polyvinyl alcohol reinforced with aligned carbon nanotubes*. Matéria (Rio de Janeiro), 2015. 20(3): p. 794-802.
103. C. Teichert, *Gwyddion: Free SPM data analysis software*

- <http://gwyddion.net>, 2002. Scanning Probe Image Processor SPIPTM (<http://www.imagemet.com>).
104. Luo, Z. and J. Koo, *Quantifying the dispersion of mixture microstructures*. Journal of microscopy, 2007. 225(2): p. 118-125.
 105. Standard, A., *Standard test method for plane-strain fracture toughness of metallic materials, E 399-90 (reapproved 1997)*. Annual Book of ASTM Standards, 2003. 3: p. 451-482.
 106. Esawi, A., et al., *The influence of carbon nanotube (CNT) morphology and diameter on the processing and properties of CNT-reinforced aluminium composites*. Composites Part A: Applied Science and Manufacturing, 2011. 42(3): p. 234-243.
 107. Martone, A., et al., *Reinforcement efficiency of multi-walled carbon nanotube/epoxy nano composites*. Composites science and technology, 2010. 70(7): p. 1154-1160.
 108. Charlier, J.-C., *Defects in carbon nanotubes*. Accounts of chemical research, 2002. 35(12): p. 1063-1069.
 109. Olayo, R., et al., *Poly (vinyl alcohol) as a Stabilizer in the Suspension Polymerization of Styrene: The Effect of the Molecular Weight*. Journal of applied polymer science, 1998. 67(1): p. 71-77.
 110. Luo, Z. and J. Koo, *Quantitative study of the dispersion degree in carbon nanofiber/polymer and carbon nanotube/polymer nanocomposites*. Materials Letters, 2008. 62(20): p. 3493-3496.
 111. Mendoza, O., G. Sierra, and J.I. Tobón, *Influence of super plasticizer and Ca (OH) 2 on the stability of functionalized multi-walled carbon nanotubes dispersions for cement composites applications*. Construction and Building Materials, 2013. 47: p. 771-778.
 112. Kondoh, K., et al., *Microstructural and mechanical analysis of carbon nanotube reinforced magnesium alloy powder composites*. Materials Science and Engineering: A, 2010. 527(16): p. 4103-4108.
 113. Xu, J., et al., *Theoretical study and pathways for nanoparticle capture during solidification of metal melt*. Journal of Physics: Condensed Matter, 2012. 24(25): p. 255304.
 114. Tiryakioğlu, M., et al., *Hardness–strength relationships in the aluminum alloy 7010*. Materials Science and Engineering: A, 2015. 631: p. 196-200.
 115. Lourie, O. and H. Wagner, *Evaluation of Young's modulus of carbon nanotubes by micro-Raman spectroscopy*. Journal of Materials Research, 1998. 13(9): p. 2418-2422.
 116. Huong, P.V., et al., *Temperature-dependent vibrational spectra of carbon nanotubes*. Physical Review B, 1995. 51(15): p. 10048.
 117. Schaufele, a. and T. Shimanouchi, *Longitudinal acoustical vibrations of finite polymethylene chains*. The Journal of Chemical Physics, 1967. 47(9): p. 3605-3610.
 118. Wagner, H.D., *Thermal residual stress in composites with anisotropic interphases*. Physical Review B, 1996. 53(9): p. 5055.
 119. Gupta, P., et al., *Electrolytic plasma technology: science and engineering—an overview*. Surface and Coatings Technology, 2007. 201(21): p. 8746-8760.
 120. Leyland, A. and A. Matthews, *On the significance of the H/E ratio in wear control: a nanocomposite coating approach to optimised tribological behaviour*. Wear, 2000. 246(1): p. 1-11.
 121. Bard, A.J. and L.R. Faulkner, *Fundamentals and applications*. Electrochemical Methods, 2001. 2.

122. Cottis, R., S. Turgoose, and B.C. Syrett, *Electrochemical impedance and noise*. 1999.
123. Mansfeld, F., et al., *Analysis of EIS data for common corrosion processes*, in *Electrochemical impedance: analysis and interpretation*. 1993, ASTM International.
124. Grahame, D.C., *The electrical double layer and the theory of electrocapillarity*. *Chemical reviews*, 1947. 41(3): p. 441-501.